Electrochemical Facilitated Transport: A Study in Synthesis, Simulation and Experimentation

by

Albert W. Wagner

Dissertation submitted to the Faculty of the
Virginia Polytechnic Institute and State University
in partial fulfillment of the requirements for the degree of

DOCTOR OF PHILOSOPHY

in

Chemistry

Approved:

R. E. Dessy, Chairman

M. R. Anderson

J. O. Glanville

J. E. McGrath

B. M. Tissue

July, 1995

Blacksburg, Virginia

ELECTROCHEMICAL FACILITATED TRANSPORT: A STUDY IN SYNTHESIS, SIMULATION AND EXPERIMENTATION

by

Albert W. Wagner.

CHAIRMAN: R.E. Dessy
DEPARTMENT: Chemistry

(ABSTRACT)

The ability to influence the movement of ions across a bulk liquid membrane through use of an electrochemically modifiable crown ether will be examined in this work. This process will be referred to as electrochemical facilitated transport. The design and synthesis of a new ferrocenophane crown ether for use in this work will be presented. Experiments using this model compound were designed and performed to demonstrate the ability to move an ion across the membrane both with and against (downhill and uphill) its concentration gradient. Experimental results are presented for the movement of silver perchlorate and thallium chloride across methylene chloride bulk liquid membranes using 2,5,8,11,14,17,20-heptaoxa[21](1,1')ferrocenophane-1,21-dione as the membrane carrier.

As a further enhancement to the understanding of the process of electrochemical facilitated transport, computer simulation modeling tools were developed with special emphasis placed on the electrochemical and carrier/ion complexation issues that are integral to the process.

Acknowledgements

I would like to start by thanking the many members of the Laboratory Automation and Design (LAID) group. This gave me the opportunity to acquire a wide, diverse set of skills and insights through interactions with them and exposure to their research projects. A special note of gratitude to Glen Wollenberg for his friendship through the years. This environment for professional development and maturity was created and maintained by Dr. Raymond Dessy and Lee Dessy. I appreciate the time and efforts Dr. Dessy put forth on my behalf to allow me to complete this project.

I also thank my father for his support through the years; I only wish my mother had survived to see my accomplishment. Further, I thank my ever present and loving spouse Kelley for her patience and encouragement that saw me through the rough times. Lastly, I thank Kelley again for waiting to deliver my son William Charles on March 30th, 1995, until after my dissertation defense, and before start of my position with Whitehall-Robins.

Table of Contents

		Page #
Abstract		ii
Acknowledgements		iii
Table of Contents		iv
List of Figures		viii
List of Tables		xiii
Introduction		1
Historical		4
(A)	Discovery of Crown Ethers	4
(B)	Crown Ether Naming Conventions	7
(C)	Nature of Crown Ether Complexation	10
(D)	Bulk Liquid Membranes	20
(E)	Control Over Transport Processes	23
1)	pH Driven	24
2)	Redox Driven	28
3)	Photo Responsive Crown Ethers	30
(F)	Summary	32
Instrumentation, Apparatus and Techniques		33
(A)	Design and Construction of the Experimental Transport Cell	34
(B)	Filling of the Experimental Cell	38

(C) Cleaning of the Transport Cell 41

(D) Choice of Solvents and Electrolytes 43

(E) Platinum as a Reference Electrode. 44

(F) Potentiostats 48

(G) Design of a Computer Controlled Potentiostat 50

(H) Calibration of the Potentiostat 57

(I) Design of the Computer Interface 58

(J) Computer Controlled Linear Sweep Voltammetry 60

(K) Metal Ion Analysis 65

Computer Simulation of Diffusion 67

(A) Development of a Computer Simulation Model for Electrochemical Facilitated Transport 69

1) Fickian Diffusion and Its Applications to Computer Simulation 70

2) Complexation Concerns 80

3) Electrochemical Considerations 84

4) Model Assumptions 85

5) Model Construction 87

6) Selection of Simulation Parameters 90

7) Collection and Handling of Simulation Data 94

8) Presentation of Data in Graphical Form 95

9) Graphical Analysis of Simulation Data Sets 96

(B) Applied Simulations 121

(C) Summary 127

Experimental 128

(A) Synthetic Organic Chemistry 128

1) Selection of Model Carrier Compound 128

2) Synthesis of Ferrocenophane Crown Ether 132

3) Characterization of the Crown Ether 135

a) Mass Spectroscopy 136

b) Analysis of Proton NMR 143

c) Ultraviolet Spectroscopy 145

d) Cyclic Voltammetry 149

4) Conclusions 154

(B) Design of the Membrane Transport Experiments 155

1) Downhill Transport 158

2) Uphill Transport 159

(C) Membrane Transport Experiments 160

1) Selection of Transport Ion 160

2) Uphill Silver Ion Transport 162

a) Preliminary Experimental Conclusions 170

b) Mass Balance for the Silver Ion 171

c) Cyclic Voltammetry of the Silver Ion System 180

d) UV Evidence for the Silver Ion System 186

e) Evaluation of the Silver Ion System 189

3) Uphill Thallium Ion Transport 190

a) Preliminary Experimental Conclusions 197

b) Mass Balance for the Thallium Ion 198

4) Downhill Thallium Ion Transport 207

a) Downhill Thallium Ion Transport (with Pumping) 207

b) Downhill Thallium Ion Transport (without Pumping) 208

c) Experimental Results 209

5) Exhaustive Electrolysis and Extraction 215

D) Summary of Transport Studies 221

Experimental Analysis 223

A) Structure of Ferrocenophane Crown Ether 223

B) Computer Generated Molecular Model Structures 229

C) Electronic Structure of Ferrocenophane 233

Conclusions: Future Work and Lessons Learned 243

Appendix I FORTH CV Routines 245

Appendix II FORTRAN Simulation Routines 251

Bibliography 258

List of Figures

Figure #		Page #
1.	Petersen's Synthesis of Dibenzo-18C6	6
2.	Crown Ethers of Varying Ring Size	8
3.	Nitrogen and Sulfur Containing Crown Ether Analogs	9
4.	Effects of Electronegative Groups on Crown Ether Membrane Transport Rates	17
5.	Bulk Liquid Membrane	21
6.	Bulk Liquid Membrane Transport Diagram	22
7.	pH Responsive N,N'-bis(2-hydroxy-5-nitrobenzyl)-2.2 Cryptand Crown Ether Ether	25
8.	pH Responsive Polyether	27
9.	Redox Responsive Dithiol/Disulfide Crown Ether	29
10.	Photo Responsive Azobenzene Crown Ether	31
11.	U-Tube Diagram	35
12.	Modified U-Tube Diagram	37
13.	Experimental Cell with Electrodes	39
14.	CV of Ferrocenophane Using Platinum Reference Electrode	46
15.	CV of Ferrocenophane Using SCE Reference Electrode	47
16.	Potentiostat Connections to Experimental Cell	49
17.	Diagram of Adder Potentiostat	51

18.	Generation of a Complex Waveform	52
19.	Improved Adder Potentiostat	54
20.	Research Potentiostat	56
21.	Computer Connections to Potentiostat	59
22.	Twelve-Bit Digital to Analog Conversion Values	62
23.	Flowchart for CV Routine	64
24.	Diagram of Simulation Model Definitions	72
25.	Species Generation at Electrode (Simulation Example)	75
26.	Growth of Depletion Layer	77
27.	Growth of Electrode Reaction Products	78
28.	U-Tube Diagram and Model Definitions For Simulation	88
29.	Diffusion Growth Profile for Neutral Carrier	98
30.	Diffusion Growth Profile for Carrier/Ion Complex	99
31.	Diffusion Growth Profile for Charged Carrier	100
32.	Diffusion Growth Profile for Charged Carrier/Ion Complex	101
33.	Depletion of Source Phase	103
34.	Growth of Receiving Phase	104
35.	Averaged Neutral Carrier Profile	106
36.	Averaged Carrier/Ion Complex Profile	107
37.	Averaged Charged Carrier Profile	108
38.	Averaged Charged Carrier/Ion Complex Profile	109
39.	Averaged Source Phase Profile	110

40.	Averaged Receiving Phase Profile	111
41.	Averaged Source and Receiving Phase Profiles (Combined)	112
42.	Effect of Equilibrium Constants on Receiving Phase Concentration	113
43.	Effect of Percent Oxidation/Reduction on Receiving Phase	116
44.	Effect of Electrochemical Redox Cycling on Receiving Phase	117
45.	Expanded View of Figure 59	118
46.	Uphill Pumping Profiles	120
47.	Simulated Uphill Transport Profiles Using Experimental Complexation Values and Conditions	123
48.	Simulated Downhill Transport Profiles Using Experimental Complexation Values and Conditions (Early Stages of Simulation)	154
49.	Simulated Downhill Transport Profiles Using Experimental Complexation Values and Conditions	155
50.	Electrochemistry of Phenazine	130
51.	Proposed Synthesis for a Phenazine-Based Crown Ether	131
52.	Phenanthroline Crown Ether	133
53.	Synthesis of Ferrocene-Based Crown Ether	134
54.	Parent Peak Mass Spectrum for Ferrocenophane Crown Ether	137
55.	Full Mass Spectrum for Ferrocenophane Crown Ether	138
56.	Theoretical Parent Peak Mass Spectrum for Ferrocenophane Crown Ether	141
57.	Proton NMR Spectrum for Ferrocenophane Crown Ether	144

58.	Ultraviolet Transmission Spectrum for Ferrocenophane Crown Ether	146
59.	UV Spectral Response of Substituted Ferrocenophane Crown Ethers	148
60.	Cyclic Voltammagram for Ferrocenophane Crown Ether	150
61.	Expanded Cyclic Voltammagram for Ferrocenophane Crown Ether	151
62.	Potential Shifts Due to Addition of Ketone Groups to Ferrocenophanes	153
63.	Downhill Transport U-Tube Diagram	156
64.	Uphill Transport U-Tube Diagram	157
65.	Calibration Curve for Silver (Uphill Pumping Experiment)	166
66.	Experimental Data (Silver/Uphill Pumping Experiment)	169
67.	Millimoles Silver (All)	175
68.	Millimoles Silver (Aqueous)	176
69.	%Moles Silver (All)	178
70.	%Moles Silver (Aqueous)	179
71.	CV Ferrocenophane (Time = 0)	182
72.	CV Silver Addition (Time = 6)	183
73.	CV Silver Addition (Time = 24)	184
74.	CV Silver Addition (Combined)	185
75.	UV Spectrum of Ferrocenophane	187
76.	UV Spectrum of Ferrocenophane (Silver Degradation)	188
77.	Calibration Curve for Thallium (Uphill Pumping Experiment)	193
78.	Experimental Data (Thallium Uphill Pumping Experiment)	196

79.	Millimoles Thallium (All)	201
80.	Millimoles Thallium (Aqueous)	202
81.	%Moles Thallium (All)	204
82.	%Moles Thallium (Aqueous)	205
83.	Calibration Curve for Thallium (Downhill Transport Experiment)	211
84.	Experimental Data (Thallium Downhill Pumping Experiment)	214
85.	ICP Working Curve for Thallium	218
86.	2,5,8,11,14,17,20-heptaoxa[21](1,1')ferrocenophane-1,21-dione	225
87.	CPK Model of Ferrocenophane Crown Ether	226
88.	CPK Model of Ferrocenophane Crown Ether Complexed With Ion	227
89.	CPK Model of Ferrocenophane Crown Ether Complexed With Ion	228
90.	Computer Model of Ferrocenophane Crown Ether Complexed With Ion (View 1)	230
91.	Computer Model of Ferrocenophane Crown Ether Complexed With Ion (View 2)	231
92.	Computer Model of Ferrocenophane Crown Ether Complexed With Ion (View 3)	232
93.	Electrostatic Repulsion Model	235
94.	Biferrocenylene	241

List of Tables

Table #		Page #
1.	Cation Radii and Crown Ether Cavity Size	12
2.	Transport Rates of Ions by Crown Ethers	13
3.	Cation Transport Rates Via Nitrogen and Sulfur Crown Ethers	15
4.	Ion Transport Rates for Electronegative Substututed DB18C6	18
5.	Growth of Diffusion Layer at Electrode Surface (Simulation Values)	76
6.	Summary of Simulation Parameters	91
7.	Uphill Silver Ion Transport (Working Calibration Curve)	165
8.	Uphill Silver Ion Transport (AE Raw Data)	167
9.	Uphill Silver Ion Transport (Experimental Results)	168
10.	Millimoles Mass Balance (Silver)	174
11.	%Moles (Silver)	177
12.	Uphill Thallium Ion Transport (Working Calibration Curve)	192
13.	Uphill Thallium Ion Transport (AE Raw Data)	194
14.	Uphill Thallium Ion Transport (Experimental Data)	195
15.	Millimoles Mass Balance (Thallium)	200
16.	%Moles (Thallium)	203
17.	Downhill Thallium Ion Transport (Working Calibration Curve)	210
18.	Downhill Thallium Ion Transport (AE Raw Data)	212
19.	Downhill Thallium Ion Transport (Experimental Data)	213

20. Thallium Extraction Data 228

21. Ferrocene Molecular Orbitals 238

22. Ferrocenium Ion Molecular Orbitals 239

INTRODUCTION

In 1967, Pedersen[1] serendipitously discovered a class of compounds he named crown ethers. Intrigued by their ability to complex with a wide variety of cations, he studied them in great detail to understand how they functioned. Many researchers have since examined these new molecules and their possible uses, and have generated several new compounds with applications in such diverse areas as synthetic organic chemistry, chromatographic separations and ion selective electrodes, modeling of enzyme systems, and carrier mediated transport of ions through solid and liquid membranes. Twenty years later, Pedersen shared the Nobel Prize in 1987 with Lehn and Cram, for their work with Crown Ethers and their analogs.

The particular direction in using crown ethers developed in this work had its beginnings in the winter of 1982-83. Upon reading a paper, published by Pannell et al.,[2] that outlined a series of substituted crown ethers and the effect of electron withdrawing and donating substituents on their ability to complex and transport ions across a bulk liquid membrane, an idea germinated. Is it possible to integrate an externally modifiable group into a crown ether to effect it's ability to transport ions? Specifically, is it possible to incorporate an electrochemical couple ("electrophore") into the crown ether system? This was a novel idea at this time, with little, if any, work being done in this area. It has been exciting to pursue the concept.

After deciding to pursue the feasibility of electrochemical modifiable facilitated transport, several questions needed to be addressed. What are the chemical, electrochemical, and physical properties a molecule must possess to be a viable candidate for study? Do any commercially available or reported compounds possess the proper attributes? If so, what do these molecules look like? If not, what compounds and what electrochemical groups may be employed? Perhaps of more importance is the question of whether the concept of externally modifiable electrochemical facilitated transport is supported by known equations of state as they apply to complexation, diffusion, and electrochemistry. Lastly, can an ion be found to experimentally validate electrochemical facilitated transport?

The selection of a model molecule and verification via theoretical mathematical simulation was attempted in parallel with the actual experimentation. No commercially available candidates were found. Searching the literature failed to produce a useful compound. To pursue this project a new class of molecules needed to be synthesized, and the author needed to develop the necessary organic skills to accomplish this task. The verification of the mathematical diffusion model through computer simulation techniques based on standard equations of state proved easier, but required more than a year to develop and refine.

It took several years, trying one synthetic system after another, reaching an impasse, trying another system, and developing additional synthetic skills, before a viable synthetic molecule was synthesized. This took the form of a new

ferrocenophane. Selection of a satisfactory ion for transport study took two years before suitable candidates in the form of Ag^+ and Tl^+ ions were found.

During this extended effort suggestions were often made by others to abandon this track of research. However, one can now report the viability of the concept of electrochemical facilitated transport, and look forward to others extending the concept, synthesizing new unique compounds, and applying them to possible areas of controlled drug release, biofermentation, or areas where it is desirable to have precise controlled delivery of a substrate or catalyst.

HISTORICAL

In 1967, Pedersen published a paper outlining his work with a new class of compound he named crown ethers, including their complexation with alkali and other metal ions[1]. While not the first to synthesize a polyether, he was the first to recognize and study the formation of stable complexes between the polyether and ions. Until this time, only biological compounds were thought capable of binding to metal ions to form stable complexes. Thus, whole new areas of research emerged to 1) probe the nature of forces involved in the complexation process, 2) create new molecules, 3) and find ever increasing numbers of uses for them. The following sections will briefly cover crown ethers and related topics of research.

(A) Discovery of Crown Ethers

While working on a project to synthesize bis[2-(hydroxyphenoxy)ethyl]ether from bis(2-chloro-ethyl)ether and 2-(o-hydroxyphenoxy)tetrahydropyran (unreacted catechol present),[1] Dr. Pedersen synthesized the first crown ether as a by-product (Figure 1). He later named it Dibenzo-18C6 as the molecule contained two benzene

rings, 18 atoms involved in the main ring, with the six oxygens in the ring reminding him of jewels in a crown. Additional naming conventions will be addressed.

Using Ultraviolet Spectroscopy to follow the course of the initial reaction, he found the new molecule exhibited an absorption curve characteristic of the phenolic starting materials. Sodium hydroxide was added to the system to test for the amount of free hydroxyl groups. Expecting the absorption curve to be unaffected if all hydroxyl groups were bound, or shifted to a longer wavelength if free, he noted an overall change in the shape of the wave form, and an increase in solubility of the unknown upon addition of any sodium containing salt. Later evidence from NMR and Infrared analysis indicated the structure of the unknown to be a cyclic hexaether. He postulated the positive sodium ion complexed with the negative dipolar charge on the oxygens in the polyether ring, and the increase in solubility was due to formation of a stable complex.

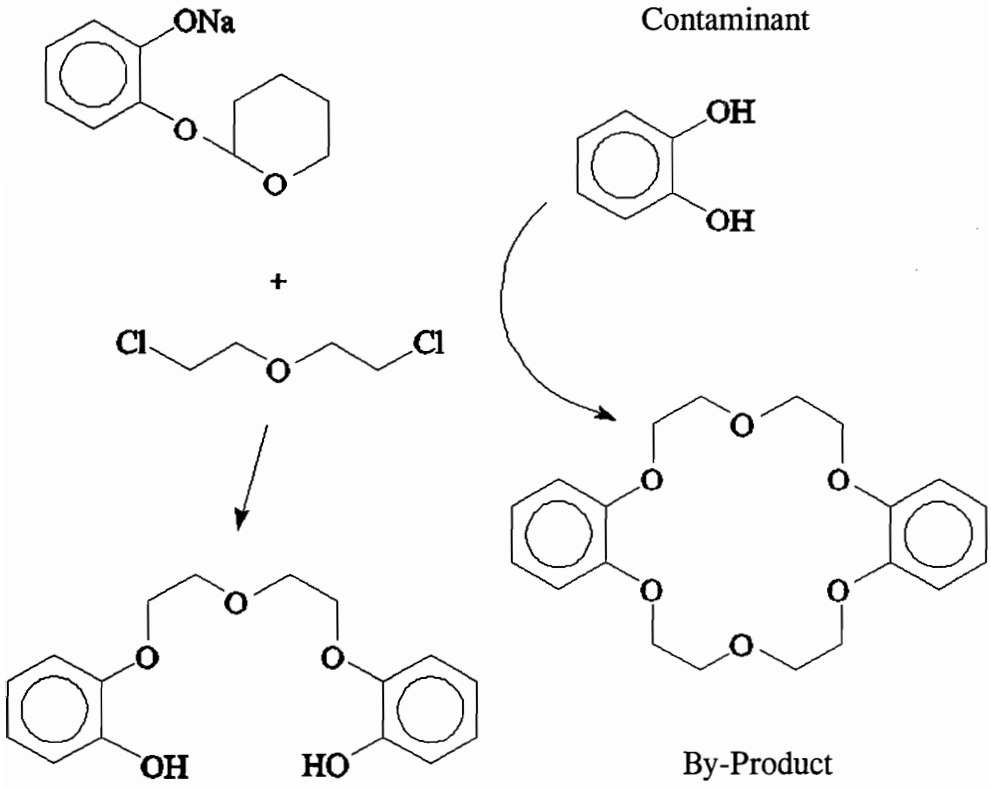

Figure 1. Petersen's Synthesis of Dibenzo-18C6 Crown Ethers[1]

(B) Crown Ether Naming Conventions

Pedersen adopted a naming convention for his new class of compounds incorporating the ring size and common names for substituents in the ring. He named his first compound Dibenzo[18]Crown-6, as opposed to using it's lengthy IUPAC (International Union of Pure and Applied Chemistry) name of 2,5,8,15,18,21-hexaoxa-tricyclo[20.4.0.0]hexacosa-1(22),8,11,13,23,24-hexaene. The utility of his naming system has been generally accepted, and has been shortened even further so that DB18C6 represents the above compound. Dibenzo-18C6 indicated two benzene rings are incorporated into a ring system of 18 atoms (counting two each from each benzene). The term crown is descriptive of the overall geometry of the compound. The number 6 refers to the number of heteroatoms (in this case, oxygen) involved in the ring system.

Since then, many additional crown-like compounds have been synthesized. The next two figures show the structures and naming conventions for crown ethers molecules that will be discussed in following sections. Figure 2 depicts crown ethers varying only in the size of the ring. Crown ether 15C5 has 15 members in the ring and 5 oxygen atoms, while 21C7 contains 21 ring members with 7 oxygen atoms. Figure 3 shows 18C6 crown ether variants with different heteroatoms such as sulfur and nitrogen in place of oxygen and introduction of a pyridine and carbonyl groups into the ring structure. The name DT18C6 represents an 18C6 crown ether with two

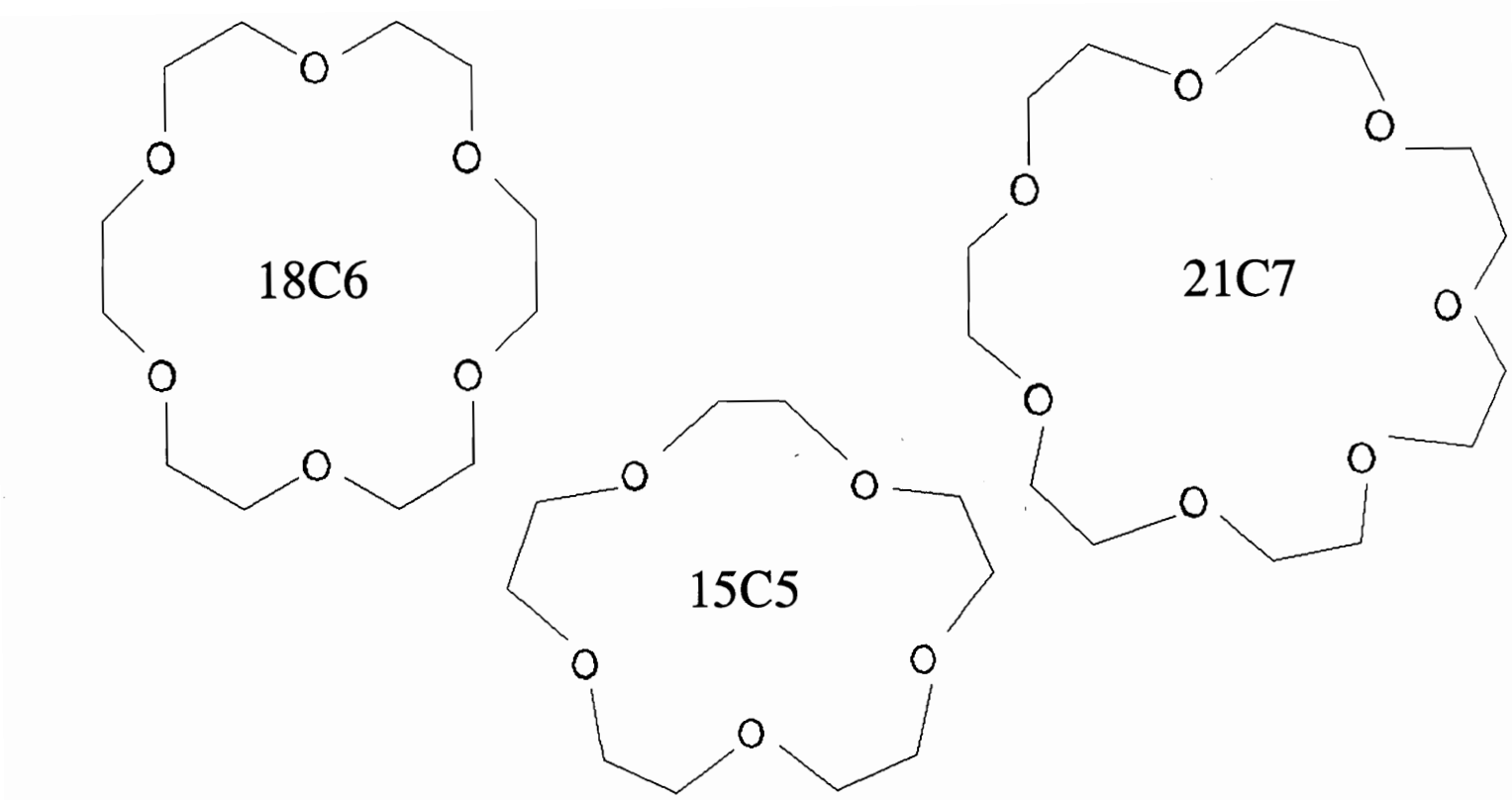

Figure 2. Crown Ethers of Varying Ring Size

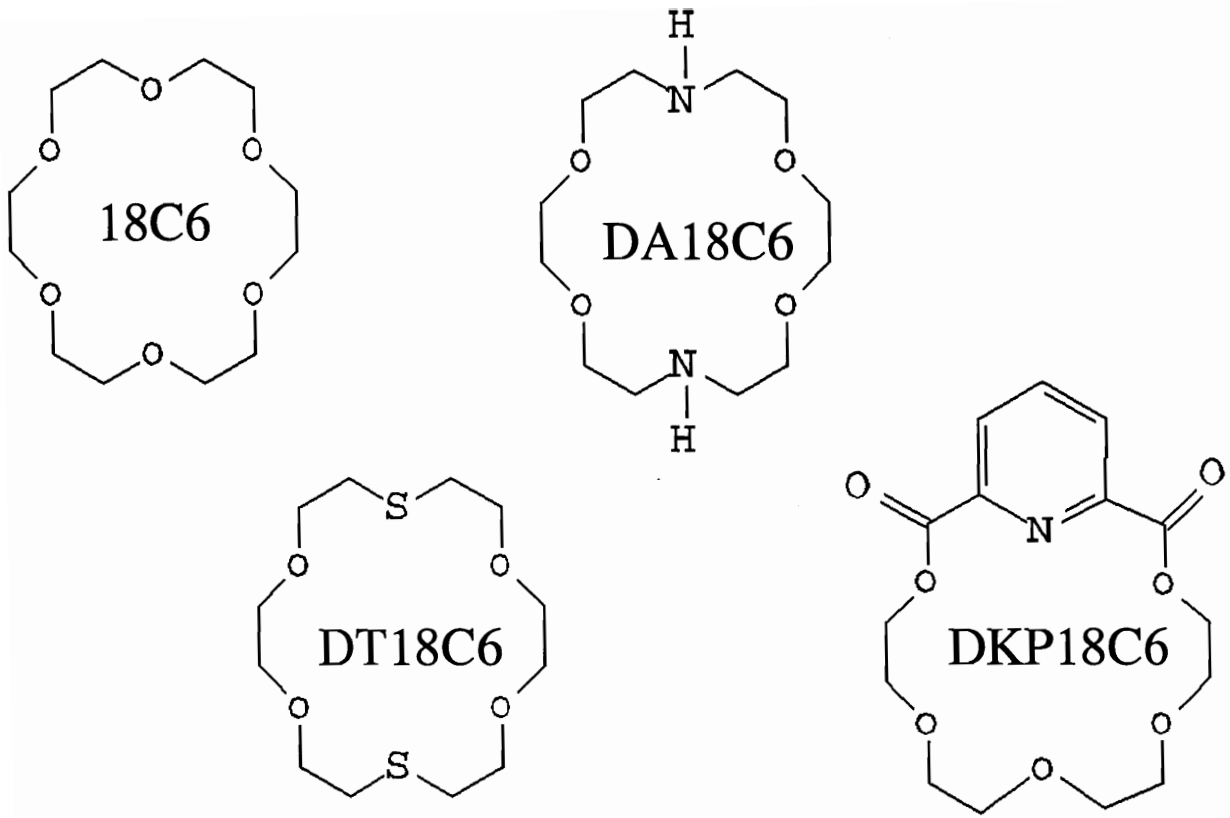

Figure 3. Nitrogen and Sulfur Containing Crown Ether Analogs

thiol (sulfur) units replacing oxygen atoms, 18 and DT as shorthand for dithiol. A more exact name would be 1,10-DT18C6 indicating the actual position of the sulfur atoms within the ring structure. Nitrogen containing crown ethers are represented by the name of Aza. Thus, 1,10-Diaza18C6 (DA18C6) describes an 18 member crown ether with two nitrogen atoms replacing oxygen atoms in ring positions one and ten. DKP18C6 represents an 18C6 crown ether with incorporation of one pyridine and 2 ketone units. Many other crown ethers continue to be synthesized and naming conventions adapted to describe the new structures. Additional compounds may be found in the literature.[3,4,5,6,7,8,9,10]

(C) Nature of Crown Ether Complexation

In 1967, Pedersen[1,11] reported the ability of various crown ethers to complex with many metal ions. Several conditions were identified for formation of stable complexes. Among them are: (1) the relative sizes of the ion and the cavity formed by the crown ether, (2) the number of oxygens in the polyether ring, (3) the coplanarity of the oxygen atoms, (4) the symmetrical placement of the oxygens in the ring, (5) the basicity of the oxygen atoms, (6) the steric hinderance of the polyether, (7) the tendency of the ion to associate with the solvent, and (8) the electrical charge on the ion.

Complexes between crown ethers and metal ions are most stable when the radii of the metal ion matches the cavity of the polyether ring. Lamb and Izatt et al.[12,13] published a study that compared transport rates for a number of cations using crown ethers differing in ring size. Table 1 lists ion and carrier molecule radii, and Table 2 reports the experimental transport rates of metal ions across a bulk liquid membrane for the various cations. Upon examination of the experimental rates, a relationship between the size of the crown ether cavity and that of the transported ion emerges. When the ion radius matches the cavity size, the metal ion comes within close proximity with the greatest number of ring oxygens. The lone pair of electrons on each of the ring's oxygens, due to the geometry of the molecule, is oriented towards the center of the ring structure. This yields a pocket of localized electronegative charge that electrostatically attracts the positively charged cation. The greater the number of oxygens that can participate in complexation, the stronger the complex.

Examining the data in Tables 1 and 2, shows the above explanation to be supported by experimental data. One observes that the maximum transport rates for Na^+, K^+ and Ag^+ occur with crown ethers that have corresponding cavity radii. The maximum for Na^+ (1.02 Å) occurs with 15C5 (0.86-0.92 A). The maximum for K^+ (1.38 Å) corresponds to 18C6 (1.34-1.43 Å). And, the maximum for Ag^+ (1.15 Å) coincides with 18C6 as well.

Table 1: Cation Radii and Crown Ether Cavity Size

Cation	Ion Radius Å	Crown Ether	Cavity Radius Å
Li^+	0.72	15C5	0.86-0.92
Na^+	1.02	18C6	1.34-1.43
K^+	1.38	21C7	1.7
Ag^+	1.15		

Table 2: Transport Rates of Ions by Crown Ethers

	Log (Moles transported x 10^7/24 hours)		
Cation / Carrier	15C5	18C6	21C7
Li^+	*	*	*
Na^+	1.45	1.05	0.68
K^+	0.53	2.44	1.83
Ag^+	2.02	2.35	2.12

* Less than 0.3 x 10^{-7} moles transported/24 hours

Note that while the transport rates maximize at best match, the rates for ions with larger and smaller cavity sizes do not drop off dramatically. Other factors such as the ring's ability to change geometry[14,15,16] and wrap itself around the ion in the case of a larger ring size, or to orient its ring oxygens towards the ion, and in the case of a smaller ring radii the possibility of having more than one crown ether unit complex with the cation[17] needs to be considered. In both cases, lack of steric hinderance allows the greatest number of ring oxygens to move into positions favorable for complexation.

J.D. Lamb, et. al[12] have reported the effects of substituting one or more nitrogen or sulfur atoms in place of the ring oxygens (Figure 3 and Table 3). Examination of the transport rates show a decrease as additional sulfur and nitrogen groups replace ring oxygens. However, comparing ion transport rates for one or more of the substituted crown ethers reveals the decrease in rate for the silver ion is less than that for sodium or potassium ions. This preference for the silver ion is explained by the theory of Hard and Soft Acids and Bases.[18]

The theory of Hard and Soft Acids and Bases defines the interactions of acids and bases in terms of their polarizability. Hard acids and bases are relatively non-polarizable, while soft groups are polarizable. In terms of Lewis acids and bases, metal ions act as acids, and atoms of oxygen, nitrogen and sulfur are bases. Alkali ions that hold tightly to their electrons are considered to be "hard", while the transition metals with more readily available electrons are considered "soft." In terms

Table 3: Cation Transport Rates Via
Nitrogen and Sulfur Crown Ethers

Cation	Log (Moles transported x 10^7/24 hours			
	18C6	DT18C6	DA18C6	DKP18C6
Na^+	1.05	0.20	0.40	0.42
K^+	2.44	*	0.60	1.97
Ag^+	2.35	1.52	1.45	2.49

* Less than 0.3 x 10^{-7} moles transported/24 hours

of the corresponding bases, oxygen is considered as "hard" with nitrogen and sulfur being regarded as "soft." In terms of complexation and equilibrium, it is generally held that like complexes with like. Experimental data supports this conclusion. The softer transition metal silver ion binds more readily with the softer nitrogen and sulfur moieties, while the harder alkali K^+ and Na^+ ions bind more readily with the harder oxygen group. Many compounds have been created with various functional groups in hopes of generating molecules that will selectively bind with only one ion.

In 1982, Pannell et.al.[2] published a paper detailing the effect of a series of substituents attached to DiBenzo-18C6 Crown ethers. The incorporated groups differed in their degree of electronegativity. Experimental data from membrane transport studies are listed in Table 4, and the molecules are depicted in Figure 4. They reported the electronegativity of the attached groups in terms of Hammett[19] (σ) values. A positive σ value indicates an electronegative (electron withdrawing) group. They found a correlation between the electronegativity of the group(s) attached to the crown, and the overall ability of the crown to transport ions across a bulk liquid membrane. It was noted that as the electronegativity and number of groups attached increased, the smaller the transport rate for the ion. They attributed the decrease of transport rate to electron withdrawal through the benzene ring and from the ring oxygens. This results in a lower available electron density for complexation with the metal ions. The withdrawal of electron density from the ring oxygens reduces the

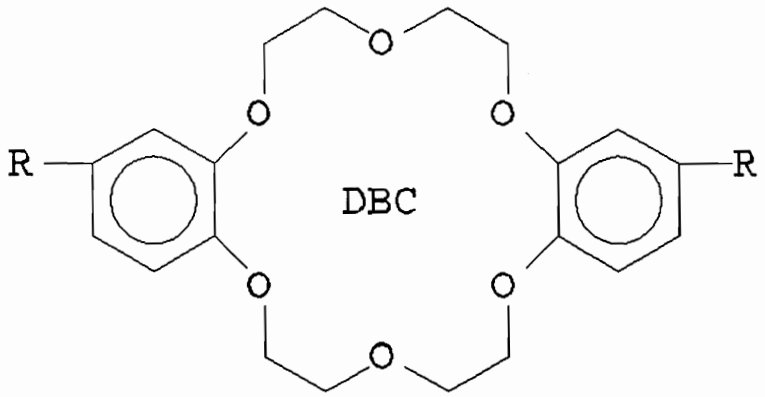

R = CH_3CHOH
$CH_3C=O$
$C_6C=O$, $C_9C=O$, $C_{12}C=O$
cis/trans NO_2
Br_2, Cl_4

Figure 4. Effects of Electronegative Groups on Crown Ether Membrane Transport Rates

Table 4: Effects of Electron Withdrawing Groups on Overall Ion Transport Rates

Crown Ether	Transport Rate -log(mol/l/min) for K^+	Na^+	Hammett Values σ
$(CH_3\text{-}CHOH)_2$DBC	6.23	6.4	
DBC	6.23	6.4	0
$(CH_3C=O)_2$DBC	6.85	7.12	1.76
$(C_6C=O)_2$DBC	6.96	7.24	1.76
$(C_9C=O)_2$DBC	6.85	7.05	1.76
$(C_{12}C=O)_2$DBC	6.92	7.20	1.76
Br_4DBC	7.27	7.92	2.49
cis-$(NO_2)_2$DBC	7.85	8.1	3.14
trans-$(NO_2)_2$DBC	7.85	7.9	3.14
Cl_8DBC	8.8	8.4	4.7

basicity of the oxygens leading to a "hard" base in accordance with the principles of Hard and Soft Acids and Bases[18].

It is important to note that this is the first instance correlating a change in transport ability with that of electron withdrawal from the binding sites. Three orders of magnitude difference exist between the observed transport rates for potassium comparing unsubstituted DiBenzo 18C6 Crown Ether with its highly electronegative electron withdrawing perchlorinated analog. This change in complexation or transport rate will be explored in later simulation modeling and experimental sections. But first, let us examine the experimental methods used to perform transport studies.

(D) Bulk Liquid Membranes

Membranes are an essential element of living cells, and are utilized in daily life in the form of soaps and detergents, protectants, filters, as well as scientific research. Liquid membranes offer a unique combination of order and disorder that allow quicker transport measurements than their solid counterparts. Due to their relative ease of implementation, bulk liquid membranes have been used extensively to study the ability of crown ethers (carrier molecules) to transport a metal ion from one side of a liquid membrane to the other. A bulk liquid membrane is usually an immiscible organic liquid that separates two aqueous phases, Aq I and Aq II, as outlined in Figure 5 (although it may be an aqueous phase separating two immiscible organic phases). The liquid membrane is defined as encompassing the entire organic and interfacial regions. The carrier molecule of interest is dissolved in the organic phase. Figure 6 depicts the transport process. The mathematics of the complexation process is described in equation below:

$$M^{+}_{Aq} + C_{Org} \rightleftharpoons (C \bullet M^{+})_{Org}$$

$$K_{eq} = \frac{[C \bullet M^{+}]_{Org}}{[M^{+}]_{Aq}[C]_{Org}}$$

The carrier molecule complexes with an ion from aqueous phase I at interface I. At the interface, cation $[M^{+}]_{Aq}$ combines with a free carrier $[C]_{Org}$ to form the complex

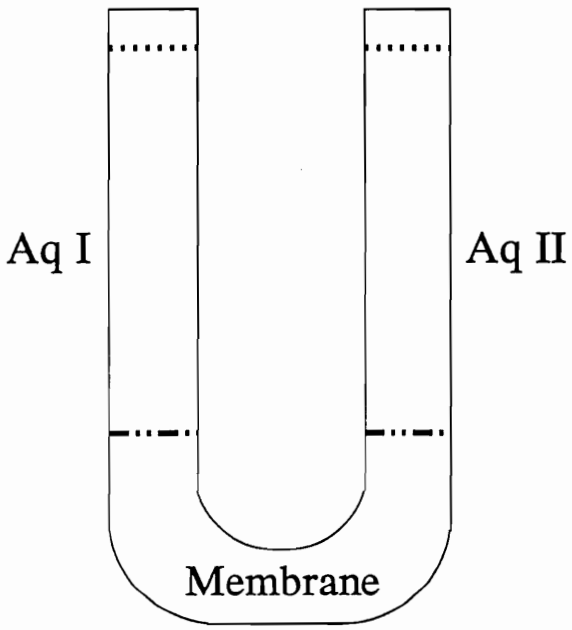

Figure 5. Bulk Liquid Membrane

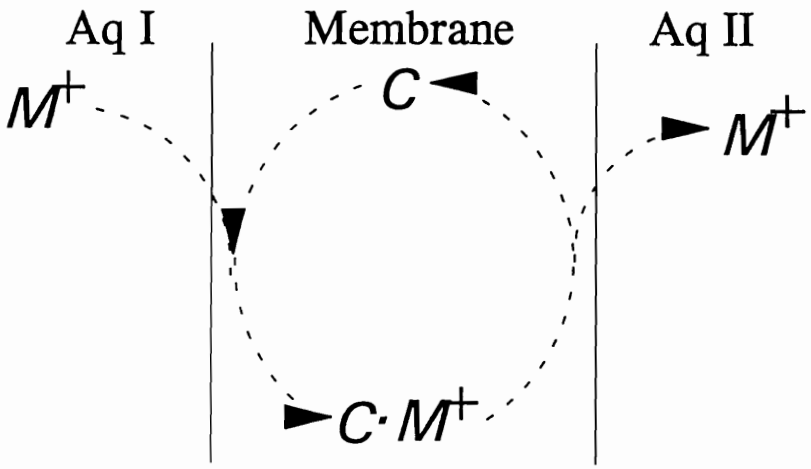

Figure 6. Bulk Liquid Membrane Transport Diagram

$[C \cdot M^+]_{Org}$ which makes the cation soluble in the membrane phase. The lipophilic complex moves across the membrane where it breaks up at interface II releasing ions into Aqueous Phase II. The freed carrier returns across the membrane to interface I to complete the cycle.

(E) Control Over Transport Processes

Traditionally, studies have been directed towards measuring a carrier's ability to transport a metal ion across a membrane based solely on interaction between the two aqueous phases. In biology, movement of substrates across living membranes controlled by differences in pH have been well documented. Researchers soon developed classes of pH responsive crown ethers and analogs to act as models for their biological counterparts[20,21]. In the same vein, other chemical gradients have been created to influence a crown ether's ability to transport ions. Even light energy has been harnessed[25].

1) pH Driven

In 1981, Nishida et al.[22] demonstrated calcium ion proton-coupled extraction utilizing a 2.2 cryptand modified with a monobasic chromatographic reagent 2-hydroxy-5-nitrobenzyl bromide (Koshland reagent). The result is N,N'-bis(2-hydroxy-5-nitrobenzyl)-1,10-diaza-4,7,13,16-tetraoxacyclo-octadecane as shown in Figure 7. The modified cryptand form stable reversible complexes with calcium, barium and strontium. A high pH gradient promotes movement of the divalent cation into the membrane phase for complexation. Bearing two chromophore subunits, the cryptand has proven useful in the photometrical determination of calcium in blood serum. Because of the cryptand's low binding affinity with sodium and magnesium, which normally interfere with blood serum calcium measurements by other means, concentrations may be measured that are in agreement with results obtained from the more stringent atomic absorption analysis methods.

The equations of complexation (extraction) are as follows:

$$(H_2L)_o + M^{++} = (ML)_o + 2H^+$$

and,

$$K_{ex} = \frac{[ML]_o \cdot [H^+]^2}{[H_2L]_o \cdot [M^{++}]}$$

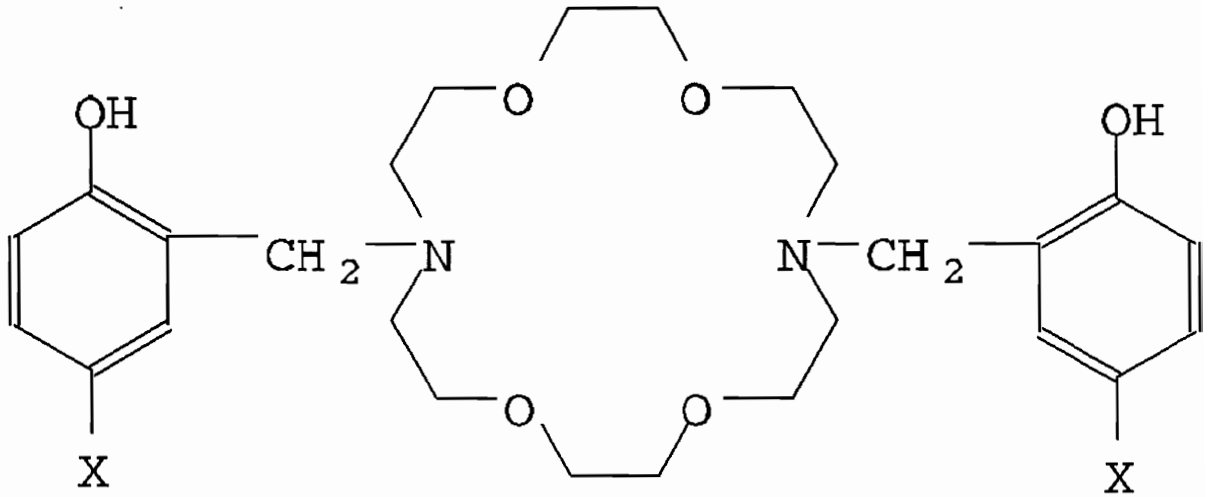

X = Nitrobenzyl

Figure 7. pH Responsive N,N'-bis(2-hydroxy-5-nitrobenzyl)-2.2 Cryptand Crown Ether

Since the complexation reaction is reversible, the above divalent metal ions can be pumped across a membrane containing the cryptand from an aqueous phase of a high pH to one of a lower value.

An example of pH facilitated transport of cation using noncyclic polyethers was published by Hiratani et. al[23] in 1982. In the study, they examined the effects of acid and cation concentrations on the uphill transport rate of the cation. The neutral form of the noncyclic polyether shown in Figure 8 does not complex as well with potassium ion as it does when the carboxylic acid group is ionized. When this occurs, the open chains of the polyether more readily wrap themselves around the cation, forming a crown ether like structure. They demonstrate that a high acid concentration at one side of the membrane can pump the potassium ion uphill across the membrane, and concentrate the ion at the expense of the chemical energy of the pH gradient.

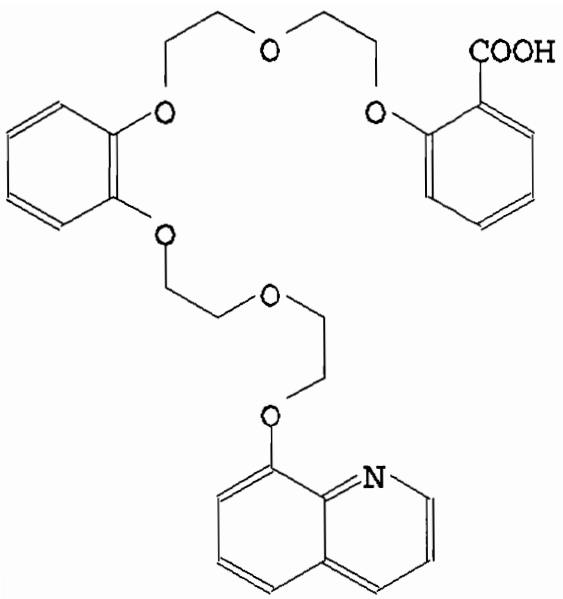

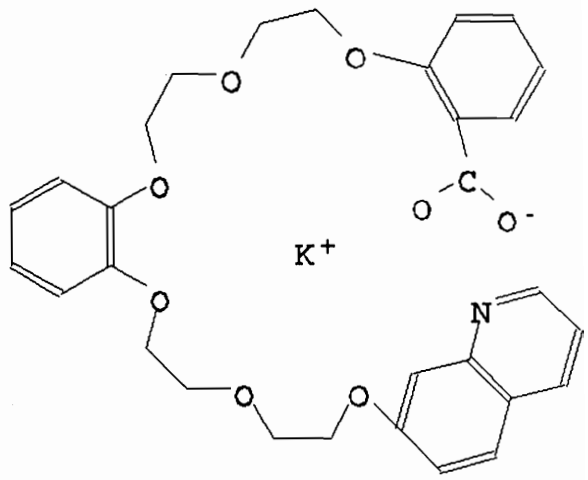

Figure 8. pH Responsive Polyether

2) Redox Driven

In 1985, Shinkai et al.[24] published results of the first redox responsive thiol-containing crown ether shown in Figure 9. When the reduced form is oxidized, a crown like disulfide compound is formed that has enhanced transporting capabilities compared to that of the reduced form. Increased transporting ability results from the formation of a crown ether cavity favorable for complexation. During the course of their experiments, they demonstrated the ability to create a chemical redox switch, in that they could selectively increase or decrease the transport of ions across a membrane. For example, if they started with the reduced form of the carrier, then oxidized it to the disulfide, the overall ion transport rate increased. Conversely, starting with the oxidized form, and then reducing the carrier molecule back to the thiol, the overall rate would decrease. Since then, several other researcher have made crown ethers incorporating quinones, porphyrins, and phthalocyanines.

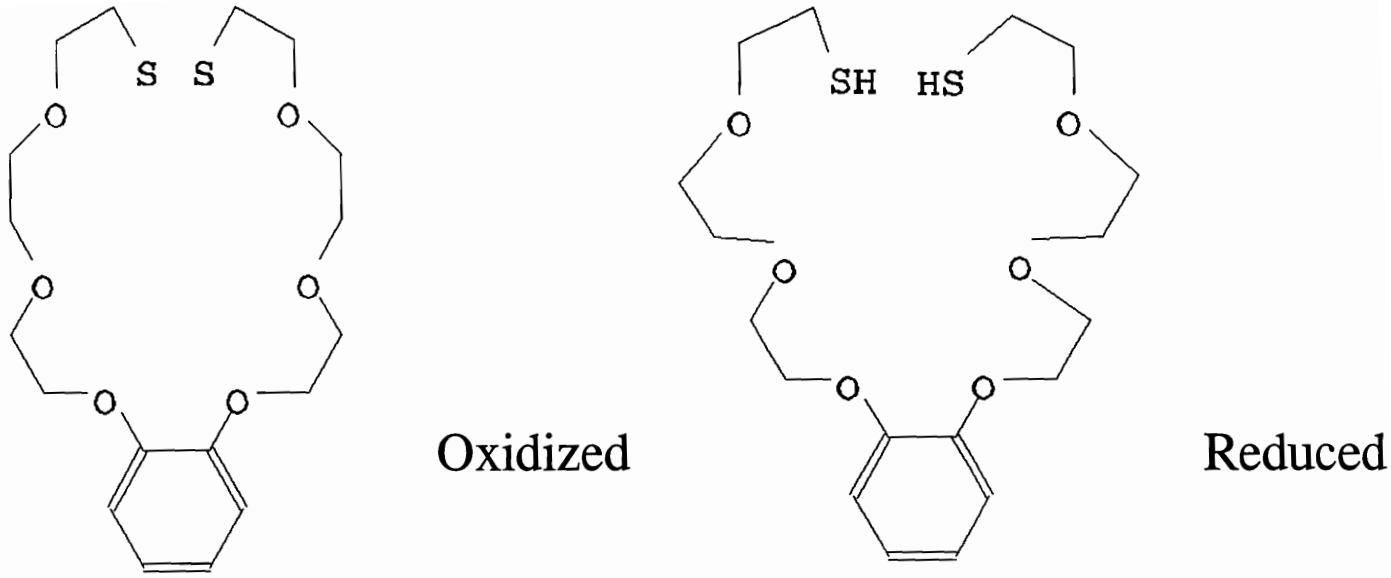

Figure 10. Redox Responsive Dithiol/Disulfide Crown Ether

3) Photo Responsive Crown Ethers

In 1985, Shinkai et al.[25] published experimental results for a photo responsive crown ether shown in Figure 10. The benzo 18C6 analog had an azobenzene structure incorporated into the crown ether. When activated by ultraviolet light at 366 nm., photoisomerization takes place converting the trans form of the molecule to the cis form. During the isomerization process, the ammonium portion of the molecule is moved into the proximity of the cavity, causing stearic hindrance to the binding site of the crown ether. In addition to blocking the binding site, the ammonium group is known to complex with the cavity of crown ethers. This not only inhibits metal ions from complexing with the crown ether, but forces ions previously complexed back into the membrane where they diffuse to the nearest aqueous phase.

Shinkai referred to this isomerization transport process as a photochemical switch. The term "switch" is not absolute in terms of "on" or "off", but describes a change in the rate of transport. Experiments were performed where transport of potassium ions across a membrane was monitored. The experiment proceeded to a point where the crown ether was irradiated with UV light, converting the complexing trans form of the crown ether into its non-complexing cis form. Measuring the transport rates of the potassium ion before and after irradiation, researchers noted the transport rate before isomerization was greater than afterwards.

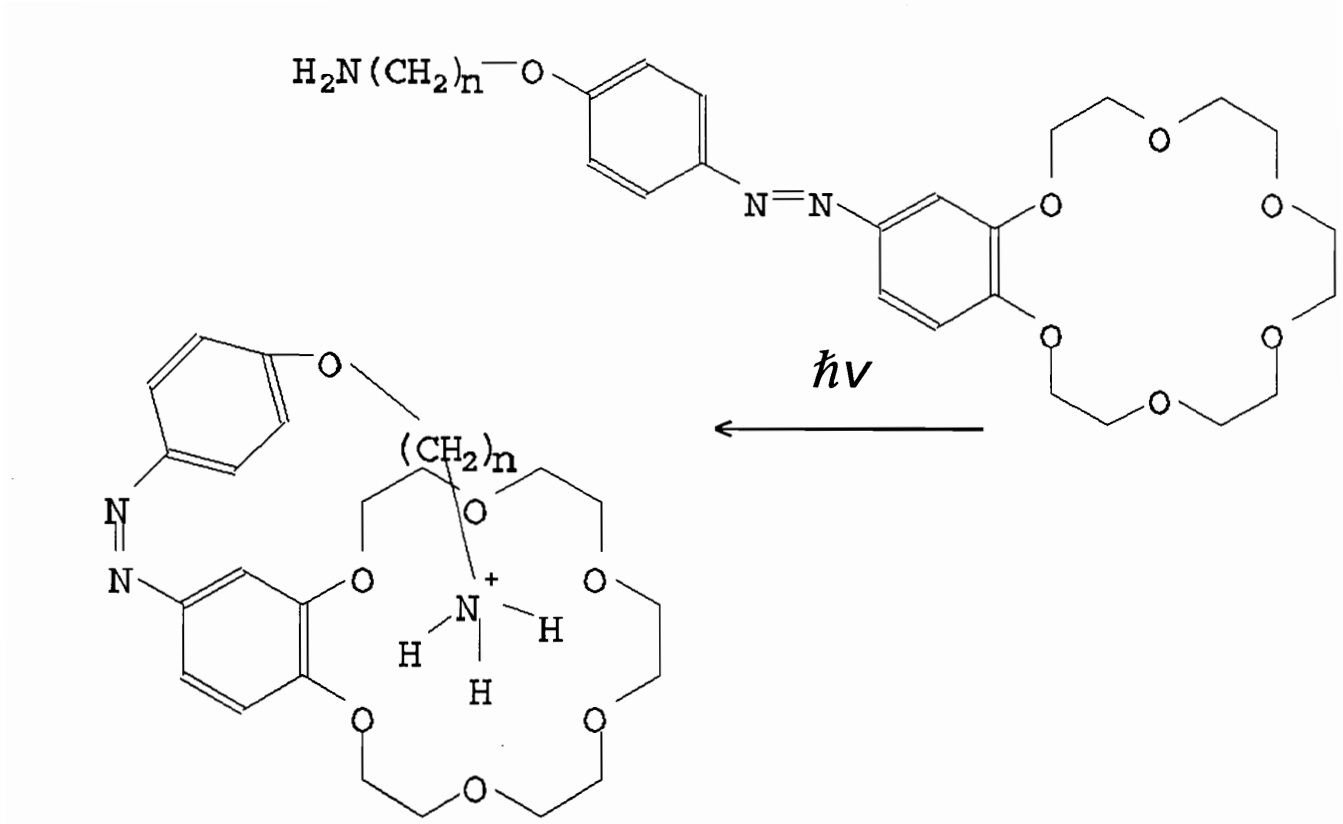

Figure 10. Photo Responsive Azobenzene Crown Ether

(F) Summary

This presentation of crown ether design and membrane transport experiments demonstrates the versatility of these unique molecules for use as models for ion complexation and transfer processes in biological systems and switchable carrier compounds in membrane/ion facilitated transport systems. The ability to be influenced by various controlled stimuli such as pH, chemical oxidation/reduction and light, and act as mediated switched transport systems suggests their potential uses are bounded only by imagination and the ability to design and synthesize new compounds. Clearly, electrochemical facilitated transport was worth pursuing.

INSTRUMENTATION, APPARATUS AND TECHNIQUES

The concept of electrochemical facilitated transport brings together areas of electrochemistry, liquid membrane transport, and metal ion analysis in forms of atomic emission, atomic absorption and inductively coupled plasma (ICP) spectroscopy. Each area encompasses a wide range of concepts, experimental apparatus and procedures. To meet the unique conditions of electrochemical facilitated transport, new experimental cells and procedures must be developed. The following topics will be addressed:

- Design and Construction of Experimental Cell
- Experimental Filling and Cleaning Procedures
- Non-Aqueous Electrochemistry
- Platinum Electrodes
- Potentiostats
  - Construction
  - Computer Control
- Metal Ion Analysis

(A) Design and Construction of the Experimental Transport Cell

The standard experimental cell for bulk liquid membrane transport studies is shown in Figure 11. It consists of a U-shaped tube in which an aqueous immiscible bulk liquid membrane layer resides in the bottom of the "U" with two aqueous phases confined within the arms of the tube. Transport cells are designed to minimize overall membrane volume, allow stirring of the various phases, and to facilitate sampling of the aqueous phases. Adapting this cell to study electrochemical facilitated transport requires additional considerations.

Several texts on electrochemistry point out the importance of proper design of electrochemical experimental cells. Utilizing the basic "U-shaped" membrane cell as a starting point, the following considerations were incorporated into the electrochemical cell design:

1 Place working, reference and counter electrode assemblies at each membrane interface.

2 Allow positioning of working and reference electrodes with respect to the interfacial region.

3 Place reference electrode in close proximity to the working electrode.

4 Place counter electrode near the reference and working electrodes.

"U-Tube"

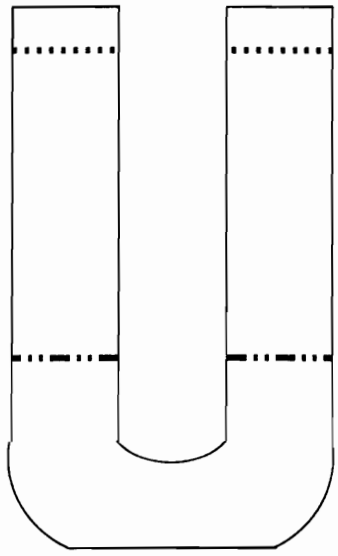

Figure 11. U-Tube Diagram

5 Isolate counter electrode compartment from the main reaction chamber keeping products formed at the counter electrode from interfering with those of the working electrode.

Incorporating these concepts, the cell depicted in Figure 12 was devised and the glass blowers at the Virginia Tech Chemistry Department fabricated the experimental cell. Controlled potential electrolysis on both sides of the experimental cell was required. Formation of separate compartments to isolate the counter electrode and material from the main transport cell was accomplished by attaching side arms to the U-tube on each side. A fine porous frit is located at the juncture of each side arm compartment with that of the main cell. The frit serves two purposes; 1) allowing the electrolyte filling solution of the counter electrode to come in contact with the membrane solution of the U-tube completing the needed electrochemical circuit, and 2) minimizing the amount of material entering or leaving the main area of the transport cell.

The overall inner diameter of the tubing used for cell construction was picked with several of the following constraints in mind:

- Minimize overall membrane solution volume
- Inner diameter of tubing large enough to:

  Accommodate positioning of electrode assemblies in the cell

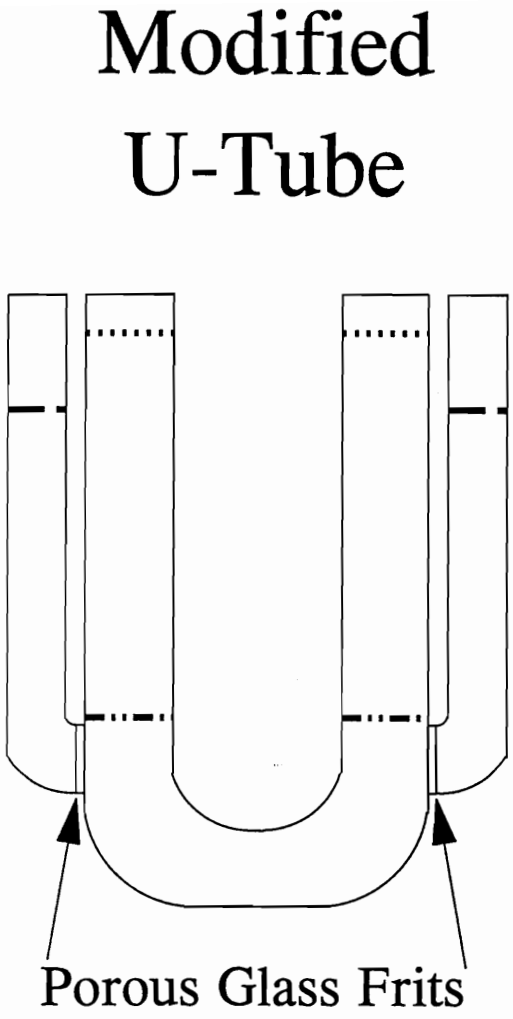

Figure 12. Modified U-Tube Diagram

Facilitate use of a small magnetic stir bar to assist in the transport experiment.

Allow for cleaning of experimental cell.

3) Utilize glass tubing large enough to allow the glass blowers to successfully incorporate glass frits.

Note: Smaller frits exist, but can seal off during the attachment process, or become brittle and shatter during the annealing or cleaning process.

Based on these constraints, the final cell shown in Figure 13 was constructed with a 25ml liquid membrane cell volume, and up to 18 ml of aqueous phase in each arm of the U-tube with the electrode assemblies in place.

(B) Filling of the Experimental Cell

Reproducible placement of the various components into the membrane cell without intermixing or delays is essential to membrane transport studies. While little is actually mentioned in the literature regarding cell filling procedures, it became readily apparent after several attempts to fill the cell that caution, a steady hand,

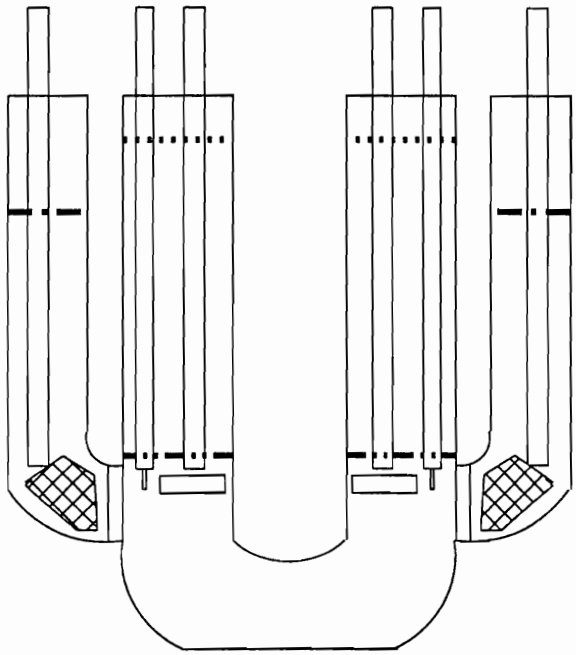

Figure 13. Experimental Cell with Electrodes

and practice are required. The following steps were identified to ensure proper filling of the experimental cell:

- Partially fill each counter electrode compartment with electrolyte solution. Observe wetting of the frits to ensure they are not clogged. Clogged frits contributes to high electrochemical cell resistance. A partial clog will diminish the electrochemical efficiency of the cell, while a completely clogged frit leads to failure of the electrochemical experiment.
- Place desired amount of crown ether solution into the bottom of the U-tube, and then add additional electrolyte solution bringing the total volume of the membrane phase to 25 ml.
- Add a portion of the left side aqueous phase, being careful not to allow the weight of the aqueous layer to force the membrane phase low enough in the curve of the U-tube to allow the aqueous phase to escape to the other side of the bulk liquid membrane.
- Add a slightly larger portion of the right side aqueous phase taking care not to allow the membrane phase to shift, intermixing the two aqueous phases
- Continue steps 3 and 4 until proper volumes are in place.

- Add filling solution to the counter electrode chambers to allow pressure equalization on both sides of the frit. Note: the density of the methylene chloride filling solution is more dense than that of the aqueous solutions. If levels in the side arm are too low, the membrane phase will be forced into the counter electrode chambers. If the levels are too high, additional filling solution from the counter electrode compartment will enter the membrane phase and add to the overall height of the liquids in the main U-tube.

(C) Cleaning of the Transport Cell

Proper cleaning of the frits is important. Prior to each experiment, the cell is thoroughly washed with alternating volumes of methylene chloride and acetone to remove materials clinging to the sides of the cell and the interior of the frits. Special attention is paid to the frits by filling the counter electrode compartments with alternating volumes of methylene chloride and acetone, allowing the liquids pass through the frits. This process continues until the elutant liquids appear to be visually free flowing and clear.

After the organic solvent cleaning, the entire cell is immersed into an acid bath consisting of approximately 1N sulfuric acid, and allowed to soak over night. The

acid bath removes metal ions and residual matter from the experimental cell. Precleaning with organic solvents before the acid bath serves three purposes; 1) it reduces the overall time needed to clean the cell in the acid bath, 2) the acid bath remains clean longer minimizing the possibility of introducing contaminants during the cleaning process, and 3) there is less chance of forming insoluble, unremovable organic oxidation materials within of the frits. After removal from the acid bath, the cell is thoroughly rinsed with distilled deionized water. Several aliquots of water are placed in the side arms of the cell and allowed to pass through the frits. This indicates the frits are not clogged, and removes excess acid that might otherwise remain trapped within the frits. The cell is placed in a drying oven to remove traces of water from the frit.

Note: A waterlogged frit can hinder the methylene chloride solution's passage through the frit.

(D) Choice of Solvents and Electrolytes

The requirement to perform electrochemistry within the bounds of the bulk liquid membrane phase necessitates a water immiscible solvent with favorable electrochemical properties. Of the water immiscible solvents, only methylene chloride and chloroform possess a dielectric constant suitable for use in electrochemical processes. Methylene chloride was picked since its dielectric constant of 9.08 is almost twice that of chloroform (4.806). Literature[34,35] sources suggest the use of tetrabutylammonium perchlorate (TBAP) as supporting electrolyte accompanied by a silver/silver iodide (TBAP) perchlorate reference electrode. More recently, researchers have published results using a standard calomel electrode (SCE) in place of the silver/silver iodide reference electrode. While the SCE is fine for short-term cyclic voltammetry experiments, a reference electrode that does not possess interfering ions in terms of potassium, mercury or silver must be found.

(E) Platinum as a Reference Electrode

The need to eliminate possible interference from cations commonly used in standard reference electrodes such as the calomel (SCE) and the silver/silver chloride reference electrodes necessitates the use of a platinum wire to act as the point of electrochemical reference potential for the membrane transport experiments. Use of platinum as a reference electrode have been reported, but problems exist in that the potential of the electrode can change with its environment. This can cause the working potential applied to a system to drift during the course of the experiment. In anticipation of possible changes, working potentials must be selected so that potential shifts, if they occur, will not traverse into regions where unwanted electrochemical reactions can occur. To verify the validity of using platinum reference electrodes, cyclic voltammetric (CV) experiments were run utilizing platinum reference electrodes on the oxidation and reduction of the ferrocene crown ether. Resulting CV's were compared with those obtained using SCE electrodes. CV's are shown in Figures 14 and 15. There are changes in the potential at which the electrochemical reaction occurs, but the difference in potentials is within the voltage shifts expected from comparison of the reference potentials for the SCE with those reported for the platinum reference electrodes. The overall shape of the CV is not appreciably different between the two reference electrodes indicating that platinum is capable of serving as a reference electrode. To obtain the above mentioned margin of safety, the

electrochemical potentials for the membrane studies were monitored to ensure they do not exceed the optimal range for the desired electrochemical reactions.

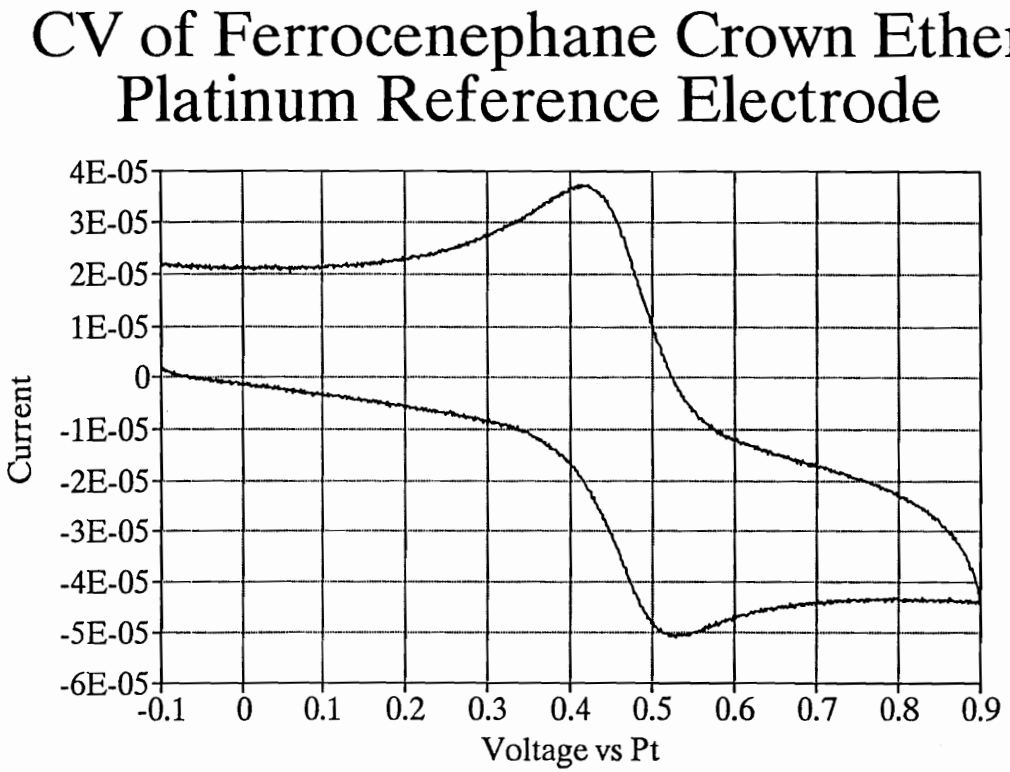

Figure 14. CV of Ferrocenophane Using Platinum Reference Electrode

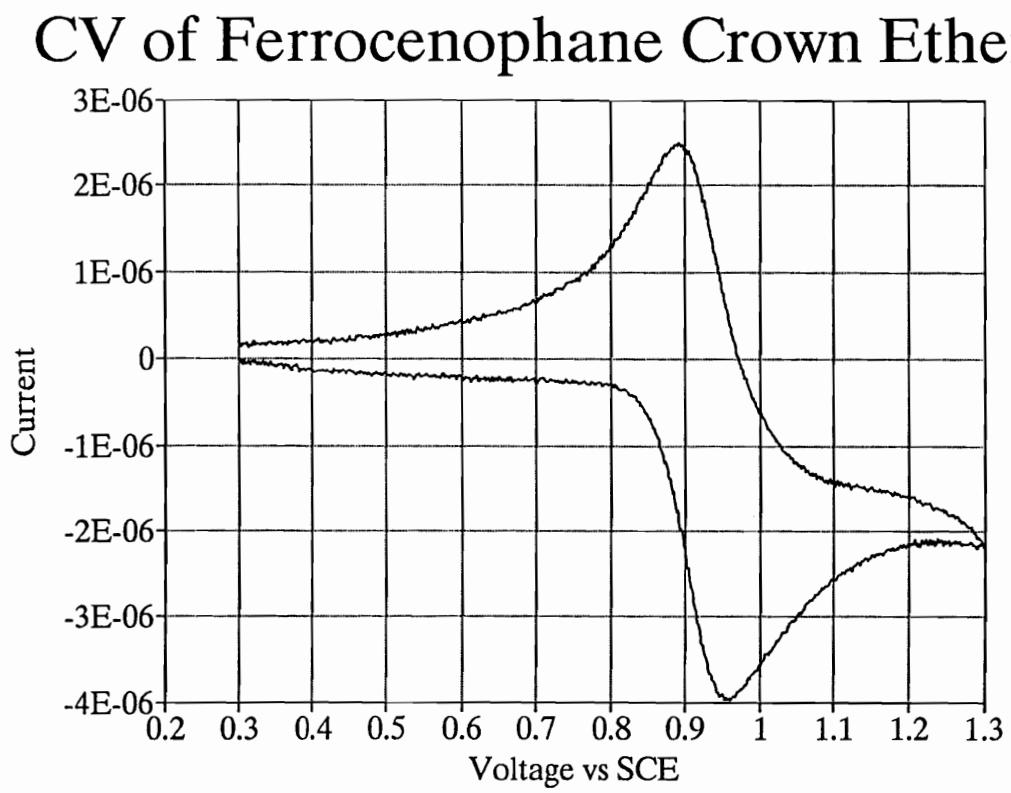

Figure 15. CV of Ferrocenophane Using SCE Reference Electrode

(F) Potentiostats

To study the phenomena of electrochemical facilitated transport, two potentiostats are required to control two separate three-electrodes assemblies positioned at just inside the liquid membrane/aqueous phase interface at either side of the experimental cell (Figure 16). The use of two separate potentiostats compensates for the electrochemical cell resistance associated with use of non-aqueous solvents of low dielectric constants, and allows better potential control of the oxidation and reduction processes on either side of the membrane. The task to assemble potentiostats from component parts was undertaken since suitable commercial models were unavailable for sustained use over the course of the experimentation. Commercial potentiostats were later made available for short term qualitative use. A Princeton Applied Research Model 173 Potentiostat was utilized to check electrochemical activity in the experimental cell prior to commencement of the transport experiment. This potentiostat, in conjunction with an in house computer controlled potentiostat, performed the electrochemical control for the electrochemical facilitated transport studies. A Princeton Applied Research Model M270 potentiostat was used characterize the ferrocenophane crown ether, and its interaction with the ions to be transported.

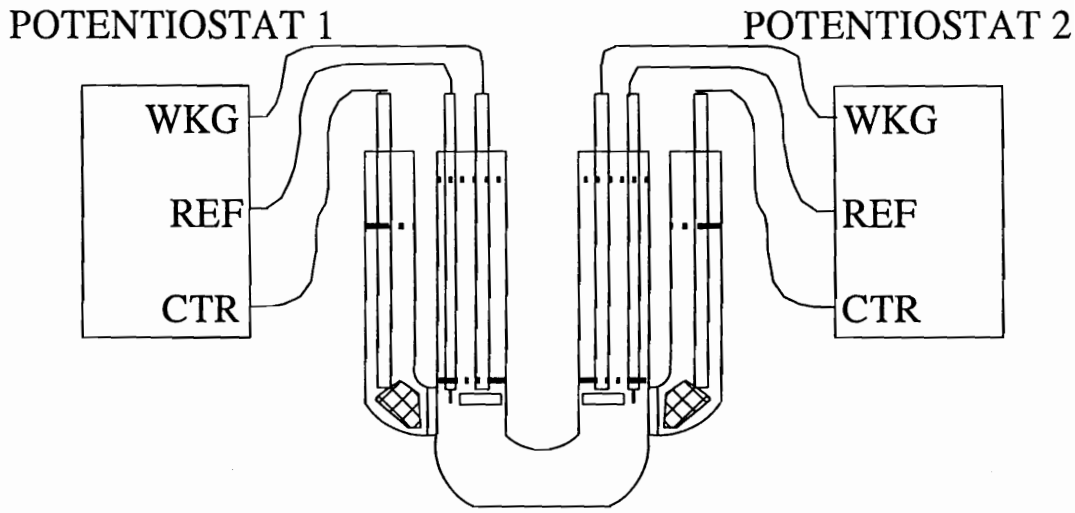

Figure 16. Potentiostat Connections to Experimental Cell

(G) Design of a Computer Controlled Potentiostat

Many reviews on potentiostat design and construction have appeared in the literature. One of the most widely used designs is called an adder potentiostat. The adder potentiostat shown in its simplest form in Figure 17. In this example the adder potentiostat allows for input signals from three sources to allow generation of complex waveforms from simple components. For demonstration purposes, Figure 18 shows a complex waveform commonly applied during the course of an A. C. polarographic experiment. While this signal could be generated by a single complex waveform generator or a computer, it can be created by combining signals from a voltage ramp generator, a sine-wave generator, and a constant voltage source.

To understand how an adder operational amplifier circuit functions, one must consider the technical specifications for the operational amplifier in a summing configuration. This mode requires the summing junction potential at point "S" be at virtual ground. This means that all currents entering point "S" must sum to zero.

$$-i_{ref} = i_1 + i_2 + i_3$$

During operation of the summing amplifier potentiostat, the output voltage of the summing amplifier oscillates about a set point that asserts a continuous changing

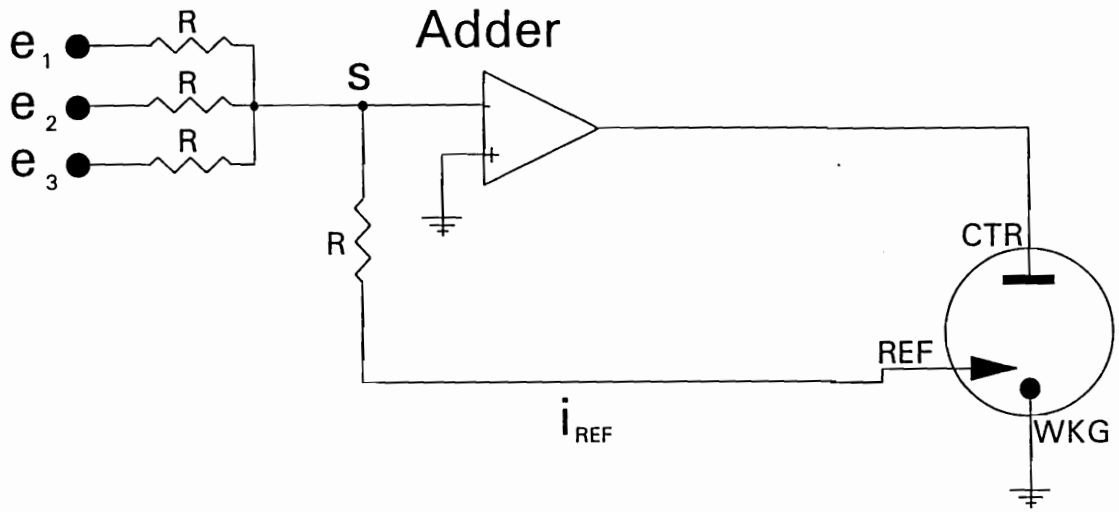

Figure 17. Diagram of Adder Potentiostat

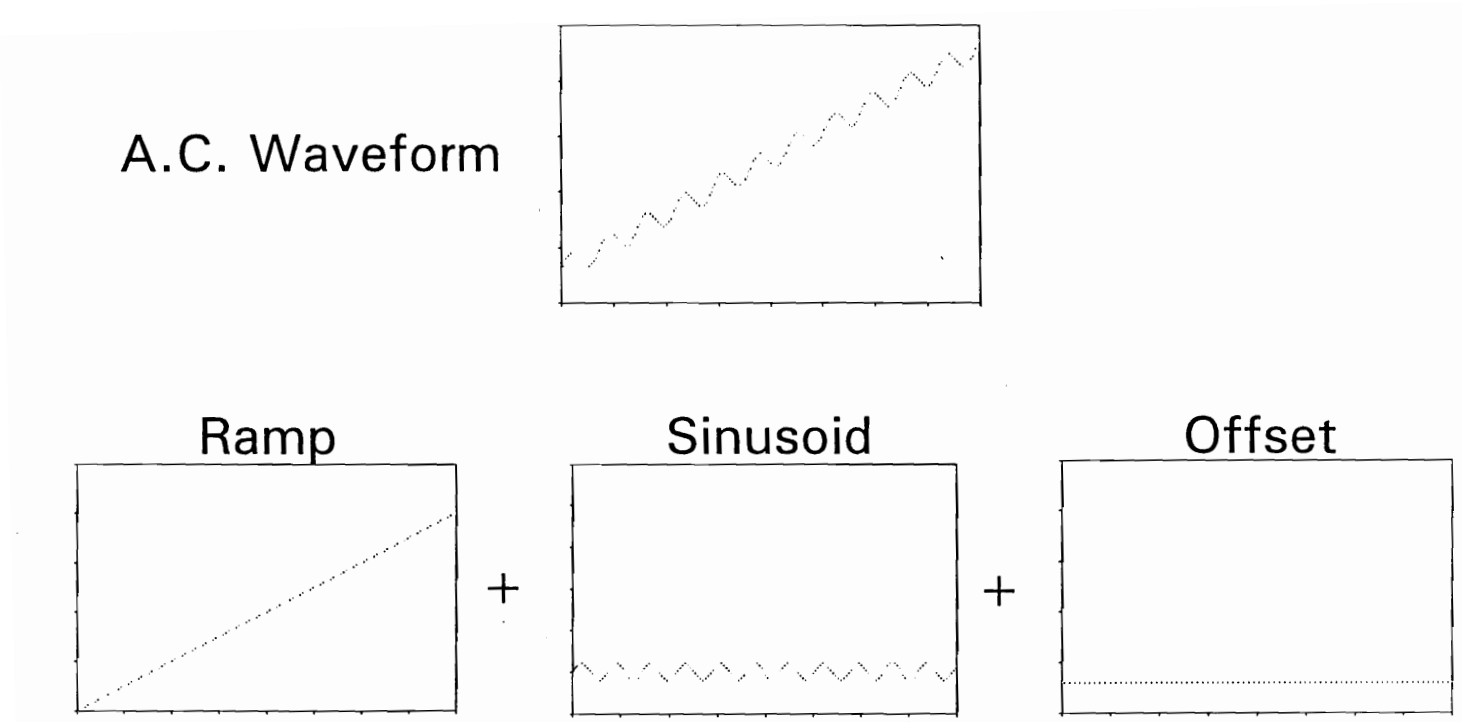

Figure 18. Generation of a Complex Waveform

voltage on the counter electrode such that the potential applied to the working electrode is consistent with and matches the voltages applied at the summing inputs e1 through e3. This oscillation results from the feedback control portion of the summing amplifier circuit. The feedback control is provided by the reference electrode. As the desired voltage for the working electrode falls short of the potential specified by the inputs e1 - e3, the potential sensed at the reference electrode is reflected in a change in the current i_{REF}. This in turn increases the potential applied to the counter electrode boosting the potential of the working electrode. As the potential of the working electrode exceeds its limits, the reverse process occurs.

While it is possible to use a single operational amplifier as a potentiostat, problems exist that make enhancements necessary. 1) The reference electrode must pass significant amounts of current during the feedback control process. This leads to degradation of the electrode as a source of constant reference potential. 2) The power available for cell reactions to occur is limited by the output of the operational amplifier. And 3), there is no means of measuring the current in the system without perturbing the electrochemical processes during the measurement. An improved version of the adder potentiostat is given in Figure 19.

Operational amplifier possess qualities that make them useful in instrument design. Due to the characteristic high input impedance of the amplifier's inputs, negligible current enters or leaves the inputs of the operational amplifier. Only the output of the amplifier has a low impedance. Thus, when an amplifier is attached to

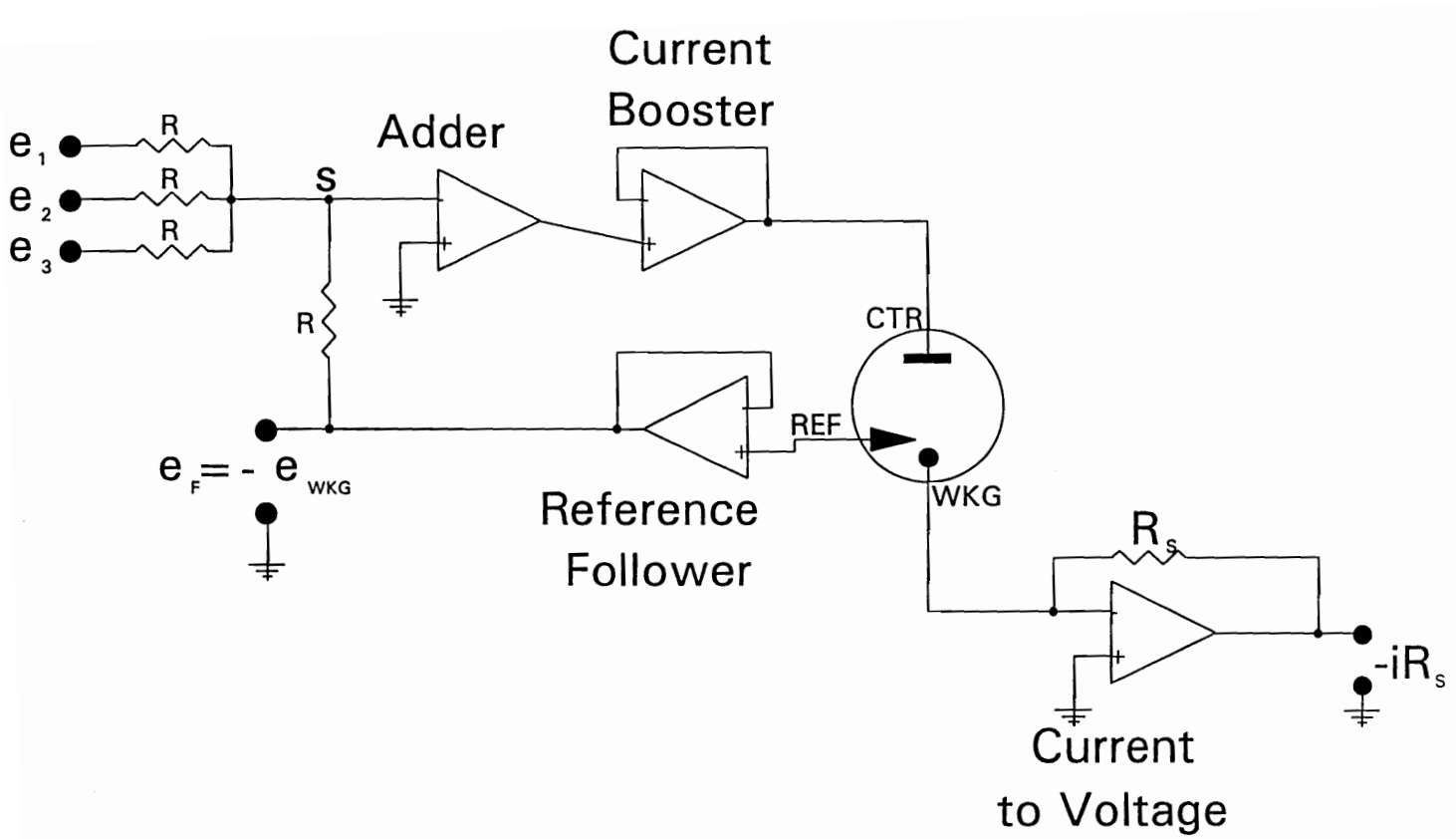

Figure 19. Improved Adder Potentiostat

a system in a voltage follower mode, as depicted for the reference follower, there is minimal current draw imposed on the reference electrode. The follower amplifier provides the voltage and currents that would normally emanate from the reference electrode, but allow the reference electrode to remain relatively unchanged.

An optional "booster" amplifier may be added to the output of the adder amplifier to provide for the additional power needs of a cell reaction that may be in excess of those obtainable from the precision summing amplifier. In the use of non-aqueous solvent, where high cell resistances are encountered, the booster amplifier is recommended. Lastly, an operational amplifier configured in a current-to-voltage mode allows the current through the working cell to be followed without disrupting the current flow of the electrochemical reaction during the measurement process.

The criteria described above were used for the design of a computer controlled potentiostat. Precision operational amplifiers with high gain and slew rates were used for the summing and voltage follower amplifier. High gain, precision power amplifiers were used for the booster amplifier and the current to voltage amplifier. The current to voltage circuit is enhanced with a user selectable switch to allow for optimal voltage gains. A precision variable 10K ten turn pot and other precision resistors with values of 10K, 100K, 1M, and 10M are incorporated to facilitate the measurement of small current processes. The schematic for the final potentiostat is shown in Figure 20.

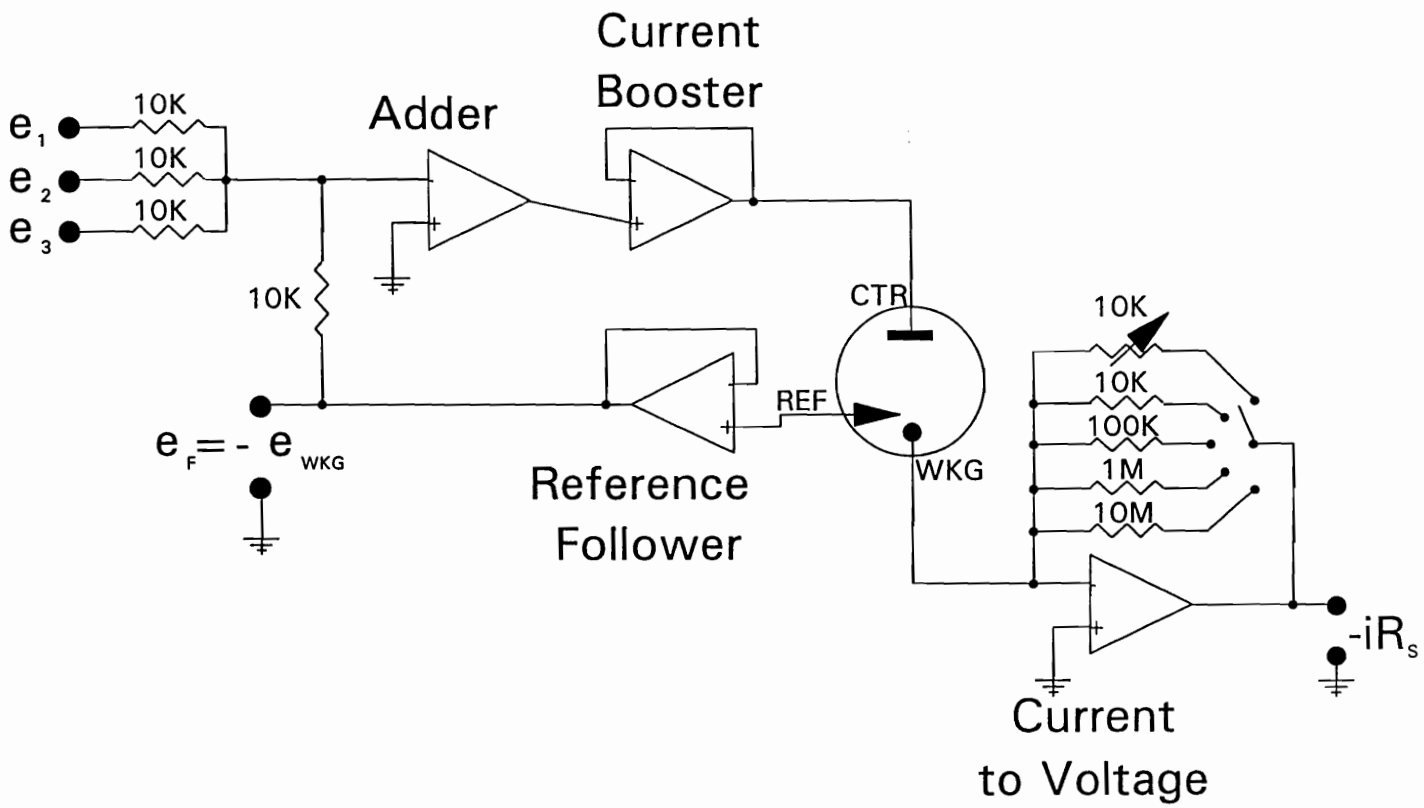

Figure 20. Research Potentiostat

(H) Calibration of the Potentiostat

Each operational amplifier used in construction of the potentiostat was incorporated with offset voltage control circuitry to compensate for potential voltage drift. Before operation, these offsets must be adjusted. A dummy cell resistance was applied to the electrode connections of the potentiostat. A 10K resistor was placed between the CRT and REF electrode connections, with a 1K resistor between the REF and WKG terminals. A constant voltage was applied to the summing junction of the potentiostat. The follower and booster amplifiers were adjusted so that their input and output voltages are the same. A 5 digit precision voltage meter was used for this process. The output of the summing amplifier was adjusted so that the voltage of applied at the inputs match the negative of the voltage measured at the voltage follower terminal of the potentiostat. The current to voltage converter was adjusted for currents calculated for the known resistances used for the dummy cell.

(I) Design of the Computer Interface

Potential control for the above potentistat is provided by a digital to analog converter controlled by a Digital Equipment Corporation's LSI/11 Microcomputer. The schematic diagram of the LSI/11 and connections to the potentiostat is shown in Figure 21. The computer itself is composed of the main processor board with 16K of main system memory, two serial cards to make connections with the controlling CRT terminal and host network disk server, a clock board providing a precision time base for software control of external devices such as a potentiostat, and a combination analog to digital and digital to analog converter board. The computer itself is controlled by the FORTH programming language, and the potentiostat control routines are programmed in FORTH. The FORTH listing for the routines are listed in appendix I.

Three coax cable connections are implemented to connect the potentiostat to the computer system. The first connects the output of the computer's digital-to-analog converter to one of the summing points on the potentiostat to apply needed voltage control waveforms to the potentiostat. The second connects output of the voltage follower amplifier of the potentiostat to the first channel of the analog-to-digital converter. This allows monitoring of the actual potential applied to the working electrode. The last connects the output of the current-to-voltage converter at the

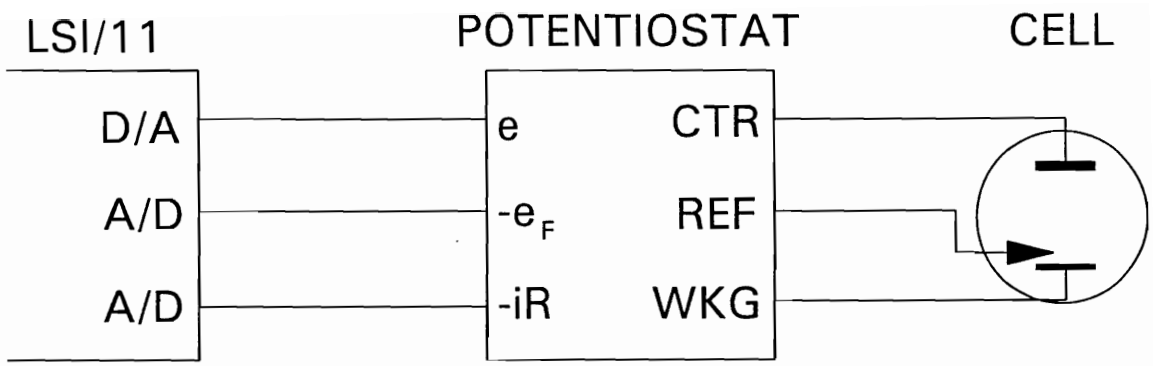

Figure 21. Computer Connections to the Potentiostat

working electrode to the second channel of the A/D converter. With the means available to control the input of voltages into the potentiostat, and to monitor the resulting currents and voltages that result from those inputs, the task of writing the waveform control and data collection software can now be addressed.

(J) Computer Controlled Linear Sweep Voltammetry

A computer generated linear sweep (ramp) waveform may be generated by successively incrementing the values supplied to a computer's digital-to-analog converter. A digital-to-analog or analog-to-digital converter allows a computer to represent real-life voltages as a number. Converter are defined as 8-bit, 12-bit 16-bit, or 24-bit based of the number of binary computer digits that are used to define the voltage range. For example, an 8-bit D/A converter can break up a 10 volt range into 2^8 or 256 steps, with the resolution of the converter being approximately 40 millivolts (10 volts/256). The same converter applied to a voltage range of only 5 volts possesses a resolution better than 20 millivolts. The resolution for a set voltage range may be increased by using a converter with a greater number of bits. Using a 12-bit converter on the same 5 volt range breaks the range into 2^{12} or 4096 steps with a resolution of better than 1.25 millivolts. The operation of an analog-to-digital converter is like that of the digital-analog converter, but allows the representation of a

real-life voltage to be represented by numbers. In general, the higher the number of bits of precision and rate of analog to digital conversion the higher the price.

Consider ADAC Corporation's Model 1030 12-bit data acquisition's D/A converter configured for a 5 volt range of -2.5 Volts to +2.5 volts. The digital representation of the voltages in the range are shown in Figure 37. A voltage ramp from -0.625 volts to +0.625 volts would be generated by sending a time measured stream of numbers to the D/A converter starting at 7000_8 and finishing when the number 1000_8 is reached. The speed at which a waveform may be changed is limited by the speed of the D/A converter and the speed of the computer processor, operating system overhead and the computer language in which the controlling routines are written. The 12-bit A/D and D/A converters are controlled by a 2MHz, 16-bit LSI/11 microcomputer, which in turn is controlled by the FORTH programming language that also serves as its operating system.

The concept of a computer generated potential ramp for use in a potentiostat turns out to be more complicated than simply sending successively higher number to the D/A converter. In addition to shipping values to the D/A converter to provide potential control for the potentiostat, software routines must be developed to tell the corresponding A/D converters to measure the potentiostat's responses in terms of the actual voltages applied to and the currents obtained at the working electrode.

12-Bit Digital to Analog
Conversion Values

Voltage	Digital Representation
-2.500 V	4000_8
-1.875 V	5000_8
-1.250 V	6000_8
-0.625 V	7000_8
0.000 V	0000_8
0.625 V	1000_8
1.250 V	2000_8
1.875 V	3000_8
2.500 V	3777_8

Figure 22

Routines must also store those values for later retrieval. Each of these steps take time and dictate a limit on the computer's ability to generate quick-changing wave forms. Through examination of hardware and software parameters, it was determined that sweep rates up to 250 millivolts per second could be obtained based on the constraints set by the hardware and software overhead.

The main sweep and data collection routine is outlined in flow chart format in Figure 22. Prior to execution of the routine, several user definable variables need to be specified by the user. The SETUP routine query the user for starting potential, upper and lower potential sweep limits, potential sweep rate, equilibration time, and data storage area. Referring to the flow chart, the following events occur:

1) Set potentiostat to initial potential, and maintain that potential for the equilibration period.
2) Increment or decrement the value to be sent to the D/A converter based on the desired sweep direction.
3) Initiate the A/D conversion for the $-e_{REF}$ voltage measurement. Wait and store the voltage when the A/D converter signals the conversion is complete.
4) Initiate the A/D conversion for the voltage measurement from the current to voltage converter. Wait and store the current representation when the A/D converter signals the conversion is complete.

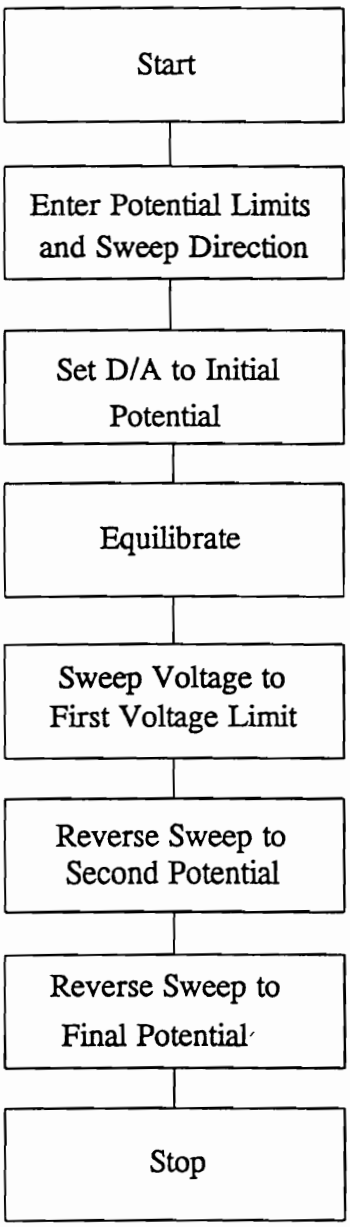

Figure 23. Flowchart for CV Routine

5) Check for completed sweep cycle, and repeat steps 2-5 until finished.

A routine for cyclic voltammetry is written by combining multiple linear sweep experiments. It starts an initial equilibration period followed by a linear sweep from the initial potential to the first limit. A reverse sweep to the second potential limit occurs, and finishes with a sweep back to the original starting potential.

(K) Metal Ion Analysis

A commercial Buck M200A atomic absorption spectrometer was utilized in the emission mode to monitor metal ion transport. Standard spectral lines[26] were used for the emission studies of the alkali metal thallium and silver ions. An air and acetylene gas mixture was used as the excitation source for most ions. A nitrous oxide and acetylene flame mixture was employed for the thallium ion to gain greater sensitivity. Later thallium samples were submitted for analysis to a departmentally constructed and operated inductively coupled plasma (ICP) spectrophotometer when the above mentioned AA unit became unavailable.

The instruments were tested for sensitivity, range and stability prior to sample analysis. Standard solutions were prepared by serial dilution techniques for each of the experimental ions with concentration ranges from 0.01M to 10^{-8}M. Linear

concentration response ranges spanning at least 2 orders of magnitude were obtained for each ion. The generation of the working curves prior to the concentration determination of the membrane samples demonstrated the that true concentration values for the experimental samples could be adequately determined generating a three point working curve that bracketed the concentration range expected for each experimental run. Data for three point calibration curves were taken immediately prior to running of the samples from the membrane transport experiments.

COMPUTER SIMULATION OF DIFFUSION

Diffusion is involved in many processes in Physics, Chemistry, Biology and Engineering. Examples include ion doping/ion migration in semiconductor fabrication,[27,28] reaction pathways, kinetics and physical properties in chemistry,[29,30,31] transport of materials in living cells,[32] and extraction/transport of materials in man-made membranes.[33,34] Computer simulation of these phenomena aids understanding of the underlying mechanisms and the effects of changing parameters on these processes.

Computer simulation applied to the study of electrochemical phenomena met with a resurgence in the early 1980's. Bard and Faulkner introduced the topic in the form of an appendix in their book "Electrochemical Methods: Fundamentals and Applications."[35] In 1984, a text called "Laboratory Techniques in Electroanalytical Chemistry" by Kissinger and Heineman upgraded the topic to a full chapter.[36] Computer simulation methodology entered the literature in areas of physical chemistry in modeling of the liquid/liquid interface in 1988,[34] and later in the area of membrane transport in 1989.[33]

The work published in 1989 by Izatt, et. al.[33] coupled results from experimental membrane transport studies with theoretical transport values generated using empirical diffusion-limited equations derived from previous experimental works.[37,38] The thrust of their work demonstrated the utility of using modeling as a

tool to predict the outcome of membrane transport systems before experiments were performed. This allows the researcher to examine the effects of varying experimental parameters on the overall membrane transport rate. The study reported theoretical and experimental results for a single cation being transported across a membrane barrier by a crown ether carrier molecule, as well as the case of two cations competing for passage across the membrane by a common carrier molecule. In the course of developing their diffusion limited model, the incorporated mathematical equations based on the following considerations:

1) DIFFUSION
2) AQUEOUS/ORGANIC PARTITION COEFFICIENTS
3) COMPLEXATION EQUILIBRIUM
4) COMPETING EQUILIBRIUM

Comparing experimental results with model predictions yielded values that agreed closely with one another in some cases, while in others the model predictions differed by as much as a factor of two from observations, being both higher and lower than other experimental values. Regardless, the model showed its utility for future membrane transport studies.

The application of computer simulation to study the feasibility of the concept of electrochemical facilitated transport of cations across liquid membranes described in this work began in 1984, prior to Izatt's work. FORTRAN was chosen as the computer programming language of choice in that FORTRAN was, and still is, a mainstay of scientific computing. The development of the FORTRAN computer programs will be outlined in the following sections and the resulting programs are listed in Appendix II.

(A) Development of a Computer Simulation Model for Electrochemical Facilitated Transport

In this section, the tools of computer modeling will be examined, modified, and where necessary, created to adapt them to the phenomena of electrochemical facilitated transport. Factors to be considered for the model include the following:

1) FICKIAN DIFFUSION
2) COMPLEXATION EQUILIBRIUM AND COMPETITIVE COMPLEXATION
3) ELECTROCHEMICAL REVERSIBILITY

4) EFFECTS OF ELECTROCHEMICALLY ALTERING A MOLECULE, AND ITS EFFECT ON THE COMPLEXATION COEFFICIENTS

5) EFFECTS OF THE ABOVE ON OVER-ALL TRANSPORT OF AN ION ACROSS A MEMBRANE.

1) Fickian Diffusion and Its Applications to Computer Simulation

Movement of a solute through a membrane may be described by application of Fick's first and second laws. Fick's first law states the movement of material in a system is governed by its flux (J). Flux can be defined as the amount of the substance (in moles) that passes through a unit area (1 m^2 or 1 cm^2) during one second.

Fick's First Law

$$-J(x,t) = D\frac{\delta C(x,t)}{\delta x}$$

Fick's second law states the change in concentration with respect to time is proportional to the change in flux with respect to its position (x).

$$-\frac{\delta C(x,t)}{\delta t}=\frac{\delta J(x,t)}{\delta x} \qquad \text{Fick's Second Law}$$

The above equations can be combined into a single equation generally known as Fick's Combined Law of Diffusion. This equation represents the concentration of a species as a function of both position and time.

$$\frac{\delta}{\delta t}C(x,t)=D\frac{\delta^2}{\delta x^2}C(x,t) \qquad \text{Combined Law}$$

The mathematical method of finite differences states that a continuous process may be approximated by a series of finite elements. Applying the method of finite differences to Fick's Combined Law facilitates conversion of it into a discrete form suitable for use with digital computers. Defining parameters as shown in Figure 24 the discrete form of Fick's Combined Laws is obtained.

$$f(j,k+1)=f(j,k)+D_M[f(j+1,k)-2f(j,k)+f(j-1,k)]$$

where:

$$f(j,k)=\frac{C(j,k)}{C^*}$$

C^* = Normalized Concentration

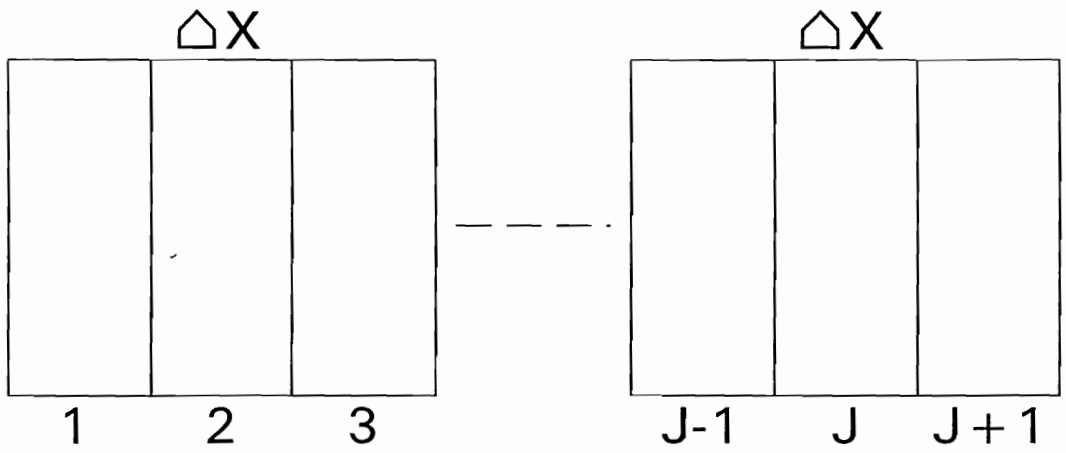

Figure 24. Diagram of Simulation Model Definitions

and:

$$D_M = \frac{D\Delta t}{\Delta x^2}$$

D = Real Diffusion Coefficient

D_M = Model Diffusion Constant

The discrete equation states the concentration of any cell j (volume element) at a point in time t + Δt (k+1 iterations), is calculable from its concentration and that of its immediate neighbors at time t (iteration k). To utilize this equation to calculate changes due to diffusion process, one divides up the medium in question into successive volume elements of thickness Δ x (Figure 24) and specifies the model concentration, f(x,t), defined above be uniform throughout each volume element. Applying the discrete form of Fick's Combined Law of Diffusion to all cell elements of the model, the model's concentration distribution profile is advanced one time step (one iteration) into the future. Continuing this process, one can chart the growth of the diffusion layers with respect to increasing iterations (time).

To demonstrate the validity of this simulation technique, consider the growth of the diffusion layers at an electrode surface for an electrochemical reaction

$$A + ne^- \rightarrow B.$$

Initially the entire solution is comprised of A until all A located in the cell volume closest to the electrode surface is electrochemically converted to B. Upon conversion of A to B an imbalance occurs so that there is an absence of A at the surface of the

electrode and a buildup of B. Diffusion processes occur in which additional A from the bulk solution migrates towards the electrode surface and the newly created B moves into the bulk solution. With increasing time the amount of A in the cell volumes nearest the electrode surface decreases while at the same time the amount of B increases.

Closed mathematical solutions to the problem of diffusion at an electrode surface generate curves representing concentration profiles for each species. The shapes of these profiles can be represented as an increasing logarithmic curve with respect to the electrode surface for A, and a decreasing logarithmic curve for B (Figure 25). Application of the discrete form of Fick's Combined Law of Diffusion generate the same patterns depicted in Figure 25. For simplicity, a model will be constructed in which the area nearest the electrode surface will be subdivided into 10 cell volumes as shown in Figure 25, and the concentration of A in each cell will be set to unity. Starting at iterative time i=0 (Figures 26 and 27) and electrochemically converting all A to B in the cell layer closest to the electrode surface yields the profiles in Figures 26 and 27 labeled i=0'. Applying the discrete diffusion equations to the ten cell volumes yield the profiles labeled i=1. Successive iteration (time steps) applying electrochemical and diffusion

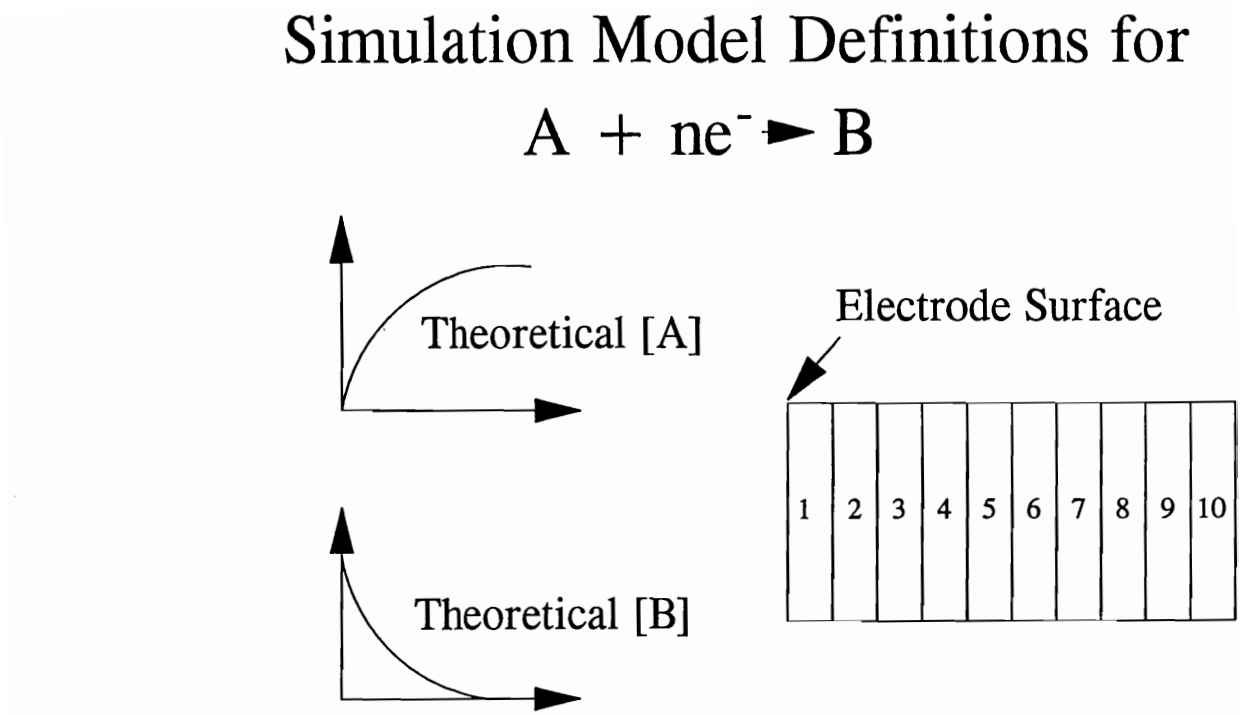

Figure 25. Species Generation at Electrode (Simulation Example)

Table 5: Growth of Diffusion Layers at Electrode Surface

Concentration [A]

Cell/Iteration	0	1	2	3	4	...	10
1	1.0	0.5	0.25	0.25	0.1875	...	0.123
2	1.0	0.5	0.5	0.375	0.375	...	0.246
3	1.0	1.0	0.75	0.75	0.625	...	0.451
4	1.0	1.0	1.0	0.875	0.875	...	0.626
5	1.0	1.0	1.0	1.0	0.9375	...	0.773
6	1.0	1.0	1.0	1.0	1.0	...	0.891
7	1.0	1.0	1.0	1.0	1.0	...	0.936
8	1.0	1.0	1.0	1.0	1.0	...	0.797
9	1.0	1.0	1.0	1.0	1.0	...	0.988
10	1.0	1.0	1.0	1.0	1.0	...	0.997

Concentration [B]

Cell/Iteration	0	1	2	3	4	...	10
1	0.0	0.5	0.75	0.75	0.8125	...	0.887
2	0.0	0.5	0.5	0.625	0.6875	...	0.745
3	0.0	0.0	0.25	0.25	0.375	...	0.549
4	0.0	0.0	0.0	0.125	0.125	...	0.344
5	0.0	0.0	0.0	0.0	0.0625	...	0.227
6	0.0	0.0	0.0	0.0	0.0	...	0.109
7	0.0	0.0	0.0	0.0	0.0	...	0.065
8	0.0	0.0	0.0	0.0	0.0	...	0.021
9	0.0	0.0	0.0	0.0	0.0	...	0.012
10	0.0	0.0	0.0	0.0	0.0	...	0.0029

Growth of Depletion Layer at Electrode Surface

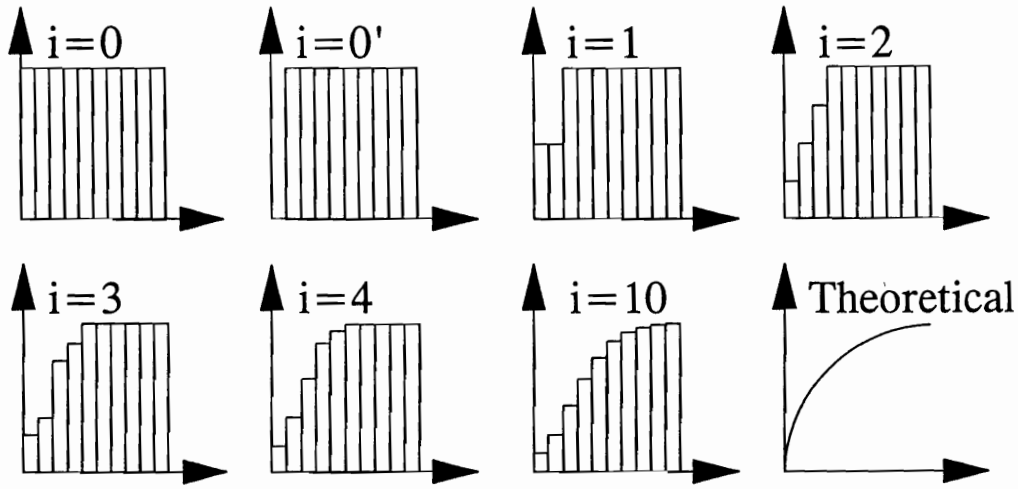

Figure 26. Growth of Depletion Layer

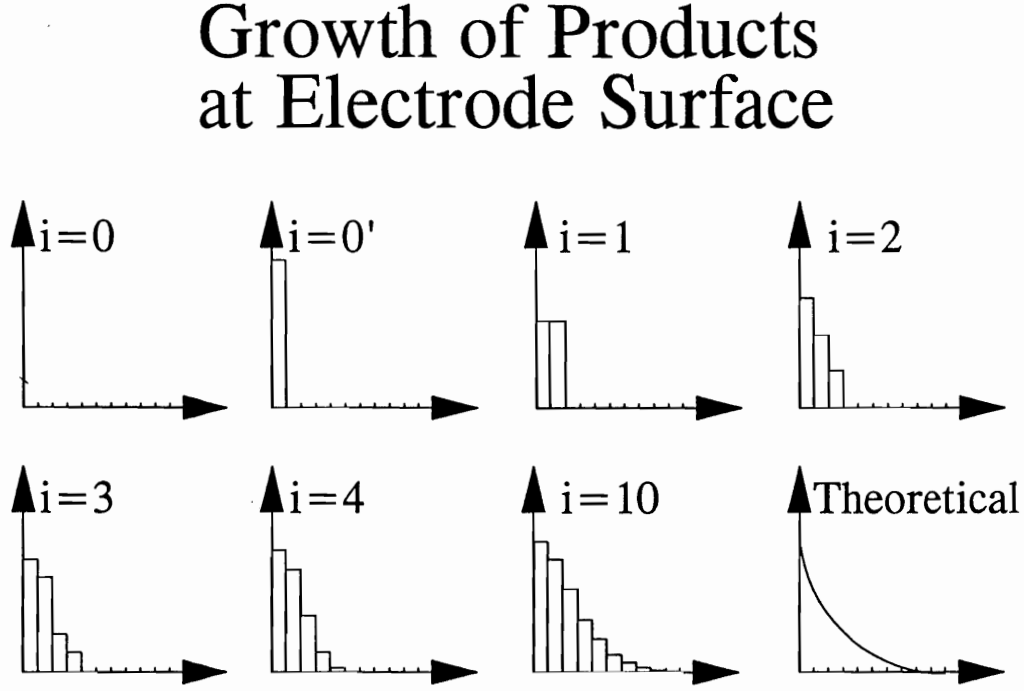

Figure 27. Growth of Products at Electrode Surface

considerations to all cells of the model yield the data values in Table 5 and the remaining profiles shown in Figures 26 and 27. As the iterations continue, the trend from the marked differences between the adjoining concentration volumes in the initial stages of the simulation model to the more continuous concentration distribution profiles that start to approximate those concentration profiles predicted by the continuous closed mathematical solutions is noted.

The success of this example in approximating the profiles generated by the continuous closed solutions verifies the validity of the technique. Further considerations and enhancements to the simulation can make the technique applicable to those systems that may not necessarily possess a closed numeric solution, or systems where mathematical equations have yet to be formulated to examine the desired phenomena. Computer programs can be written to calculate and track each set of concentration profiles for each species involved as the number of iterations increase. The computer program written to generate the values in Table 5 and Figures 26 and 27 for the above electrochemical experiment is listed in appendix II. The techniques of discrete digital diffusion illustrated above, along with other criteria to be discussed later, will be combined to create a computer program to generate concentration profiles expected from electrochemical facilitated transport and allow the user to change the simulation parameters to evaluate the effects of changing parameters on the overall concentration profiles.

2) Complexation Concerns

Complexation of a solute by a carrier molecule to make it soluble and transportable through a membrane phase has both theoretical and practical aspects. In terms of membrane transport processes, for a carrier molecule to possess good transport properties the compound must form a reversible complex with the solute being transported. Experiments have shown that the more stable the complex, the better the overall transport efficiency of the system. Understanding electrochemical facilitated transport relies heavily on the concepts of what happens when a carrier molecule is converted into another form with a different binding affinity. The idea that a carrier molecule can be changed into another entity of varying complexing ability makes it necessary to consider the effect of competing ligands (carriers) for a common solute, and the effect it has on the over all transport rate of solute across a membrane phase. To incorporate complexation criteria into a discrete digital simulation model, an exact mathematical solution containing the interrelationships between the solute and the various states of the carrier molecule must be determined.

The case of competing ligands for a common metal ion is addressed by Ramette in his book entitled "Chemical Equilibrium and Analysis.[39] In the case of two ligands competing for complexation with a common solute, the ligand with a combination of the higher complexation coefficient and number of complexing forms binds with a higher percentage of the available solute. Ramette represented the

magnitude of the "winning" complexation agent in terms of a ratio comparing the relative amounts complexed by one ligand versus that of the other. The use of ratios provides a useful method for evaluating amounts of material (ligands and solute) in its free and complexed form. For a compound with a single complexing form per oxidation state, theory predicts that the larger the difference in the solute complexation ability between the two ligands, the greater the differences in the amounts of solute complexed by each competing ligand. In the case of electrochemical facilitated transport where the two carriers (C and C^*) that are actually the same molecule differing only in its electrochemical state, two equations for complexation can be written.

$$C+S \overset{k}{\rightleftarrows} CS$$

$$k = \frac{[CS]}{[C] \cdot [S]}$$

$$C^*+S \overset{k^*}{\rightleftarrows} C^*S$$

$$k^* = \frac{[C^*S]}{[C^*] \cdot [S]}$$

Where: C ⇒ Carrier Concentration

C^* ⇒ Oxidized Carrier Concentration

S ⇒ Solute Concentration

k ⇒ Equilibrium Constant for Neutral Carrier

k^* ⇒ Equilibrium Constant for Oxidized Carrier

The above equations, combined with the following mass balance considerations for each of the equation components, make it possible to derive additional equations to calculate the concentration of each species in its free and complexed form. The mass balances for each species are:

$$[C]_T = [C] + [CS]$$

$$[C^*]_T = [C^*] + [C^*S]$$

$$[S]_T = [S] + [CS] + [C^*S]$$

Note: Concentrations shown with a subscripted T refer to total concentration of species in the system regardless of complexation state.

Manipulating the equations and making substitutions, the following equations are obtained.

$$Ratio = \frac{k[C]}{k^*[C^*]}$$

$$[S] = \frac{[CS]_T}{1+[C]\cdot(Ratio+1)}$$

$$[C^*S] = \frac{[CS]_T-[S]}{Ratio+1}$$

$$[CS] = [CS]_T-[S]-[C^*S]$$

$$[C] = [C]_T - CS$$

$$[C^*] = [C^*]_T - [C^*S]$$

Using these equations one can define the new equilibrium concentration values of all species in the simulation based on the effects of electrochemical redox processes and diffusion processes. These equations were incorporated into a computer simulation program written in FORTRAN, with the competing equilibrium considerations separated from the main routine in the subroutine named EQUIL.

3) Electrochemical Considerations

In electrochemical systems the amount of material oxidized or reduced at an electrode, at a given electrochemical potential, may be calculated using the Nernst Equation. The Nernst equation for the reaction $O + ne^- \rightleftarrows R$ may be expressed as:

$$E = E^{\circ} + \frac{RT}{nF} \ln \frac{O}{R}$$

where

E	=	Applied Electrochemical Potential
E°	=	Reference Potential
R	=	Gas Constant
T	=	Kelvin Temperature (°K)
n	=	Number of electrons transferred
f	=	Faraday's Constant
ln	=	Natural Logarithm
[O]	=	Concentration of Oxidized Species
[R]	=	Concentration of Reduced Species

For the case of controlled potential voltammetry where the potential is held fixed, several terms of the Nernst Equation may be combined into a single constant. At a given potential, the ratio of the oxidized and reduced species is a constant.

$$\frac{[O]}{[R]} = Constant$$

Knowing the total amount of materials diffusing into and out of the cell element where electrochemical reaction takes place, algebraic expressions can be derived to determine what portion of the material will be oxidized or reduced. This result will be employed in the study of electrochemical facilitated transport. For the purposes of the simulation model, values of 90%, 50% and 0% conversion with respect to oxidation and reduction processes will be used to address the effect of electrochemical conversion on the overall transport rate across a membrane as it pertains to the concept of electrochemical facilitated transport. The results of the simulation runs will be presented later.

4) Model Assumptions

Before a computer simulation model can be constructed, several items must be addressed. Typical questions involve (1) what physical phenomena should be considered, and (2) what constraints need to be applied. During the development of a

computer simulation model for electrochemical facilitated transport the following assumption were made.

(1) Total immiscibility of aqueous and bulk liquid membrane phases.

(2) Local physical and chemical properties do not change between the aqueous and membrane phases.

(3) No internal interfacial resistance to movement of species across the membrane interface. Physical partition coefficients between the aqueous and membrane are constant.

(4) Electrochemical reversibility is maintained and degradation products do not occur.

(5) Complexation constants of the oxidized and reduced form of the carrier are different, with the oxidized form having the lower complexation constant. The simulation model utilizes a ratio of complexation constants assigning a normalized value of unity (1) to the reduced form, and values of 0.1, 0.01 and 0.001 for the oxidized form of the carrier molecule.

5) Model Construction

In the Historical section (pages 21-23, Figure 5), the experimental U-tube construct was introduced as the experimental cell of choice for liquid membrane transport studies. In testing the feasibility of the concept of electrochemical facilitated transport, the method of finite differences was applied to this cell. Imagine taking the U-tube assembly in Figure 5, straightening it into a linear form and then subdividing it into a number of discrete volume units as was done with the electrochemical example discussed previously. The result is shown in Figure 28. Unlike the previously described electrochemical example, the current model possesses two aqueous phases and one non-aqueous phase. The two aqueous phases are subdivided into 200 subunits each, while the membrane is divided into 100 parts. The interface between the aqueous and organic phase is represented by cell 1 of the aqueous phase and either cell 1 or cell 100 of the membrane phase. In Figure 28, interface I is represented as a combination of cell 1 of aqueous phase I and cell 1 of the membrane. Interface II is defined by cell 1 of aqueous phase II and cell 100 of the membrane cell volumes. The working electrodes that convert the carrier molecule between its oxidized and reduced state are located at the interfaces as defined above. Electrochemical conversions occurs in the boundary cell locations 1 and 100 as defined above.

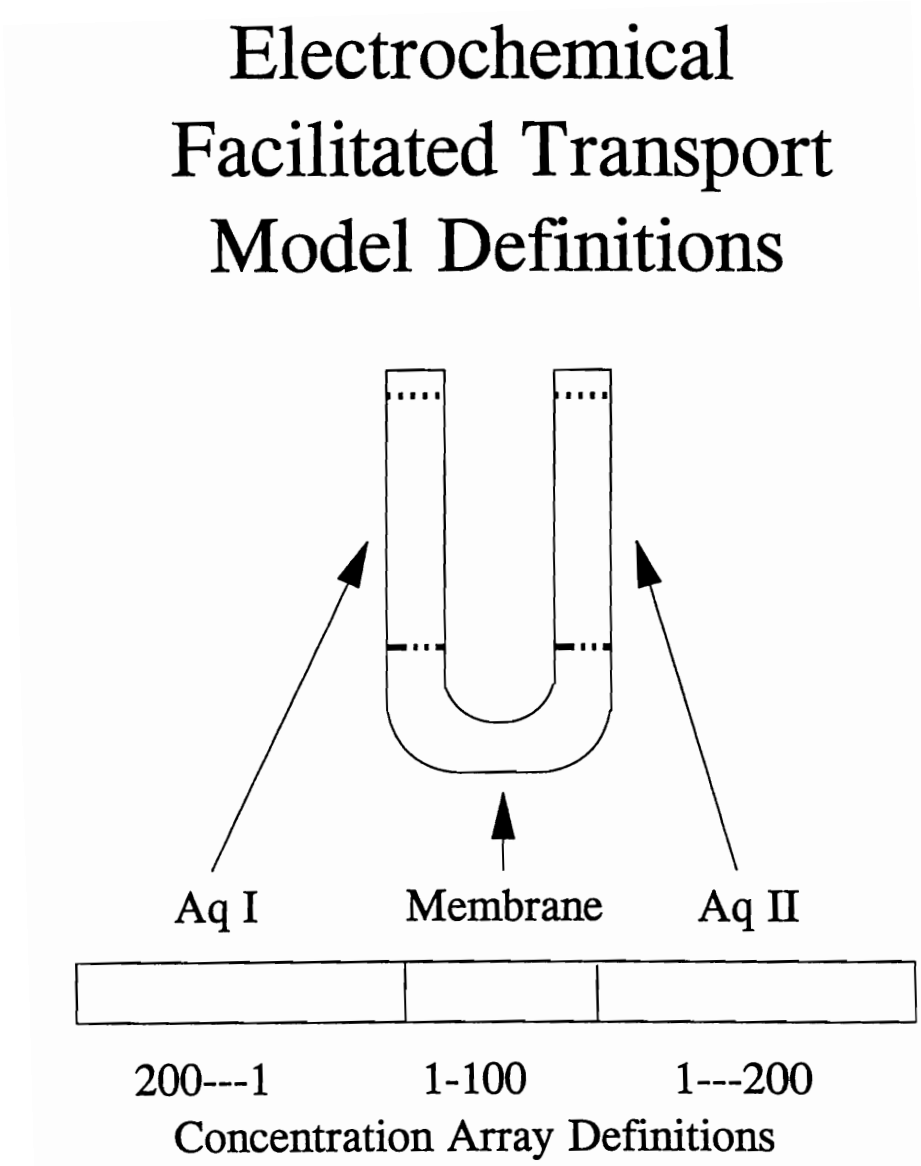

Figure 28. U-Tube Diagram and Model Definitions for Simulation

To calculate the amount of solute that may enter or leave the membrane at any given time, equations defining the complexation ratios between the oxidized and reduced membrane carrier molecule and the aqueous solute are used. To implement discrete simulation of electrochemical facilitated transport, the order of calculations for each iterative step of the model is as follows:

(1) Perform controlled potential electrochemical conversion of the carrier molecules at their respective interfaces. Conversion includes both complexed and uncomplexed forms of the ligand.

(2) Perform equilibrium calculations for the case of competing ligands to determine how much material will enter or leave the membrane phase.

(3) Apply discrete diffusion to membrane and aqueous phase species.

(4) Save concentration profiles at user defined intervals.

(5) Repeat steps 1-4 till finished.

The initial starting condition for the following parameters are user definable at the start of the simulation:

(1) Concentration

  (a) Solute in aqueous phase I (Source)

  (b) Solute in aqueous phase II (Receiving)

(c) Free Carrier Molecule (Membrane)

(d) Free Charged Carrier Molecule (Membrane)

(e) Complex of Carrier and Solute (Membrane)

(f) Complex of Charged Carrier and Solute (Membrane)

(2) Amount of Electrochemical Conversion at interfaces.

(a) Amount oxidized at receiving phase interface

(b) Amount reduced at source phase interface

6) Selection of Simulation Parameters

Several digital simulations were run with varying conditions to look for effects of changes in key parameters on the overall rate of simulated transport. Key parameters identified for study are 1) change of equilibrium complexation between the cation and the carrier based on its electrochemical oxidation state, and 2) percentage of electrochemical conversion (0-100%) at each interface. A simulation run was performed for the case of no electrochemical action to serve as a baseline case for comparison with other facilitated rates.

The simulation conditions are listed in Table 6. Most simulations will assume 90 percent electrochemical conversion at interface electrodes (discussion follows), and have initial concentrations for the source and receiving phase and the carrier molecule

Table 6: Simulation Parameters

Simulation #	1	2	3	4	5	6	7
Percent Oxidation at Receiving Phase	0.9	0.9	0.9	0.9	0.9	0.5	n/a
Percent Reduction at Source Phase	0.9	0.9	0.9	0.9	0.9	0.5	n/a
Equilibrium Constant for Neutral Carrier	1	1	1	1	1	1	1
Equilibrium Constant for Charged Carrier	0.01	0.001	0.001	0.1	0.001	0.001	n/a
Source Phase Concentration	0.002	0.002	0.002	0.002	0.002	0.002	0.002
Receiving Phase Concentration	0.0	0.0	0.002	0.0	0.0	0.0	0.0
Carrier Concentration	0.0005	0.0005	0.0005	0.0005	0.0005	0.0005	0.0005

of 0.002 M, 0.0M and 0.0005M respectively. These concentration values are representative of the concentrations of cations and carrier compounds used in Downhill membrane transport experiments. Exceptions are: 1) simulation 3 where both source and receiving phase concentrations are 0.002M (Uphill Transport); and 2) simulation 6, where 50% electrochemical conversion is assumed.

The value of 90% for electrochemical conversion was chosen instead of 100% to approximate real experimental conditions where the selection of oxidation and reduction potentials are limited by the solvent system being employed, or that of unwanted electrochemical side reactions. Using the Nernst Equation, one can calculate how much the applied potential must be varied from the $E_{1/2}$ for the electrochemical reaction to achieve the desired percentage of conversion products. A 90% conversion may be achieved setting the voltage one volt in excess of the $E_{1/2}$, while 99.99% (100%) conversion requires a much larger variation (4 volts). Calculated values are listed below:

E (versus E½)	% Conversion (Red ⇒ Ox)
0.000 V	50.00
0.954 V	90.00
1.996 V	99.00
2.999 V	99.90
3.999 V	99.99

Examination of these values, combined with electrochemical consideration of competing reactions and useful electrochemical voltage range from the solvent/electrolyte systems confirms the selection of 90% to approximate real experimental conditions.

Simulations numbers 1,2,4 and 7 demonstrates the effect of assumed changes in the complexation coefficients based on effects influenced by the oxidation state of the carrier molecule. In these runs the complexation coefficients of the oxidized carrier molecule was chosen to be ten, one hundred, and one thousand times poorer than that of the neutral carrier. These values were chosen as reasonable based on previous experimental studies referred to in the historical section detailing the changes in transport rates of crown ethers with varying electronegative attached substituents. The overall transport rate of a crown ether with highly electronegative groups attached has been shown to transport cations at least one thousand times less efficiently than its neutral counterpart.

Simulations 2, 5 and 6 demonstrate the effect of the amount of electrochemical conversion on the overall transport rate. As will be seen, the more efficient the conversion process, the higher the transfer rate of substances across a membrane.

7) Collection and Handling of Simulation Data

Because of the large amount of numbers being generated by the simulation model, it is very important to realize that while it is possible to save all calculation for each iteration, it is more practical to save "snapshots" of the concentration profiles at predetermined steps in the iterative process. These "snapshots" contain all parameters for the simulation and allow the user to reconstruct at a later date those intermediate iterations not previously saved. This is accomplished by loading the iterative "snapshot" prior to the desired iterative time frame and instructing the user program to save the desired steps. This procedure also enables the user to recover from computer related failures, and to continue the simulation runs from the last successfully collected data set. [Historical Note: When the initial simulation calculation were performed, on an original IBM PC with 640K of memory and a math coprocessor chip, a simulation run of 2 million iterations would took up to 2 days of continuous processing. With newer faster machines, this time can be reduced to a few hours.]

8) Presentation of Data in Graphical Form

The large numeric data sets generated during the simulation runs dictate a need to analyze the data through graphical formats. Appropriately used, graphs allow to user to visualize the information content of one or more data sets to identify trends associated with the experimental parameters of interest. Many graphical representations were evaluated for their ability to convey information imbedded in the data sets. The following graphical representation were chosen:

(1) Plotting concentration vs position within the membrane or aqueous phase for each species. Several increasing iterative time steps for a single simulation are placed on a common graph to examine the formation of steady state equilibrium profiles for each phase.

(2) Phase averaged concentration values vs iterations (time) were plotted for each species. Values for each phase were averaged to obtain one number representing the concentration of the species within each phase. This allows visualization of overall change in the bulk concentration with respect to time for each species.

(3) Combined results from different simulations together on one graph. This allows examination of the effect of change in parameters on the over-all transport rate. Parameter changes considered were (1)

equilibrium, (2) oxidation/reduction conversion rates and (3) changes in initial starting concentrations.

9) Graphical Analysis of Simulation Data Sets

Before continuing with the analysis of the concentration profiles, please refer back to Figure 28 which defines the division of the experimental membrane transport cell into a discrete numbered cell locations. The membrane location defined by zero is the source phase/membrane interface, while location 100 defines the receiving phase/membrane interface. Raw data generated from the simulations consist of numeric data sets representing the concentrations of each species with respect to its location in membrane, source and receiving phase as defined by the discrete approximation model of the membrane transport cell shown in Figure 28. A complete set concentration profiles are saved for each iterative time step of interest. Let's consider the data sets from the first simulation dealing with Downhill transport, 90% electrochemical conversion at each membrane interface. Initial concentrations for the membrane carrier molecule, the source phase and the receiving phase are 0.0005 M, 0.002 M and 0.000 M respectively. Plotting data for the case of the neutral carrier molecule (Figure 29), one can see that with increasing iterations the overall amount of

free carrier in the membrane phase decreases until it reaches a "steady state" concentration profile at approximately 10000 iterations.

An explanation for the formation of the steady state concentration profiles will now be considered. At the source phase side of the membrane, the free carrier binds with metal ions from the source phase to form a neutral carrier complex shown in Figure 30. At the receiving phase membrane interface, a decrease is noted as the neutral carrier is converted into its charged carrier form (Figure 46). Comparing Figures 30 and 31 with that of Figure 29, the losses in the free carrier concentration may be matched with corresponding gains in the charged and complexed forms of the carrier. These initial losses in free carrier concentration continue until around 10000 iterations where increasing iterations deviate little from previous or future iterations and a "steady-state" condition has been achieved. The attainment of a "steady-state" in the concentration profiles of the neutral carrier molecule are matched by "steady-states" in the neutral complex (Figure 31), charged carrier (Figure 32) and the charged carrier complex in Figure 32.

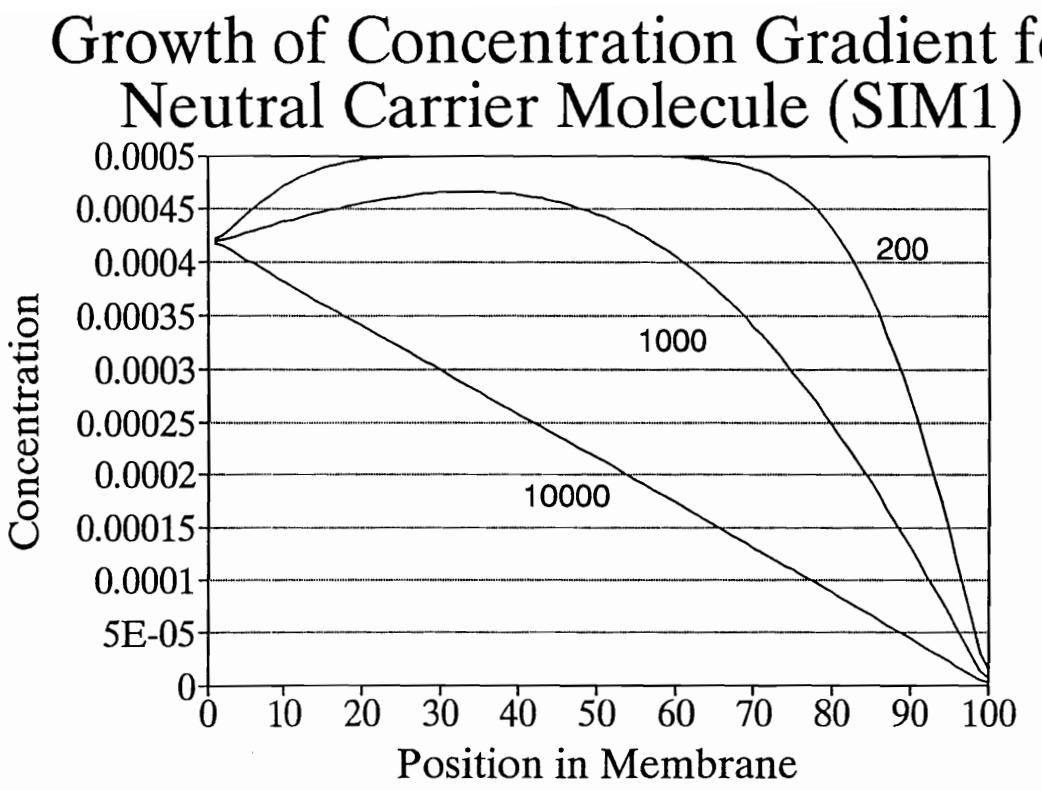

Figure 29. Diffusion Growth Profile for Neutral Carrier

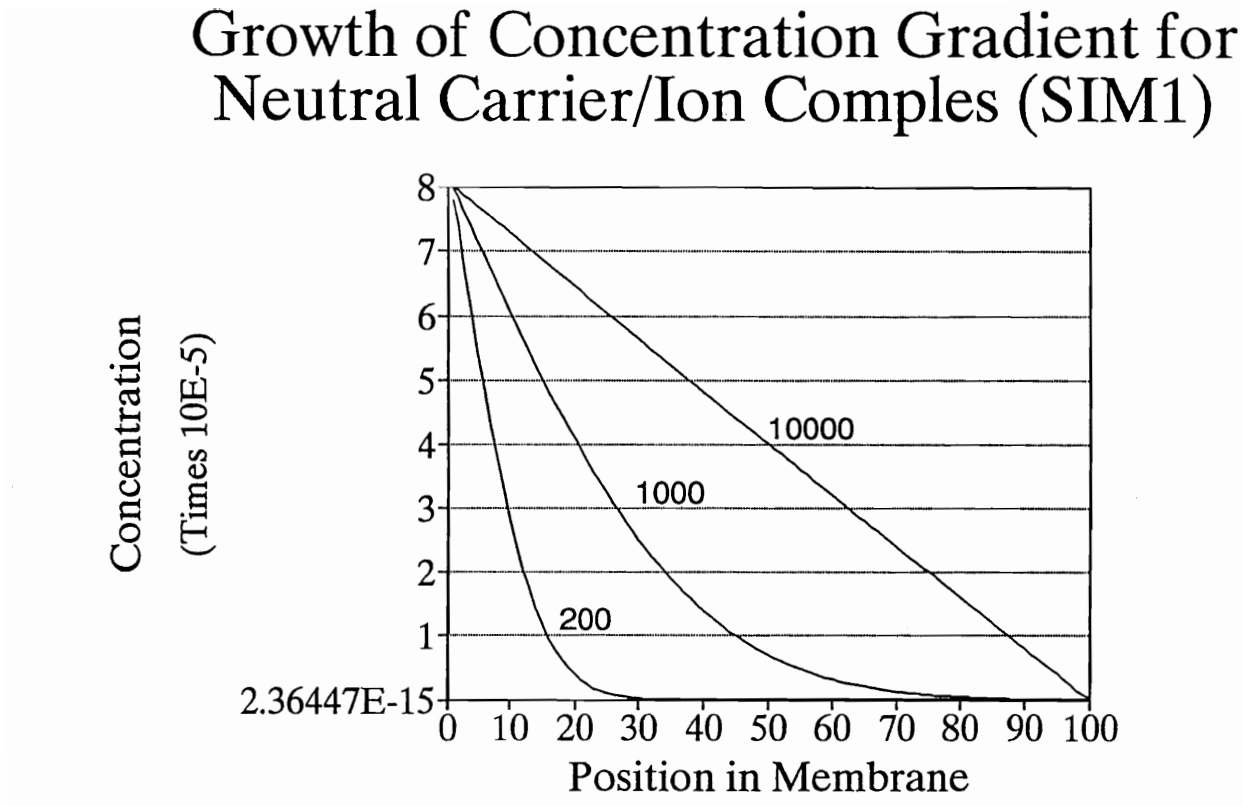

Figure 30. Diffusion Growth Profile for Carrier/Ion Complex

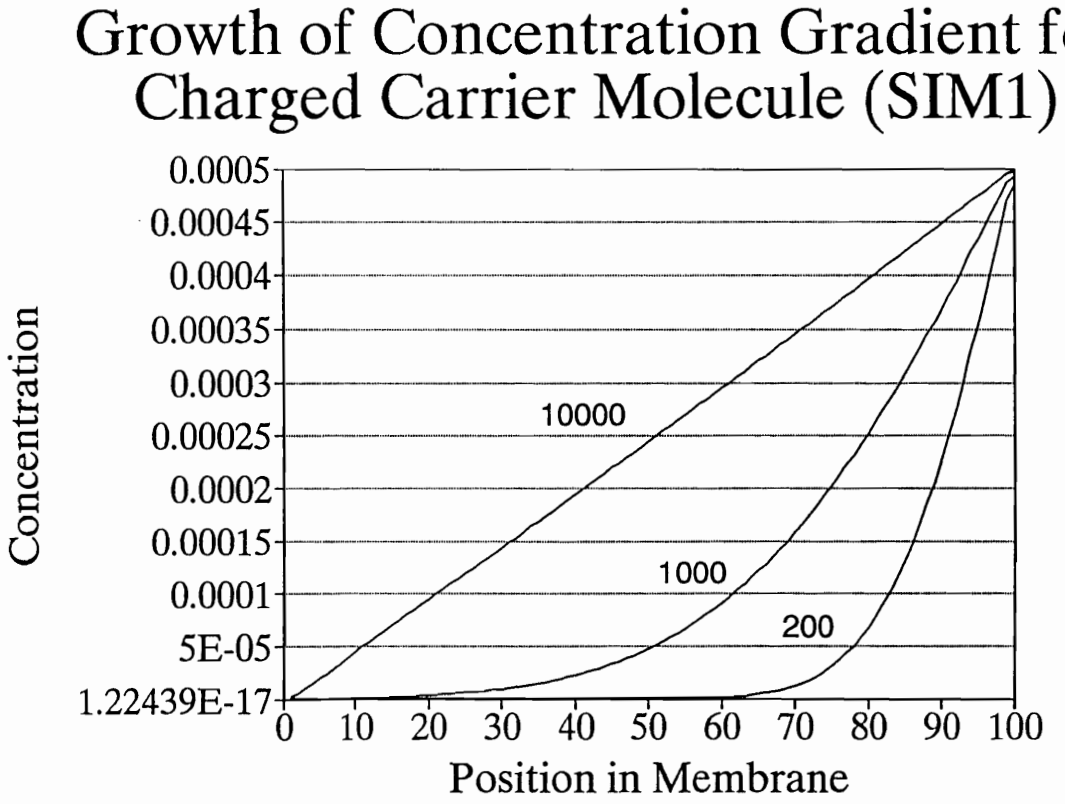

Figure 31. Diffusion Growth Profile for Charged Carrier

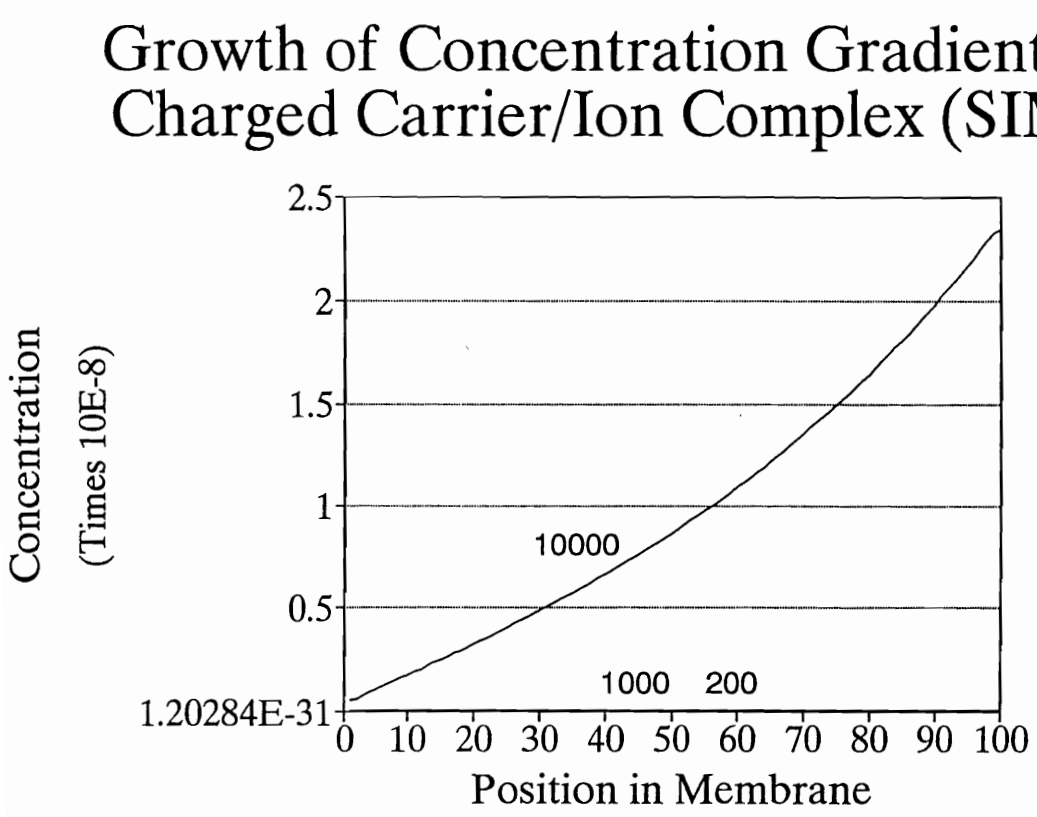

Figure 32. Diffusion Growth Profile for Charged Carrier/Ion Complex

Additional graphs showing the solute concentration profiles in the source (Figure 33) and receiving phases (Figure 34) further support the above explanation of the neutral carrier molecule concentration profiles. In Figure 33 one notes the solute concentration in the cell locations of the source phase nearest the membrane interface are increasingly depleted as the number of iterations increase. Figure 34 shows the introduction of solute into the receiving phase that was previously devoid of the material. It is difficult to see the concentration profiles shown for early simulation iterations 200 through 1000, since their overall concentration is small with respect to values achieved by the time frame of 10000 iterations. One also notes that decreases in the source phase do not appear to be matched by corresponding increases in the receiving phase. This apparent discrepancy is readily explained when the contribution of the membrane species are considered (Figures 29 and 32), and it is realized that the membrane phase does initially contain a significant amount of solute. These trends, as described for the first simulation, are present in all simulations defined in Table 6.

The trend to form "steady-state" unchanging concentration profiles for membrane species suggests a reduction of the data sets is feasible and that concentration profiles for each iteration may be effectively represented by a cell averaged value for both source and membrane species. A cell averaged value for one iteration is obtained for the source phase by averaging the concentration values in each of the 200 cell division. This is done for the species in the membrane and

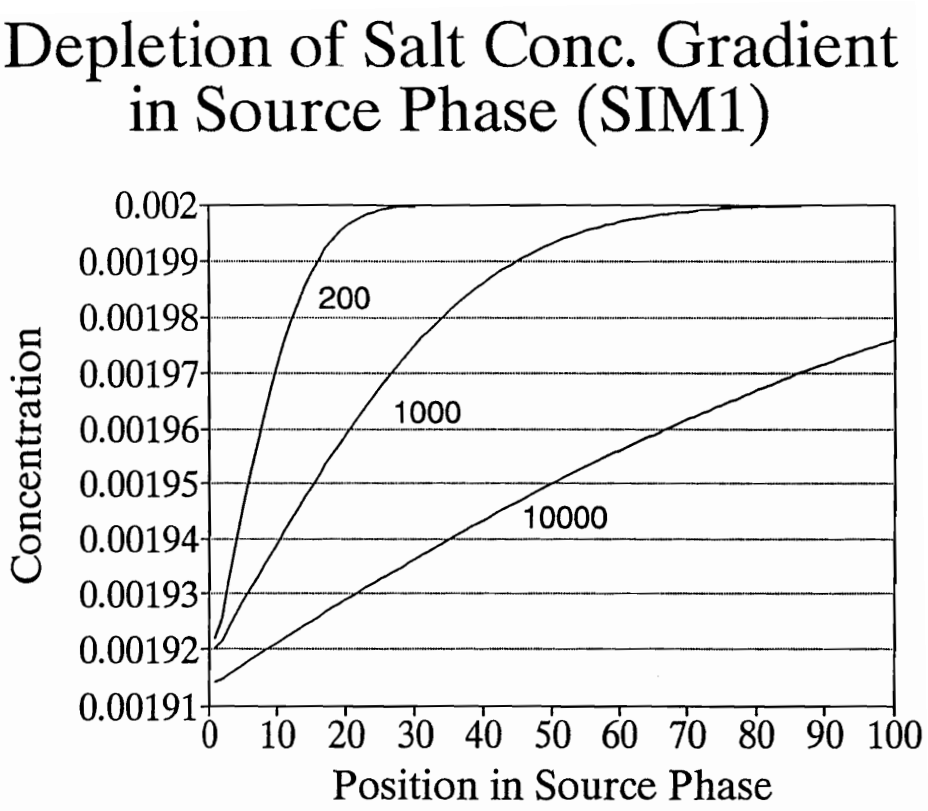

Figure 33. Depletion of Source Phase

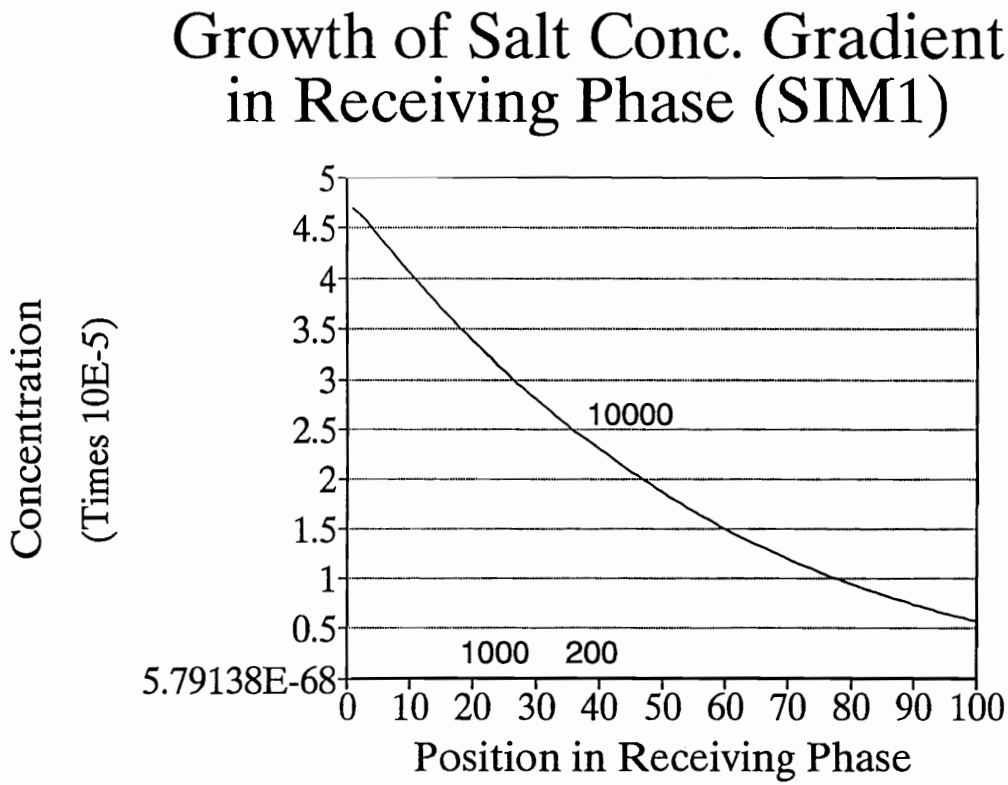

Figure 34. Growth of Receiving Phase

receiving phases. This has been done for every saved iteration, and a graph-type plotting averaged concentration values versus increasing iteration for the first simulation are shown in Figures 35 through 40. Looking at the free carrier concentration in Figure 35, the over-all concentration decreases with increasing iteration and approaches a limiting value at around iteration 10000. This corresponds with that of the complexed carrier in Figure 36 showing attainment of a steady state at 10000 iterations. As before, loss of the free carrier is shown to be accompanied and explained by gain in the other membrane species (Figure 35-38).

Expanding the time scale on the X-axis of the graphs to cover the full time scale of the simulation, loss of material from the source phase and gain in the receiving phase can be examined in a clearer fashion. Separate plots for these are given in Figures 39 and 40 for the source and receiving phases respectively. Combining both on a common graph in Figure 41, it can be seen that losses in the source phase are complemented by gains in the receiving phase.

The last graphical data treatment combines results from simulations varying only in one parameter to elucidate effects of that parameter on the over-all transport rate of solute across the liquid membrane. Figure 42 compares the amounts entering the receiving phase for simulation results varying only the magnitude of change in the equilibrium constant due to the electrochemical oxidation state of the carrier molecule. Initial conditions for the simulations are 90% electrochemical conversion rate and

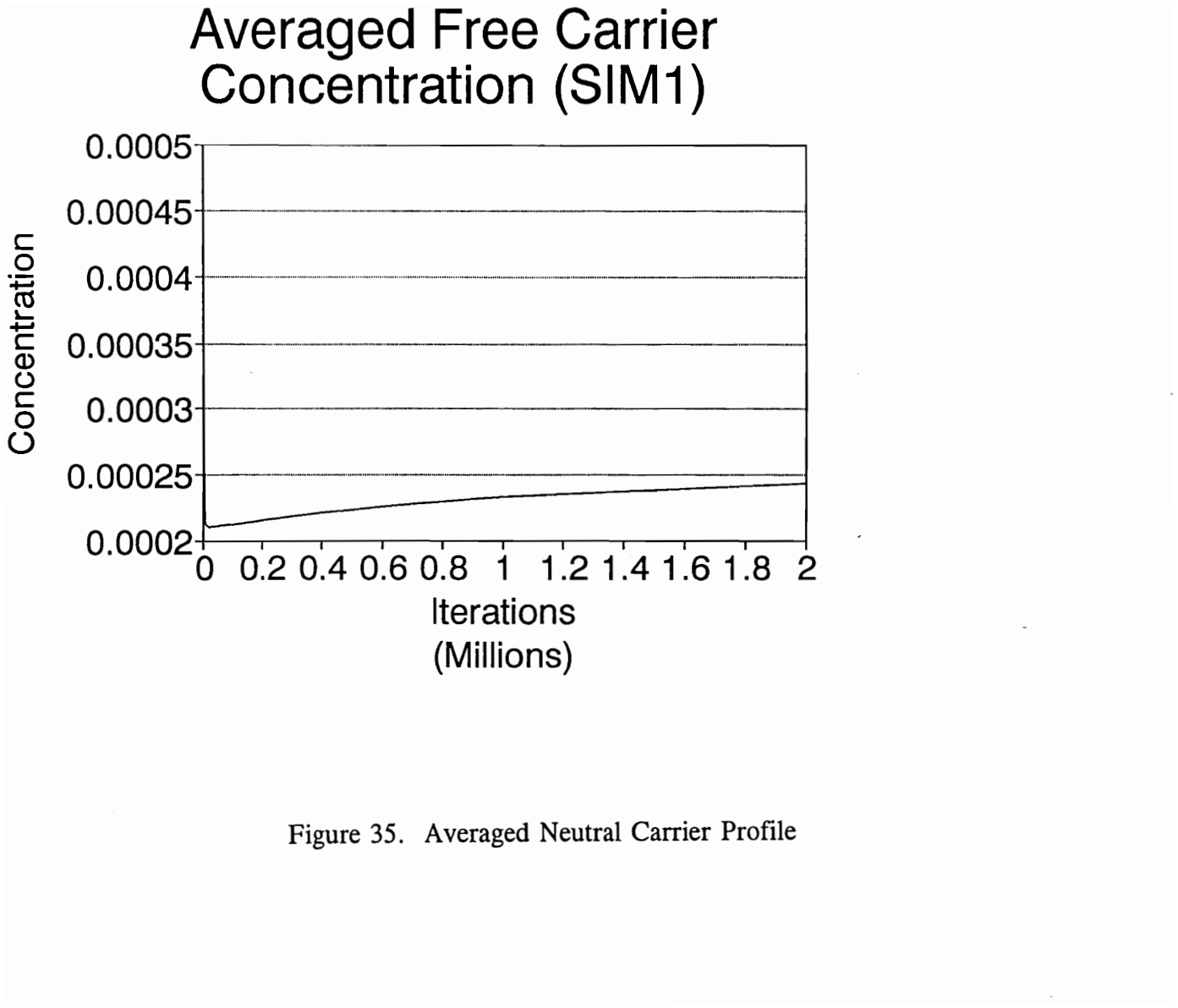

Figure 35. Averaged Neutral Carrier Profile

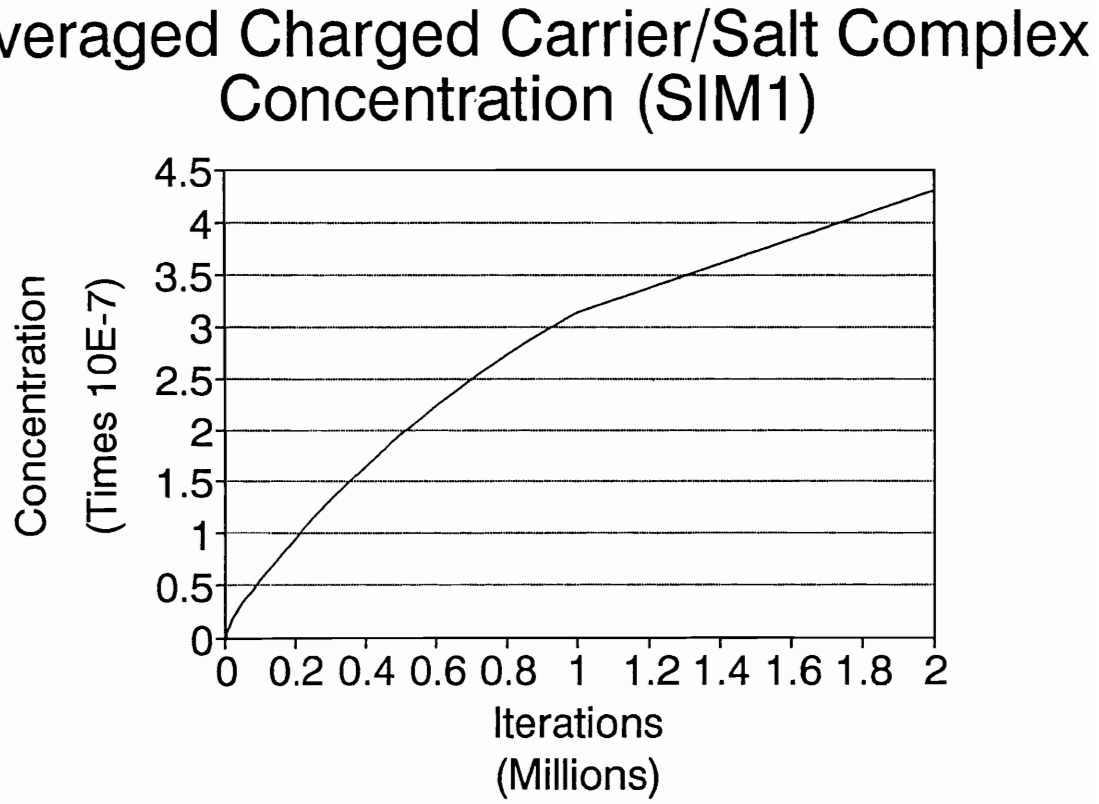

Figure 36. Averaged Carrier/Ion Complex Profile

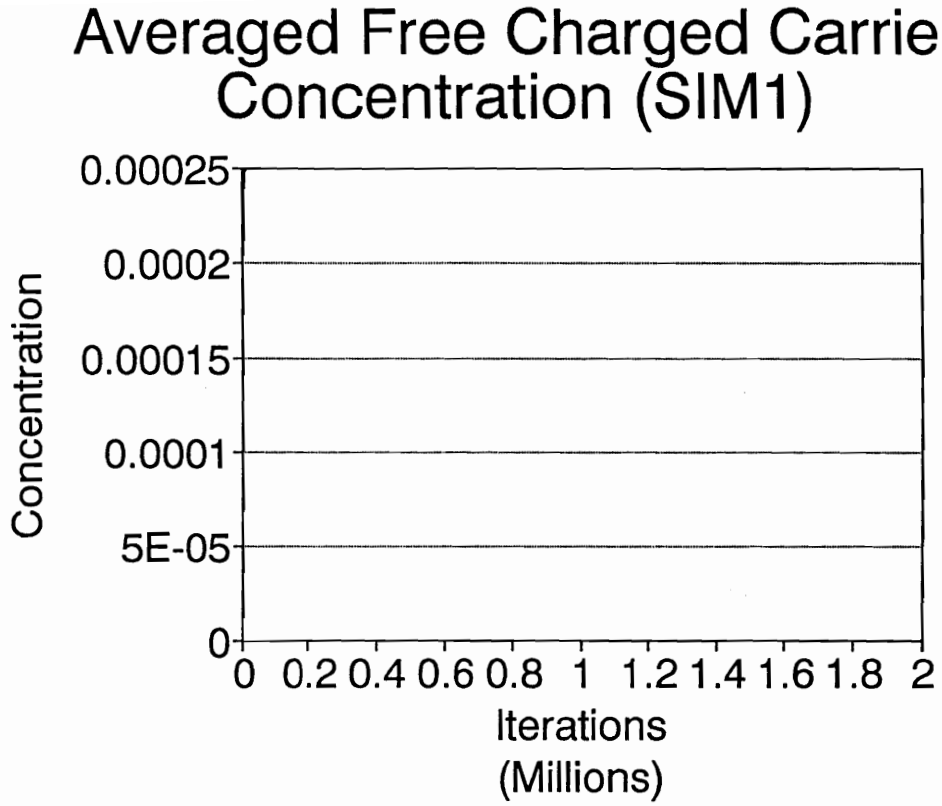

Figure 37. Averaged Charge Carrier Profile

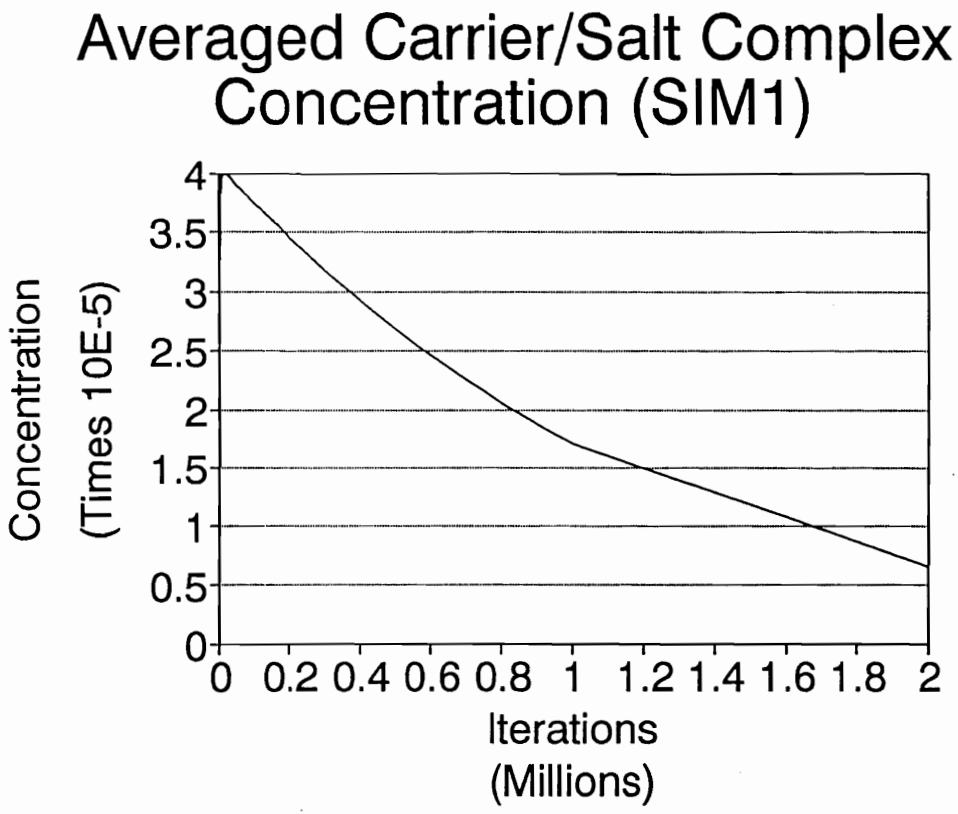

Figure 38. Averaged Charged Carrier/Ion Complex Profile

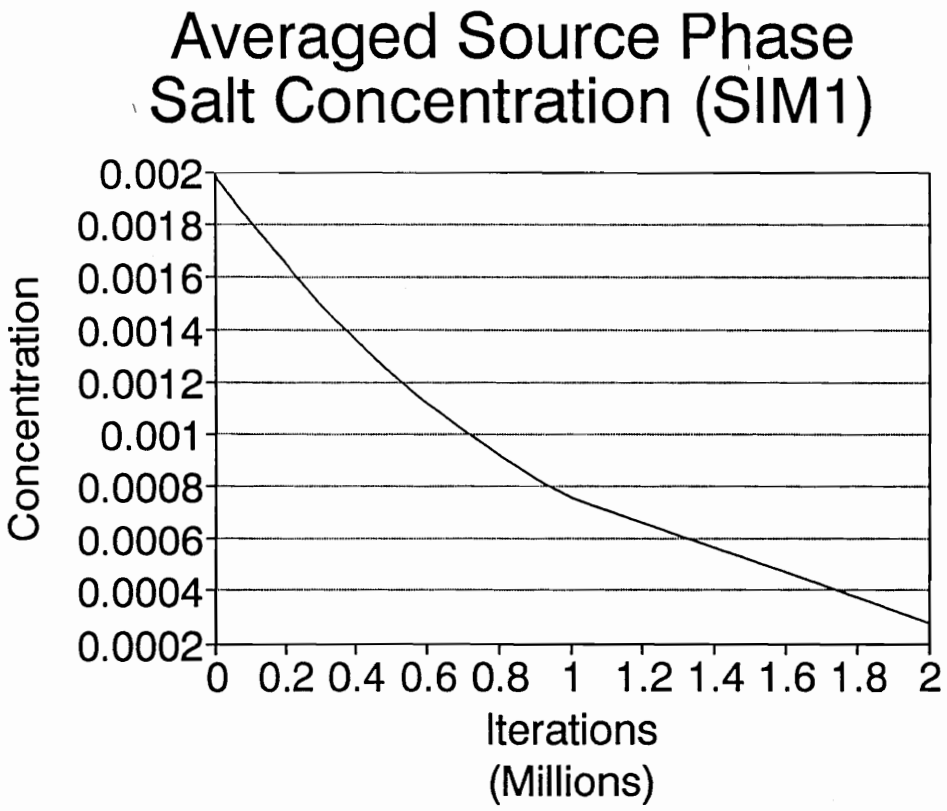

Figure 39. Averaged Source Phase Profile

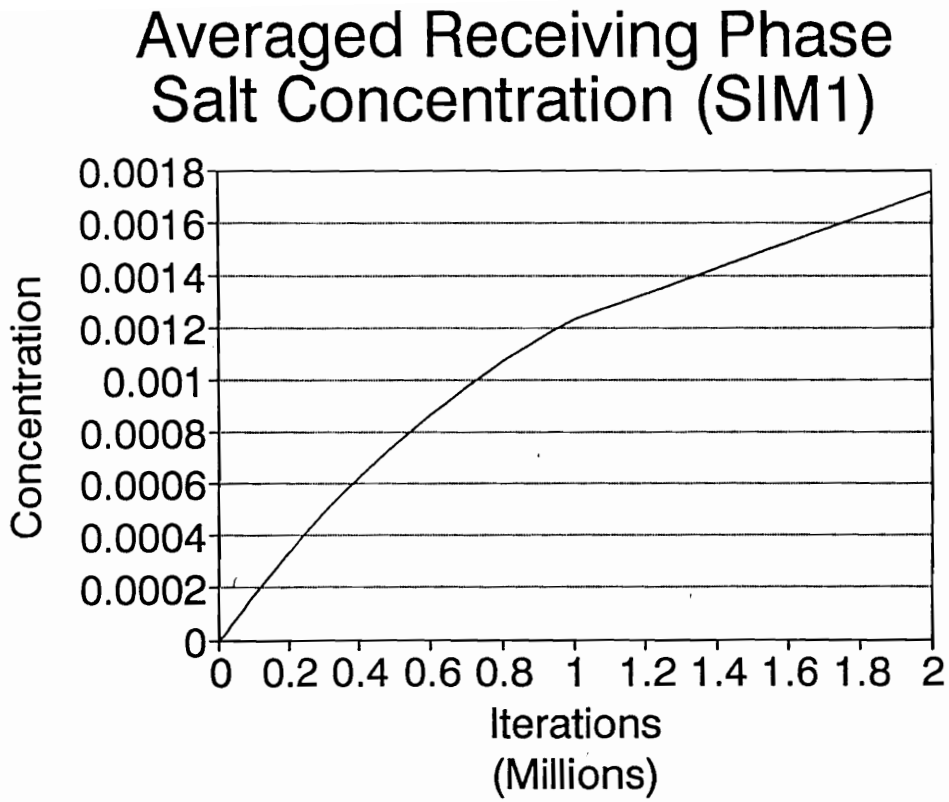

Figure 40. Averaged Receiving Phase Profile

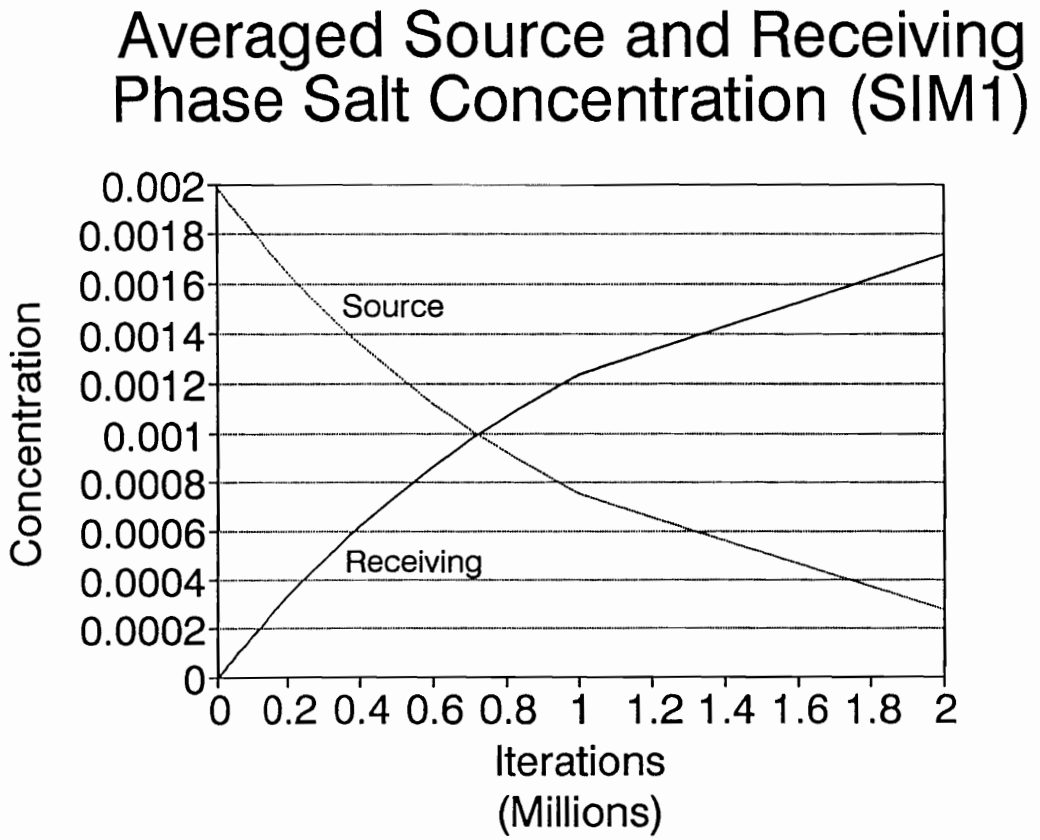

Figure 41. Averaged Source and Receiving Phase Profiles

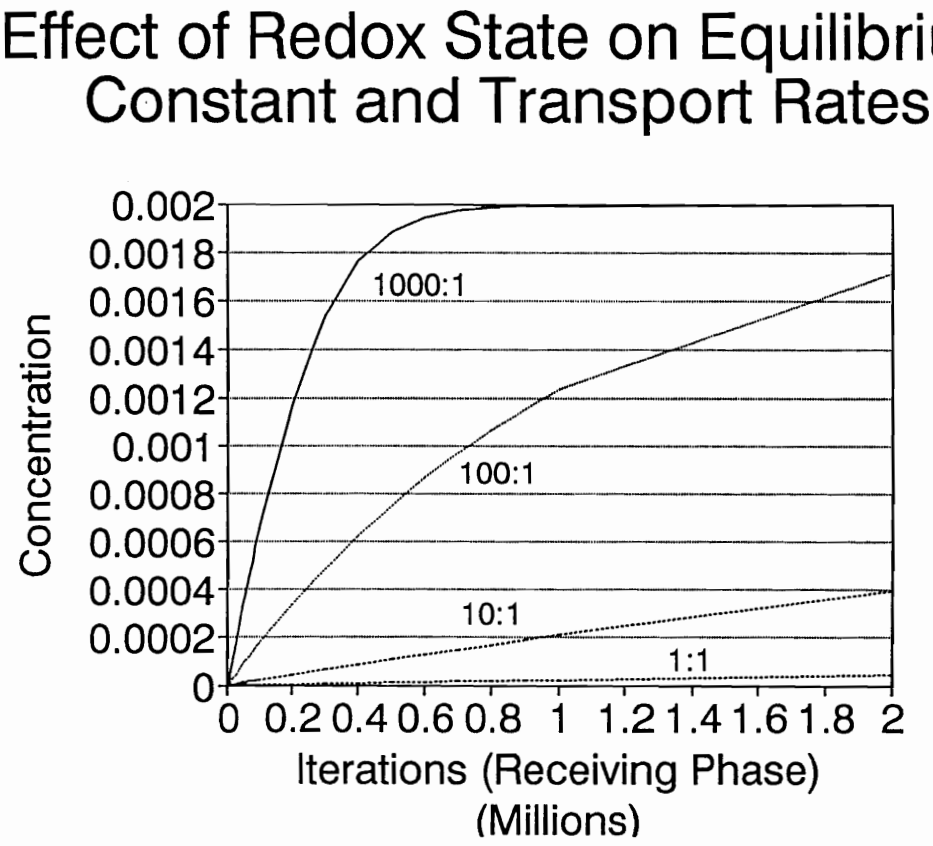

Figure 44. Effect of Equilibrium Constants on Receiving Phase

0.002 M and 0.000M for the source and receiving phases respectively. The change in complexation based on oxidation states for the 4 simulations are 1000:1 (SIM 2), 100:1 (SIM 1), 10:1 (SIM 4) and 1:1/NoEffect (SIM 7). The ratios are based on the complexation ability of the neutral molecule to that of the charged "deactivated" carrier. Thus the 1000:1 ratio states the neutral carrier is 1000 time better a complexing agent than the electrochemically oxidized form of the molecule. Examination of Figure 42 shows the rate at which material is moved into the receiving phase is fastest when the assumed change in oxidation state is 1000:1 followed in sequence by 100:1, 10:1 and lastly by the base line simulation of membrane transport without electrochemical activity. This result is agreement with the experimental evidence presented in the historical section dealing with transports rates of a series of DB18C6 crown ethers differing only in the electron withdrawing substituents placed on the benzene rings. That study showed that electro-negatively substituted carrier molecules transported material less efficiently that the unsubstituted form of the carrier.

The effect of electrochemical conversion at the membrane interfaces was studied in simulations 1, 5, 6 and 7. The initial conditions for the simulations were 0.002M for the source phase and 0.000 M for the receiving phase, and a 1000:1 change in the complexing ability of the carrier molecule based on its oxidation state. The electrochemical oxidation conversion at the receiving phase, and the corresponding reduction back to the neutral complexing carrier compound at the

source phase, are detailed below. The term n/a states that no electrochemistry is being applied.

Simulation #	Source Conv.	Receiving Conv.
1	90%	90%
5	90%	n/a
6	50%	50%
7	n/a	n/a

n/a: No Electrochemistry

Figure 43 demonstrates a comparison of 90% versus 50% electrochemical conversion rate at both the source and receiving phase interfaces. As expected, the larger the amount of conversion in the carrier molecule, the larger the overall transport rate.

Figure 44 demonstrates the predicted result of full electrochemical pumping versus partial pumping versus no electrochemical pumping. The results are as expected. Based on the previous results the larger the effective change of the carrier molecule, the larger the effective transport rate of material across the membrane phase. Figure 45 focuses on the case of electrochemical oxidation only at the receiving phase versus that of no electrochemical activity. The expanded graph shows there is an initial influx of material into the membrane phase for the simulation where

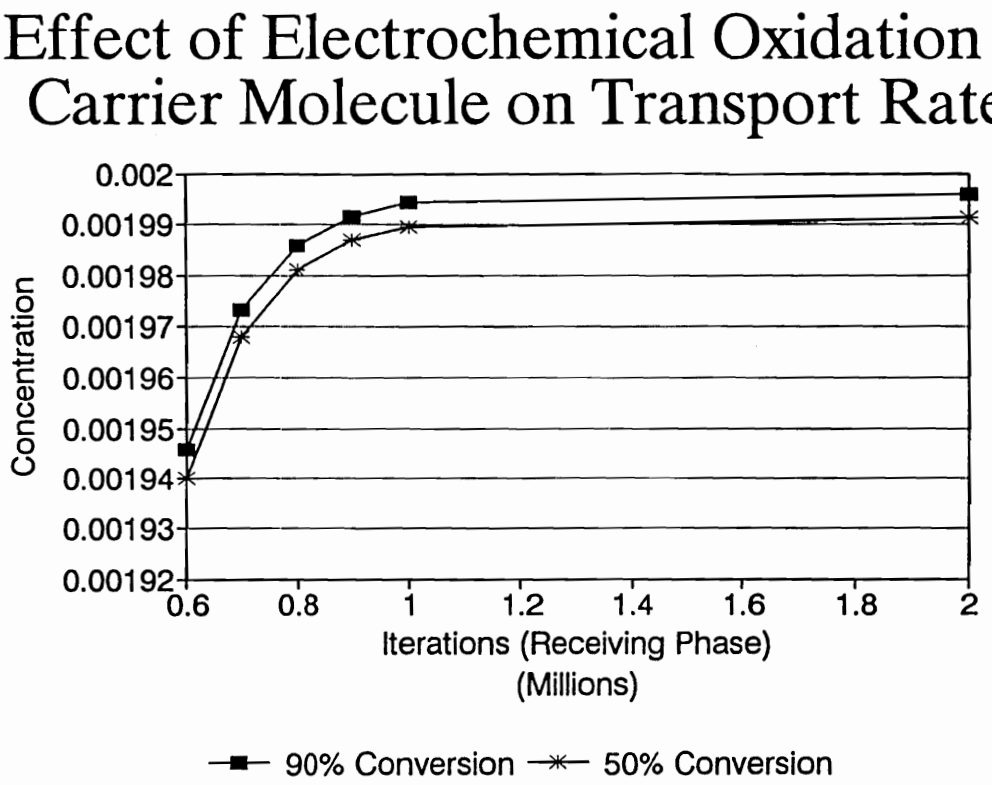

Figure 43. Effect of Percent Oxidation/Reduction on Receiving Phase

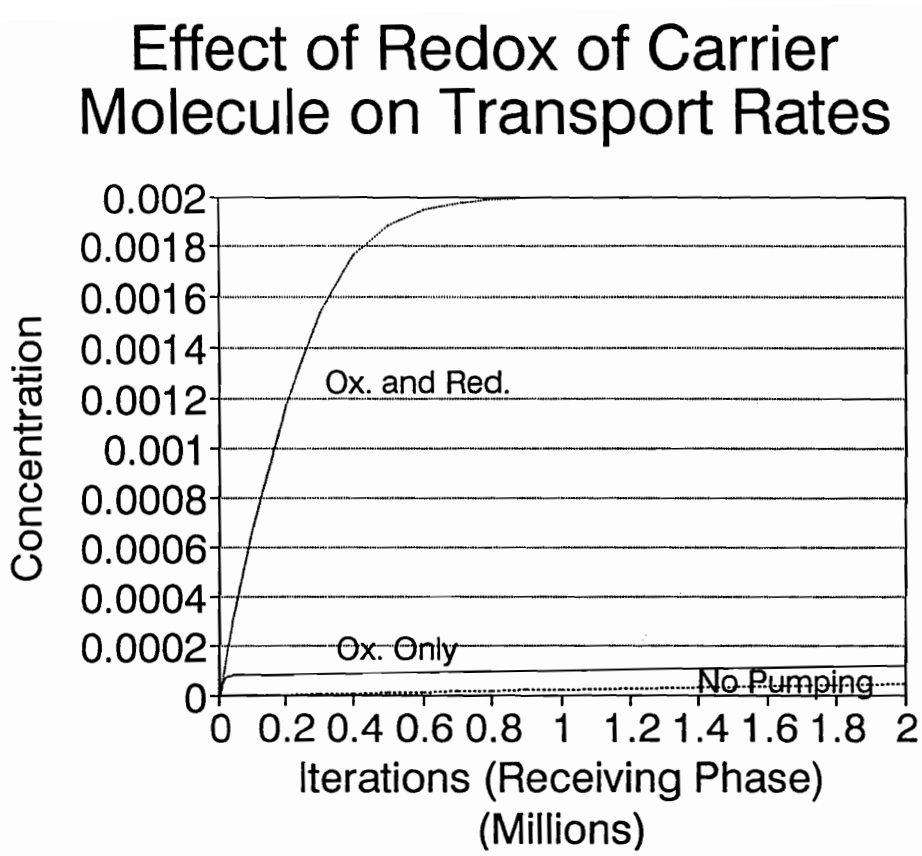

Figure 44. Effect of Electrochemical Redox Cycling on Receiving Phase

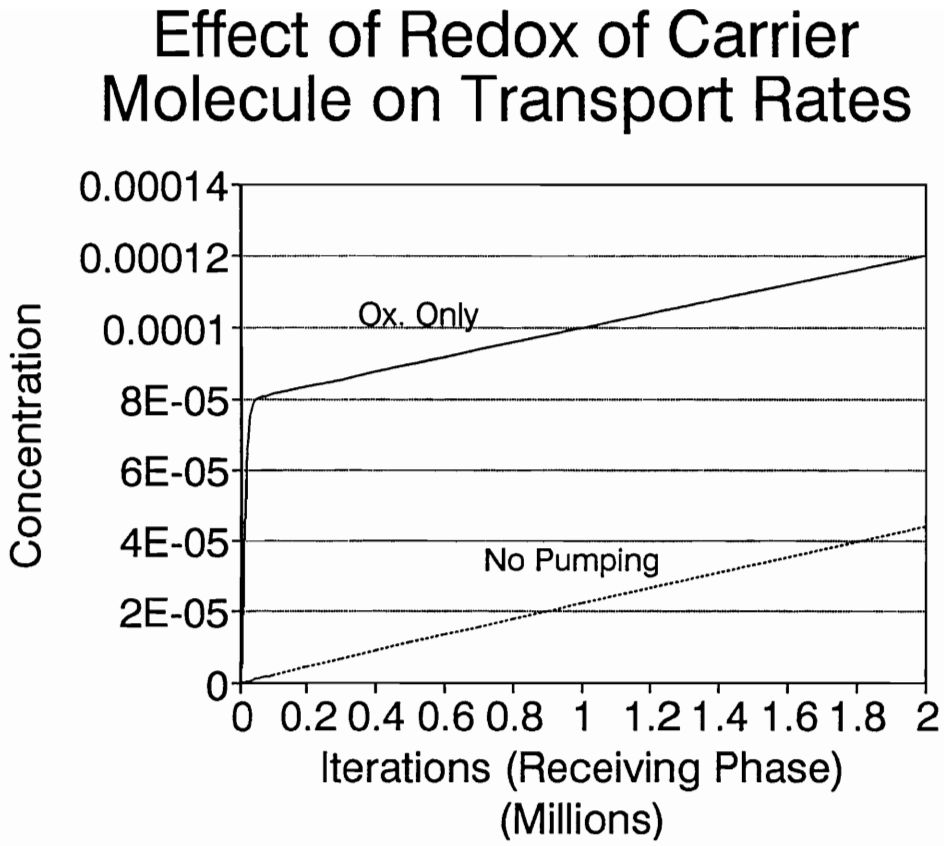

Figure 45. Expanded View of Figure 44

electrochemical activity at the receiving is present. The explanation for this result is based on the consideration that the membrane phase is initially charged with a significant amount of solute in a complex form with the carrier. Having charged membrane with solute, the effect of exhaustive electrolysis on the membrane forces the complexes to break up upon electrochemical conversion of the carrier molecule complex to its non-complexing form at the receiving phase interface. This releases the solute into the receiving phase. This charging of the membrane followed by discharging of the solute is responsible for the initial jump in concentration of the receiving phase compared with the case of membrane transport without the aid of electrochemical transport.

The last, and most significant result of the simulation deals with the concept of the possibility of "Uphill" electrochemical facilitated transport. The conditions for the experiment are 0.002 M in both source and receiving phase, 0.0005 M carrier concentration in the membrane phase, 1000:1 complexation change and 90% electrochemical conversion rate at both interfaces. The graph is Figure 46 clearly shows it is theoretical possible to electrochemically move solute from the source phase, through the membrane, and into the receiving phase. This simulation indicates that "Uphill" electrochemical facilitated transport in viable and worthy of consideration.

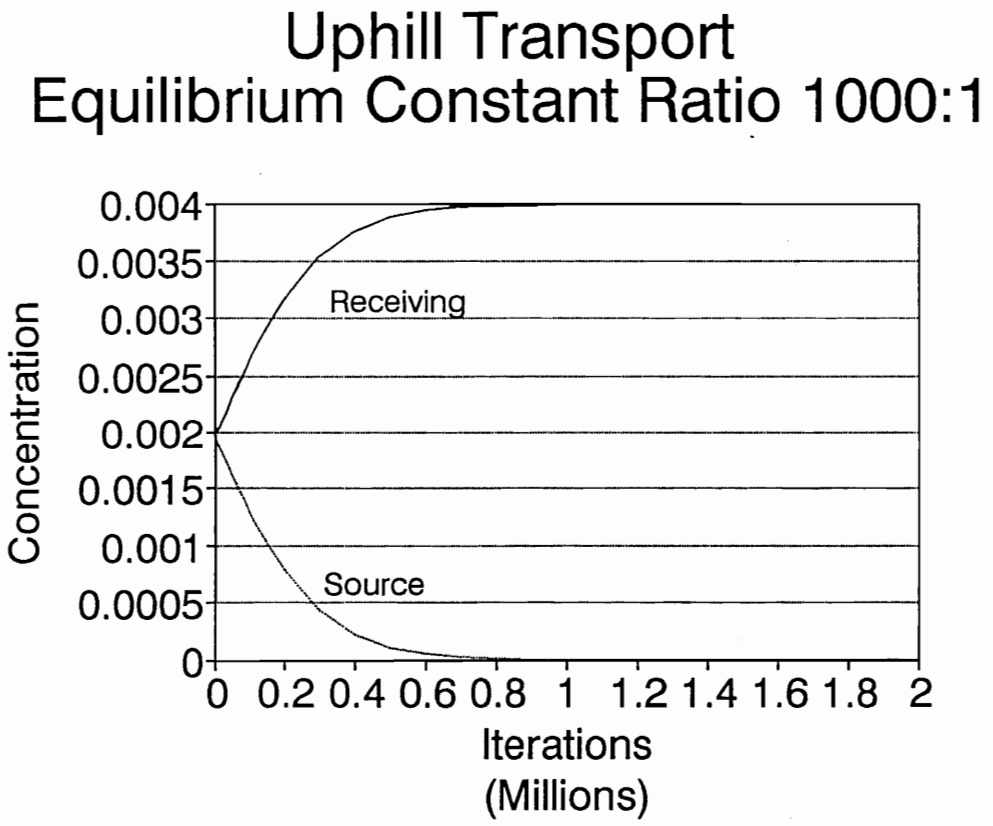

Figure 46. Uphill Pumping Profiles

(B) Applied Simulations

Previous simulation parameters were picked as representative of experimental conditions found in the literature. Hence, values of 0.0005 molar concentration for the carrier molecule, and 0.001 molar concentration for the solute to be transported. The values for change in equilibrium constants on the basis of the oxidation state of the carrier were chosen to reflect those found in the literature study comparing effect of electronegative substituents on the overall downhill transport rate of metal ions across a bulk liquid membrane. Three orders of magnitude were found between the unsubstituted crown ether and the crown ether with a high number ("eight") of attached electronegative chloride ions.

In the upcoming experimental chapter, evidence in the form of ion extraction experiments show the change in equilibrium constants between the neutral and oxidized form of the carrier molecule for thallium differs by only a factor of two. Additional uphill and downhill simulations were run using complexation constants from the thallium extraction experiments with the concentrations of the thallium ion and the ferrocenophane from those the corresponding uphill and downhill experiments. The complexation formation constant is defined as:

$$K_{eq} = \frac{[C \cdot Tl(I)]_{org}}{[C]_{org}\,[Tl(I)]_{aq}}$$

Using the above equation and experimental values from the extraction experiment, the complexation constant for the neutral complexation is 2338, and 1481 for the charged form of the carrier.

The uphill simulation parameters involved 0.01 M thallium ion concentration for both source and receiving phase, and 0.003232 M for the ferrocenophane carrier molecule. Complexation constants are as described above. Electrochemical conversion efficiencies are taken as ninety percent for both source and receiving phase membrane interfaces. Additional equilibrium calculations are performed to acquire simulation conditions analogous to those obtained during the pre-equilibrium stage of the thallium uphill transport experiment. Thus, at the start of the uphill simulation, the membrane phase will possess a quantity of thallium ion complexed with the ferrocenophane crown ether. The resulting graph for the concentration profiles for the source and receiving phase is shown in Figure 47. The trends predicted by the simulation show the familiar increase in the receiving phase concentration combined with a decrease in the source phase concentration.

This simulation provides additional basis for the conclusion reached in the based on the results obtained in the uphill transport experimental sections.

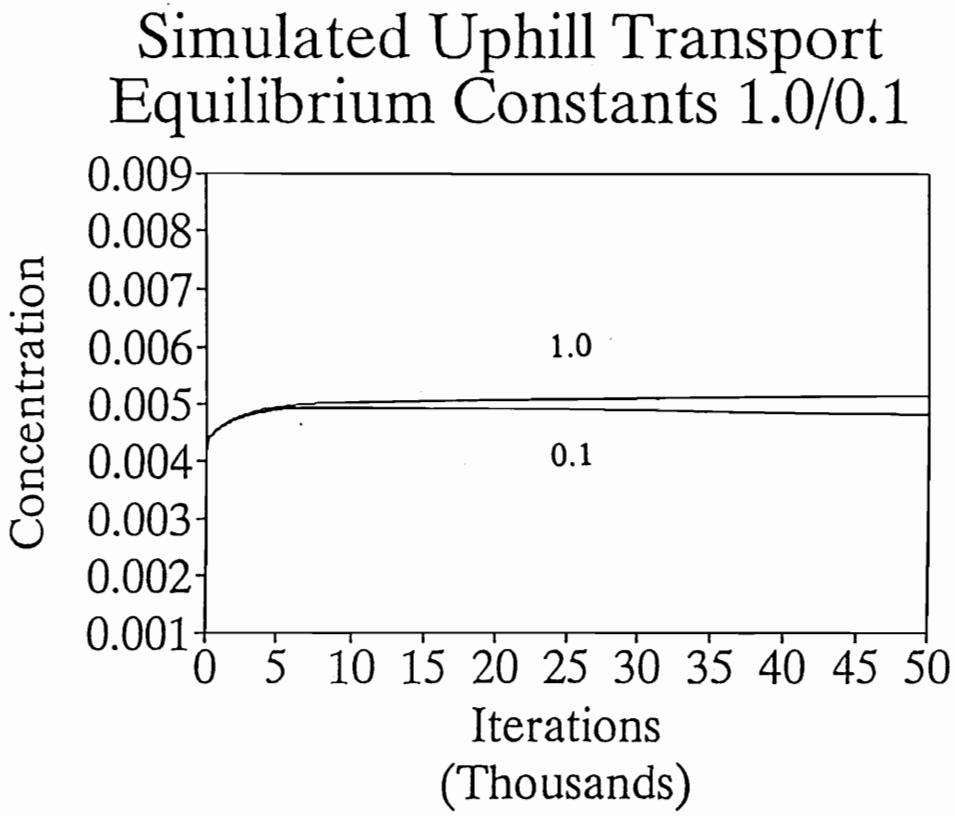

Figure 47. Simulated Uphill Transport Profiles Using Experimental Complexation Values and Conditions

Examination of both the silver and thallium uphill experiments showed initial increases in the receiving phase without similar decreases in the source phase. It is deduced that this increase in the receiving phase was a direct result of the decrease in carrier molecule's ability to complex with the cation due to the oxidation of the carrier molecule. This decrease in complexation ability forces the complexed ion to leave the membrane phase and enter the nearest aqueous phase. This results in an apparent increase of that aqueous phase without a corresponding change in the other aqueous phase. Examining the initial stages of the above simulation (Figure 48), it can be seen that this behavior is predicted from the model. The receiving phase, and to a lesser extent the source phase, receive an increase in concentration due to the oxidation of the carrier molecule.

The Downhill simulation parameters involved 0.01 M thallium for the source phase and 0.0 M for the receiving phase. The concentration for the ferrocenophane carrier is 0.003232 M. Complexation constants are as defined above, and electrochemical efficiencies are taken as ninety percent for the pumped experiment, and not implemented for the non-pumped experiment. The results are shown in Figure 49. Once again, the trends predicted by the simulation correspond with those in the experimental section.

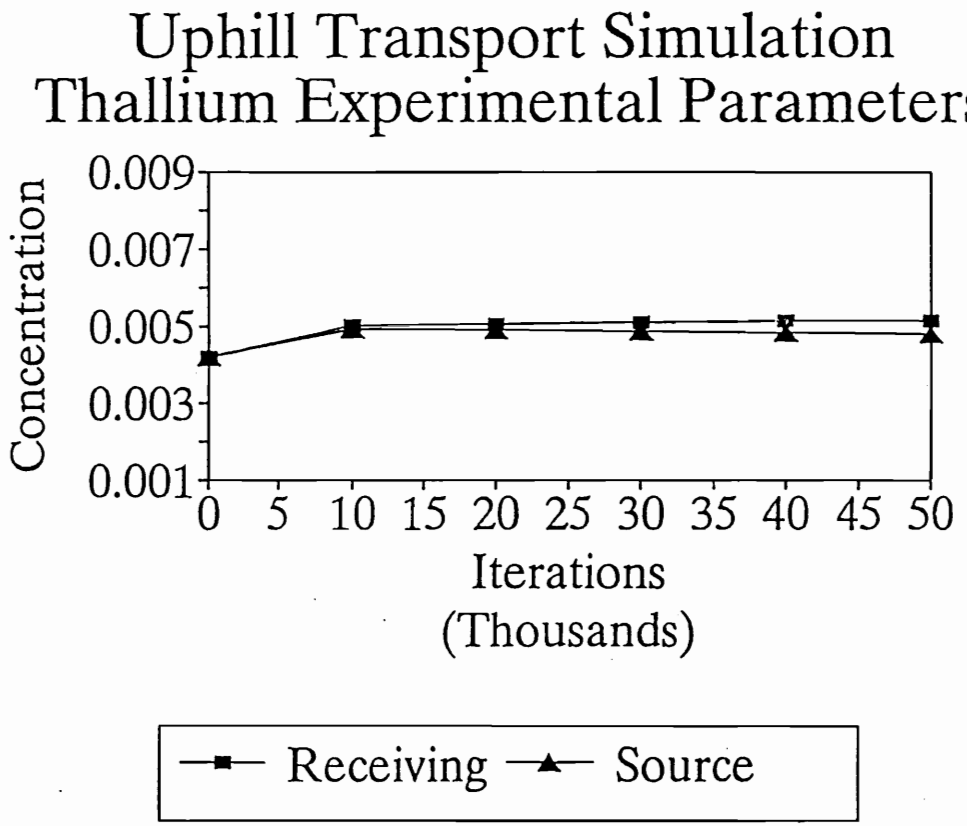

Figure 48. Simulated Uphill Transport Profiles Using Experimental Complexation Values and Conditions (Early Stages of Simulation)

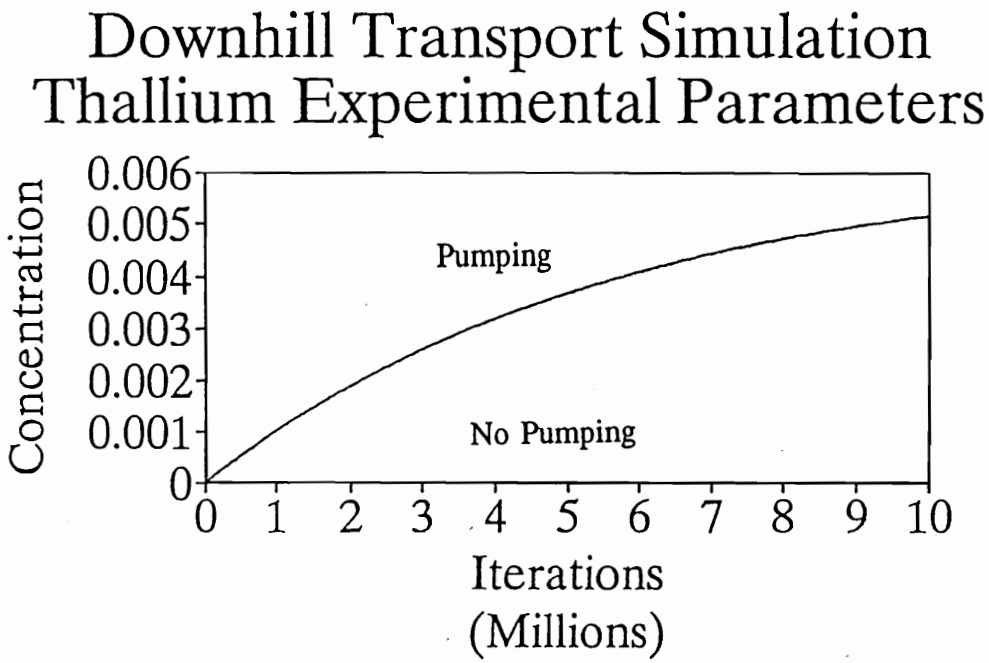

Figure 49. Simulated Downhill Profiles Using Experimental Complexation Values and Conditions

(C) SUMMARY

Digital simulation of electrochemical facilitated transport have revealed the following:

1) **The concept is theoretically valid for both downhill and uphill pumping.**
2) **The larger the difference in equilibrium constant between the neutral and oxidized forms, the larger the pumping rate.**
3) **The larger the amount of electrochemical conversion at the source and receiving phase, the larger the pumping rate.**

With these theoretical concepts in mind and the capability to synthesize appropriate carrier molecules, the idea of electrochemical facilitated transport promises many avenues for research. The basic tools (computer programs) described in appendix II provides the future researcher a starting point with which to modify the simulation, adding parameters as needed, to meet those future needs.

EXPERIMENTAL

A) Synthetic Organic Chemistry

1) Selection of Model Carrier Compound

The study of the viability of electrochemical facilitated transport requires selection of a suitable membrane transport compound. A survey of commercial specialty chemical catalogs failed to yield promising candidates. To proceed with the project, properties of an ideal model compound needed to be defined. Literature searches were performed. Synthetic design routes were proposed followed by synthesis and characterization of the new compound and its intermediates. The design criteria for the model compound is as follows:

- Crown ether moiety (metal ion complexation).
- Electrochemically reversible functional group.
- Chemically and electrochemically stable in a water saturated methylene chloride/tetrabutyl ammonium perchlorate (TBAP) media.
- Complexation between carrier molecule and metal ion influenced by electrochemical redox state of the carrier molecule.

- Oxidation/reduction potential of carrier molecule outside the range of that of the metal ion being transported.

Examination of reference sources for organic electrochemistry,[40,41,42] and searching for water resistant, electrochemically reversible functionalities, lead to few candidates suitable for incorporation into a crown ether. Of the few compounds not exhibiting irreversible side reactions (degradation products) upon reaction with water, phenazines seemed the best class of compounds on which to base a new crown ether. These generate a stable radical ion[43] even in the presence of water,[44] and are electrochemically reversible (Figure 12). The synthesis of the phenazine diol[45,46,47,48,49,50,51,52,53] required as an intermediate for the creation of the target phenazine crown ether using conventional crown ether condensation reactions is reported in the literature (Figure 13). Synthesis of the reported diol crown ether failed despite many experimental attempts and variations of synthetic methods. Synthesis of additional phenazine crown ethers were attempted using the diamino phenazine and phenazine dioxides as intermediate starting materials. Here to, intermediates for the desired phenazine crown ethers were not isolated, or proved unreactive when attempts to form the final crown ether were made. To date, phenazines have not been reported as functionalities within crown ethers.

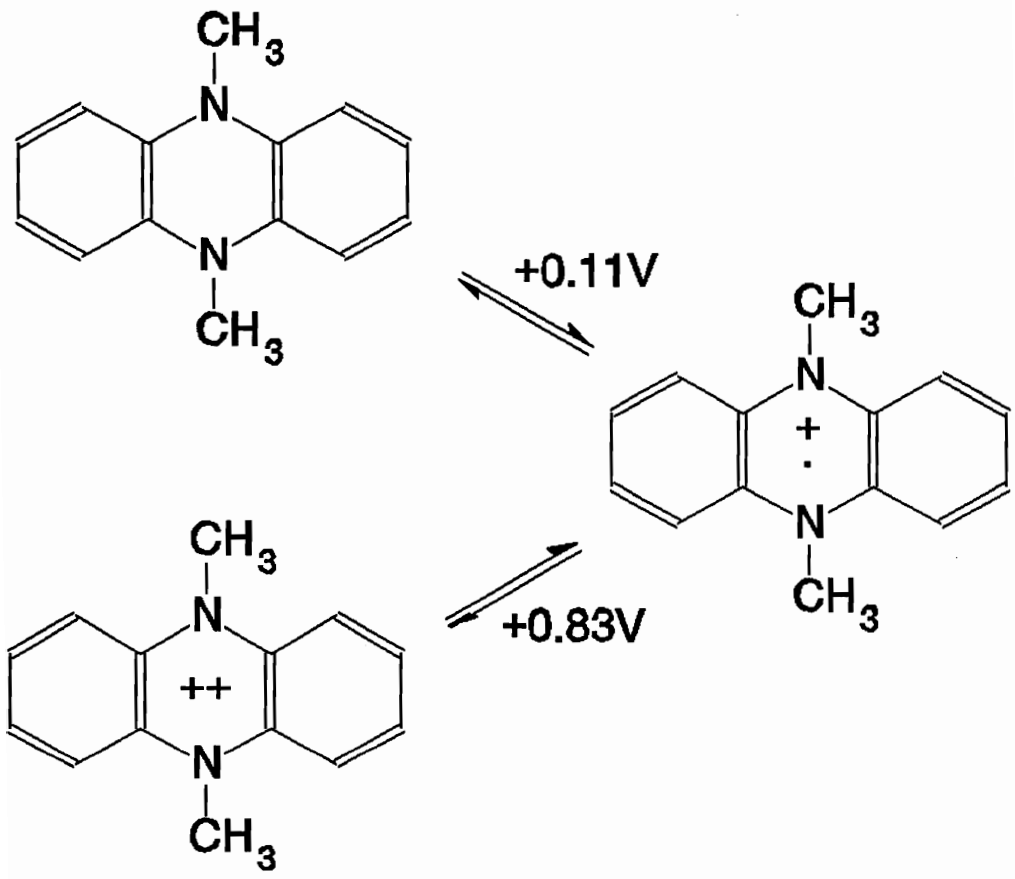

Figure 50. Electrochemistry of Phenazine

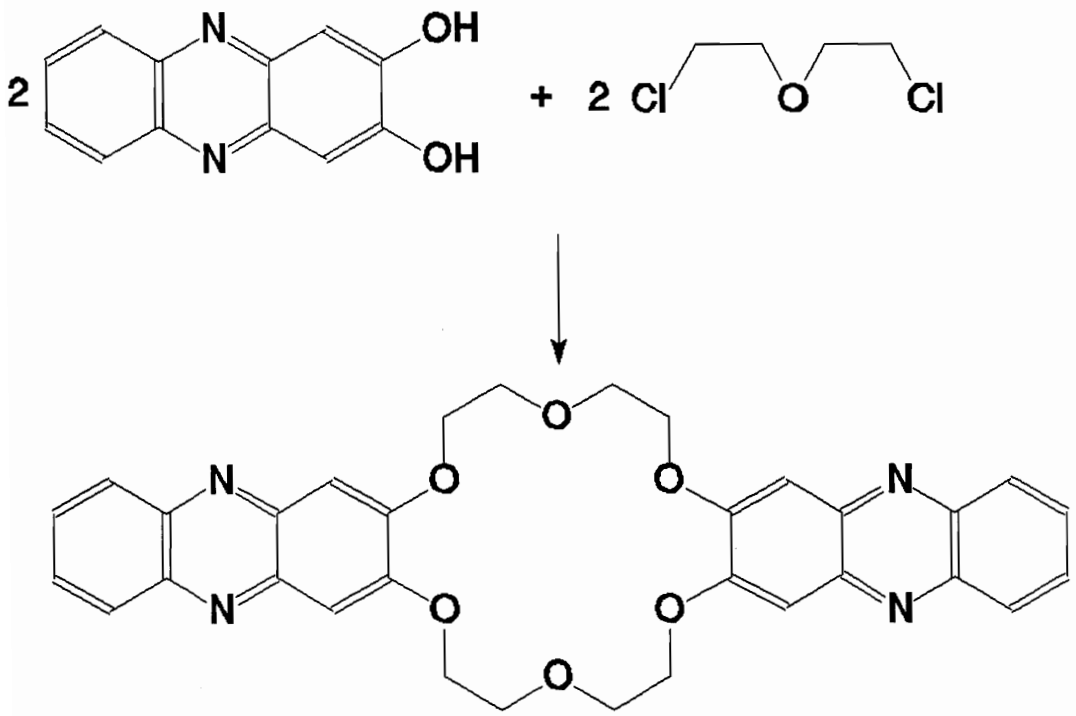

Figure 51. Proposed Synthesis for a Phenazine-Based Crown Ether

The electrochemically reversible class of phenanthrolines[54] (Figure 52) were tried, but compounds containing the hydroxyl or carboxylic acid groups necessary for creation of the crown moiety were not commercially available, and the synthetic routes reported in the literature again failed to yield the desired intermediates. However, during the course the aforementioned synthetic attempts, an increasing aptitude for organic chemistry techniques was developed so that when the literature searches located a class of ferrocenophanes, a useable crown ether was suggested.

2) Synthesis of Ferrocenophane Crown Ether

The reaction pathway outlined in Figure 53 depicts the condensation of 1,1'-dichlorocarbonyl ferrocene with hexaethylene glycol to make a new ferrocenophane with the IUPAC name of 2,5,8,11,14,17,20-heptaoxa[21] (1,1')ferrocenophane-1,21-dione. The 1,1'-dichlorocarbonyl ferrocene was obtained from the commercially available diacid using oxalyl chloride as the chlorinating agent in place of the thionyl chloride as described in literature preparation[55]. Reaction conditions for the ferrocenophane crown ether follows.

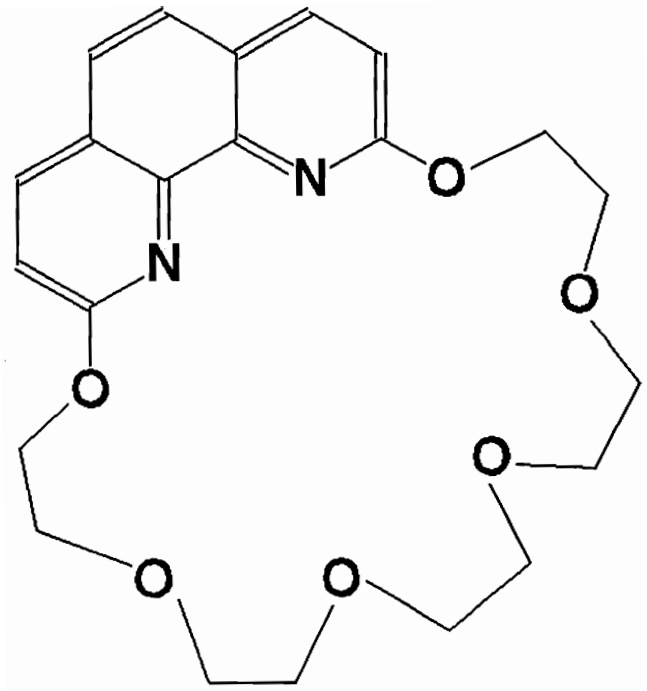

Figure 52. Phenanthroline Crown Ether

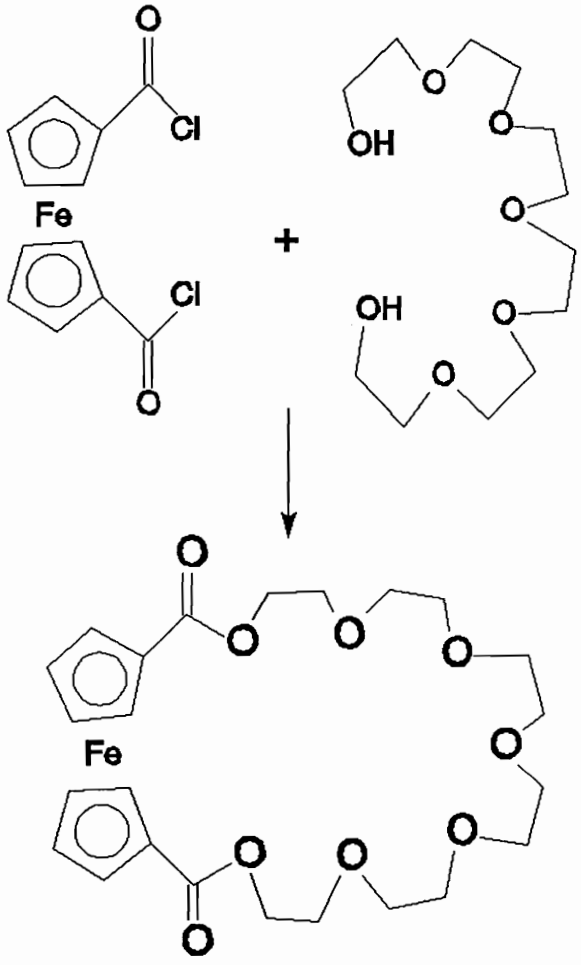

Figure 53. Synthesis of Ferrocene-Based Crown Ether 2,5,8,11,14,17,20-heptaoxa[21] (1,1')ferrocenophane-1,21-dione

2,5,8,11,14,17,20-heptaoxa[21](1,1')ferrocenophane-1,21-dione. A solution of 1,1'-dichlorocarbonyl ferrocene (4.5 g, 0.0145 mol) and benzene (200 ml) is dripped slowly into a gently refluxing benzene (200 ml) solution containing hexaethylene glycol (4.1 g, 0.0145 mol), and refluxed for twenty four hours. Another equivalent of the glycol solution is added and refluxed for 24 hours. The benzene is removed in vacuo, and separation is obtained using a silica gel column and elutant a mixture of 4:1 Ethyl Acetate:Hexanes. The ferrocenophane crown ether elutes as an orange-red oil (first orange band, 0.211 g, 1.58% yield). Purity is confirmed using thin layer chromagraphy (4:1 Ethyl Acetate:Hexanes).

3) Characterization of the Crown Ether

Proton NMR, mass spectroscopy, ultraviolet spectroscopy, and cyclic voltammetry were utilized to identify, characterize and evaluate the new compound. NMR and mass spectroscopy verified the structure of the molecule. Ultraviolet spectroscopy and cyclic voltammetry provided complementary evidence for its structural components. Cyclic voltammetry also demonstrated the electrochemical reversibility of the compound. Spectra and interpretation of the spectra for the ferrocenophane crown ether are now presented.

a) Mass Spectroscopy

Figures 54 and 55 show the isotopic fragmentation pattern of the parent peak and the fragmentation pattern for the entire compound respectively. Both show a single parent peak at 520 mass units consistent with the molecular weight of the target ferrocene crown ether. The identification of the parent peak is further confirmed by the absence of peaks above 520 mass units. In Figure 54, the peaks surrounding the parent 520 peak conform with isotopic abundance patterns for a molecule containing 24 carbons, 32 hydrogens, 9 oxygens, and 1 iron. Referring to a standard text on Mass Spectral analysis[56], the relationship between the parent peak M, M+1 and M+2 peaks for molecules containing only carbon, oxygen and hydrogen, can be approximated by the following formulas. These formulas are obtained by considering the natural isotopic abundances for hydrogen, carbon and oxygen and scaling their relative percentages taking the main peak to have the value 100.

$$\%(M+1) = 1.1 \times \text{number of carbon atoms}$$

or

$$\%(M+1) = 1.1 \times 24 = 26.4$$

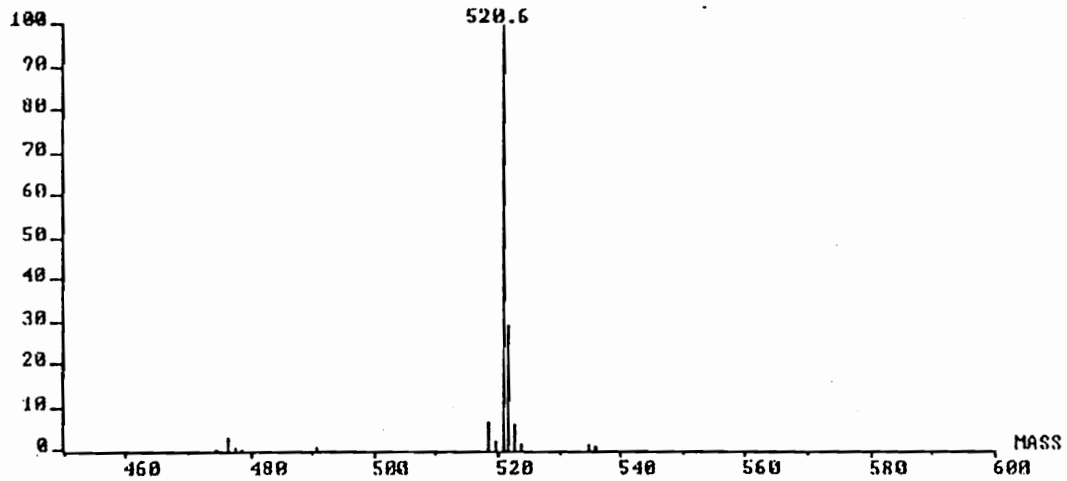

Figure 54. Parent Peak Mass Spectrum for Ferrocenophane Crown Ether

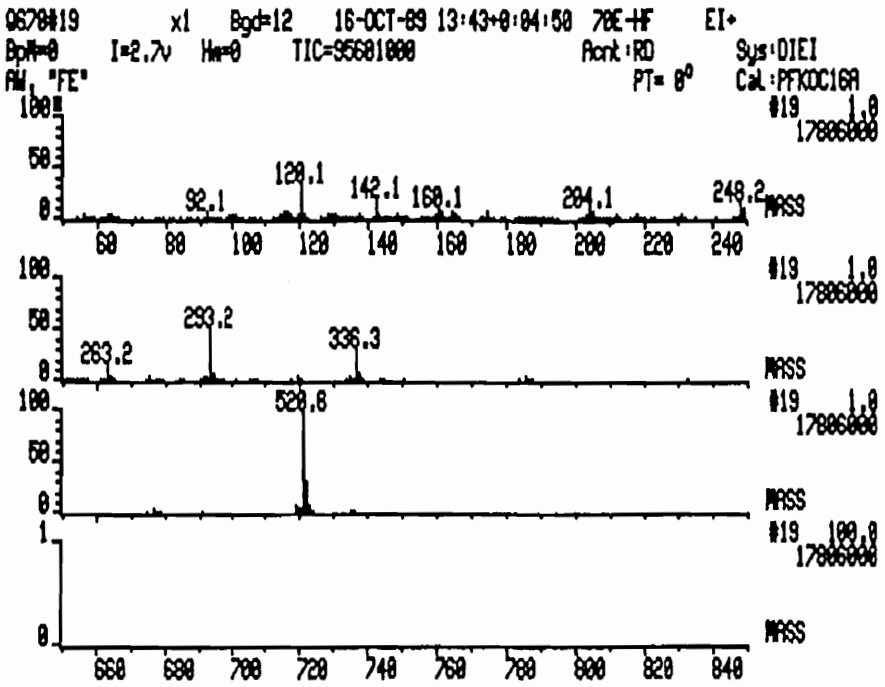

Figure 55. Full Mass Spectrum for Ferrocenophane

and

$$\%(M+2) = (1.1 \times \text{number of carbon atoms})^2/200 + 0.20 \times \text{number of oxygen atoms}$$

or

$$\%(M+2) = (1.1 \times 24)^2/200 + 0.20 \times 9 = 5.3$$

The calculated values considering only the carbon, oxygen and hydrogen atoms do not exceed the magnitudes of the experimentally determined (M+1) and (M+2) peaks, but does not account for the entire magnitude of the (M+1), (M+2), or the appearance of the (M-2) peak at 518 mass units. The iron atom must be examined for its isotopic contribution to the isotopic peak patterns.

Iron consists of four major isotopes with the percentages listed below. The percentages are scaled taking the largest component to be 100% as is customary in mass spectrum isotopic analysis. The values for iron are as follows:

Isotope	Abundance	Scaled Abundance
Fe^{54}	5.82%	6.35
Fe^{56}	91.66%	100
Fe^{57}	2.19%	2.39
Fe^{58}	0.33%	0.36

The peaks are assigned as follows: (M-2) to Fe^{54}, (M) to Fe^{56}, (M+1) to Fe57, and (M+2) to Fe^{58}. The peak ratios of the single iron atom accounts for the peak at 518 mass units, as well as the remaining magnitudes for the peaks at 521 and 522 mass units. The results of these theoretical calculations are shown in Figure 56, and the theoretical isotopic peak pattern matches that of the experimental pattern in Figure 16. This completes the parent peak analysis, and confirms the parent peak has a molecular formula of $C_{24}H_{32}O_9Fe$.

The full mass spectrum in Figure 55 shows fragmentation patterns with characteristic losses of the ethylene oxide crown ether repeating unit. This is compatible with fragmentation patterns found in long chain crown ethers. Other peaks can be assigned to substituted ferrocene and cyclopentlydienyl ring fragments. The following peak assignments have been made.

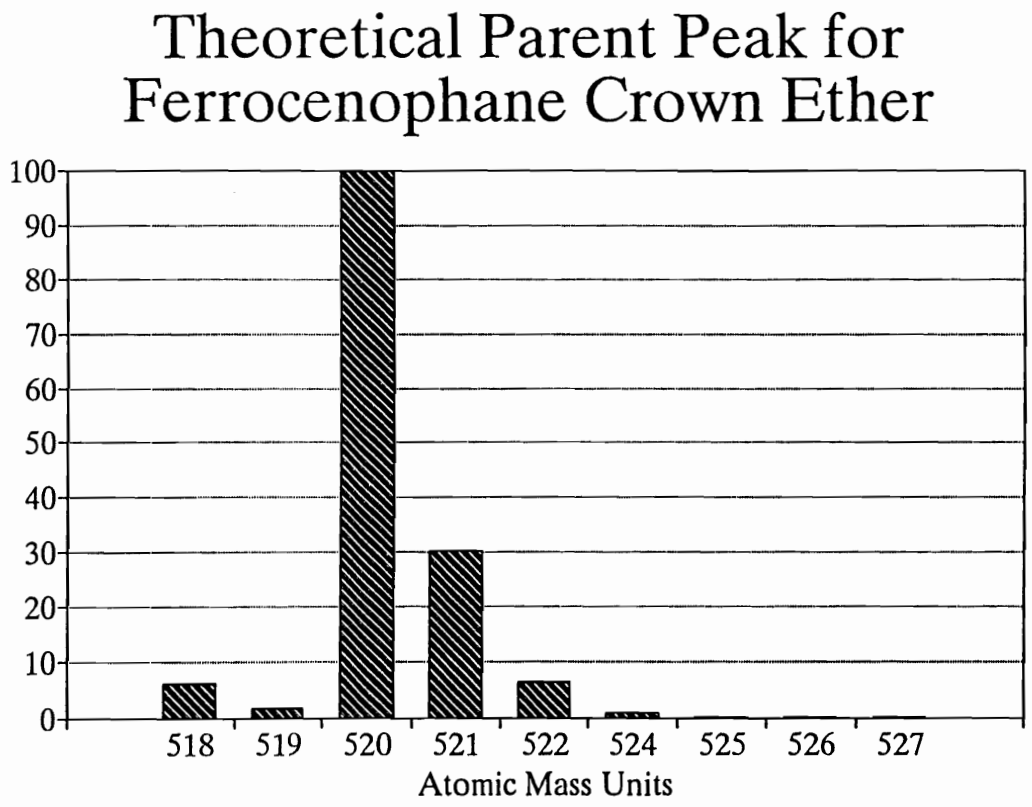

Figure 56. Theoretical Parent Peak Mass Spectrum for Ferrocenophane Crown Ether

Peak	Identification
520	Parent Peak
336	Parent less ferrocene unit
293	Parent less ferrocene and ethylene unit
263	Ferrocene with $CO\text{-}(CH_2\text{-}CH_2\text{-}O)_4$
120	cyclopentadienyl iron
92	cyclopentadienyl aldehyde

From analysis of the isotopic peak patterns of the parent peak in Figure 54 and identification of the peak fragment and mass losses in Figure 55, the structure for the unknown is consistent with the structure expected for the ferrocenophane crown ether in Figure 53.

b) Analysis of Proton NMR.

Proton NMR spectrum (deuterated chloroform) for the ferrocenophane crown ether is shown in Figure 57. From literature proton NMR studies of substituted ferrocene compounds,[57] each peak in Figure 57 can be assigned to a unique group of chemically equivalent protons in the target molecule (Figure 53). The integrated peak heights for each peak support these assignments.

Peak (ppm)	Integration	Assignment
5.2	4H	H_α Ferrocene Protons
4.95	4H	H_β Ferrocene Protons
4.9	4H	Chain Protons Nearest Carbonyl Group
4.65	8H	$-CH_2-O-CH_2-$ Protons
3.35	12H	Remaining Chain Protons

The peaks at 7.25 and 1.15 ppm corresponds to the isotopic impurity of hydrogen in the deuterochloroform solvent and the internal standard.

c) Ultraviolet Spectroscopy

The ultraviolet transmission spectrum for the ferrocenophane crown ether is shown in Figure 58. Alkyl and acyl substituted ferrocenophane compounds typically exhibit absorption bands at 325 and 440 nm that are attributed to symmetry forbidden excitations of the electrons in the d-orbitals of the metal. The d-orbitals of iron are proposed to be split by the perturbing field of the π-electrons of the cyclopentadienyl rings. Changes in the energy levels of these transitions are further influenced by substituents placed on the cyclopentadienyl rings that may interact with the ring electrons and/or the iron atom. Barr and Watts studied a number of substituted ferrocenophanes.[58,59,60,61] They focused on the 325 and 440 nm bands for ferrocenophanes incorporating various placements of carbonyl groups and chain-lengthening methylene groups in the bridging linkage and examined the effects of increased conjugation and chain length on the absorption bands. The incorporation of carbonyl groups into the molecule introduces possible coplanar interactions between the π-systems of the cyclopentadienyl ring and that of the carbonyl groups leading to a blueshift in the 440 nm band. The effect is enhanced as the chain is lengthened as the π-π orbital overlap becomes more significant.

Of the several compound evaluated in Barr and Watt's studies, substituted [5]ferrocenophane-1,5-diones approximate the geometry of the model ferrocenophane

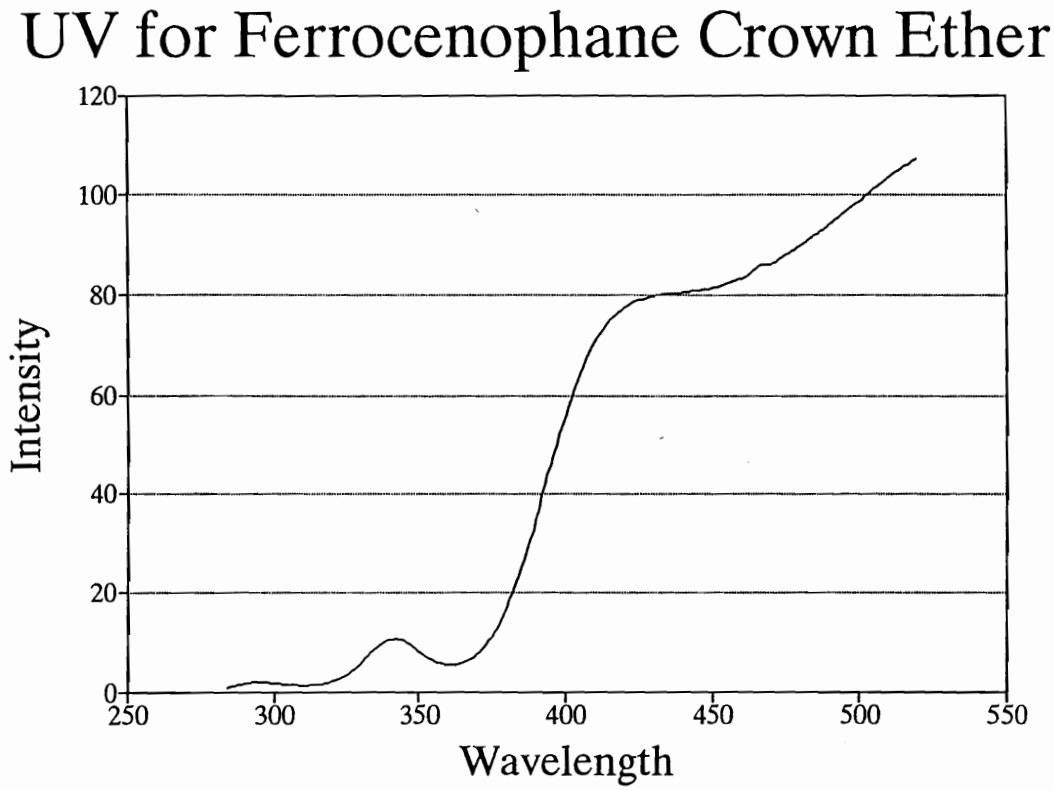

Figure 58. Ultraviolet Transmission Spectrum for Ferrocenophane Crown Ether

of this study. The two structures are contrasted in Figure 59. The absorption values for the [5]ferrocenophane-1,5-dione vary from 465 nm with an electron withdrawing group attached to the bridging linkage to a low of 455 nm due to the electron donating nature of the attached phenyl group. The crown ether for this study possesses an absorption peak at 445 nm. This is consistent with the trend demonstrated by the substituted [5]ferrocenophane-1,5-dione. Combined with the effects of blue-shifting of the absorption peak due to increase in chain length, conjugation of the carbonyl groups, and electron donating properties of the ether linkages found in this study's ferrocenophane of this study, the absorption value of 445 nm provide further evidence for the identification of the synthesized ferrocenophane molecule as that depicted in Figure 53.

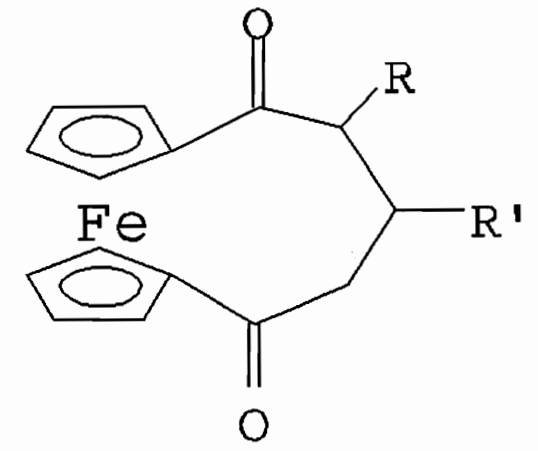

UV Peak Position
(%T) (nm)

465 (R=CH_2OEt,
R'=H)
462 (R=R'=H)
455 (R=H,R'=Ph)

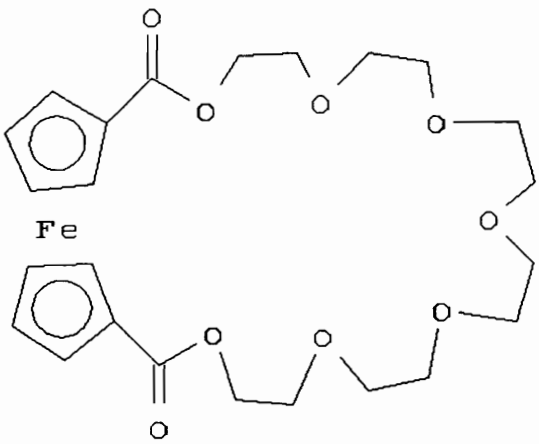

445

Figure 59. UV Spectral Response of Substituted Ferrocenophane Crown Ethers

d) Cyclic Voltammetry

A small quantity of the ferrocenophane crown ether was dissolved in 0.10M solution of tetrabutylammonium perchlorate (TBAP) in methylene chloride. Figure 60 depicts a characteristic cyclic voltammetry scan for the crown ether using platinum counter and working electrodes, and an standard calomel electrode (SCE) as the reference electrode. The sweep rate for the run was 100 millivolts per second. The scale for the voltammegram was expanded and is shown in Figure 61. The half-wave potential $E_{½}$ for the crown ether is 0.9235 volts. Measurement of the peak separation of the forward and reverse waves is 63 millivolts. This is close to the optimal theoretical value of 59 millivolts expected for a one electron electrochemical process. For non-aqueous systems, this value is considered a strong indication of an electrochemically reversible system. This, combined with the equivalent heights of the forward and reverse waves, as well as the symmetry of the waves, indicates the electrochemical process is reversible. Thus, another condition for the model compound is satisfied.

The half-wave potential is much more positive than one would expect for most substituted ferrocene molecules. Toma and Solcaniova[62] studied the effects of the number of carbonyl substituents on the overall potential of oxidation/reduction on a series of bridged ferrocenophane compounds. The potentials are summarized in

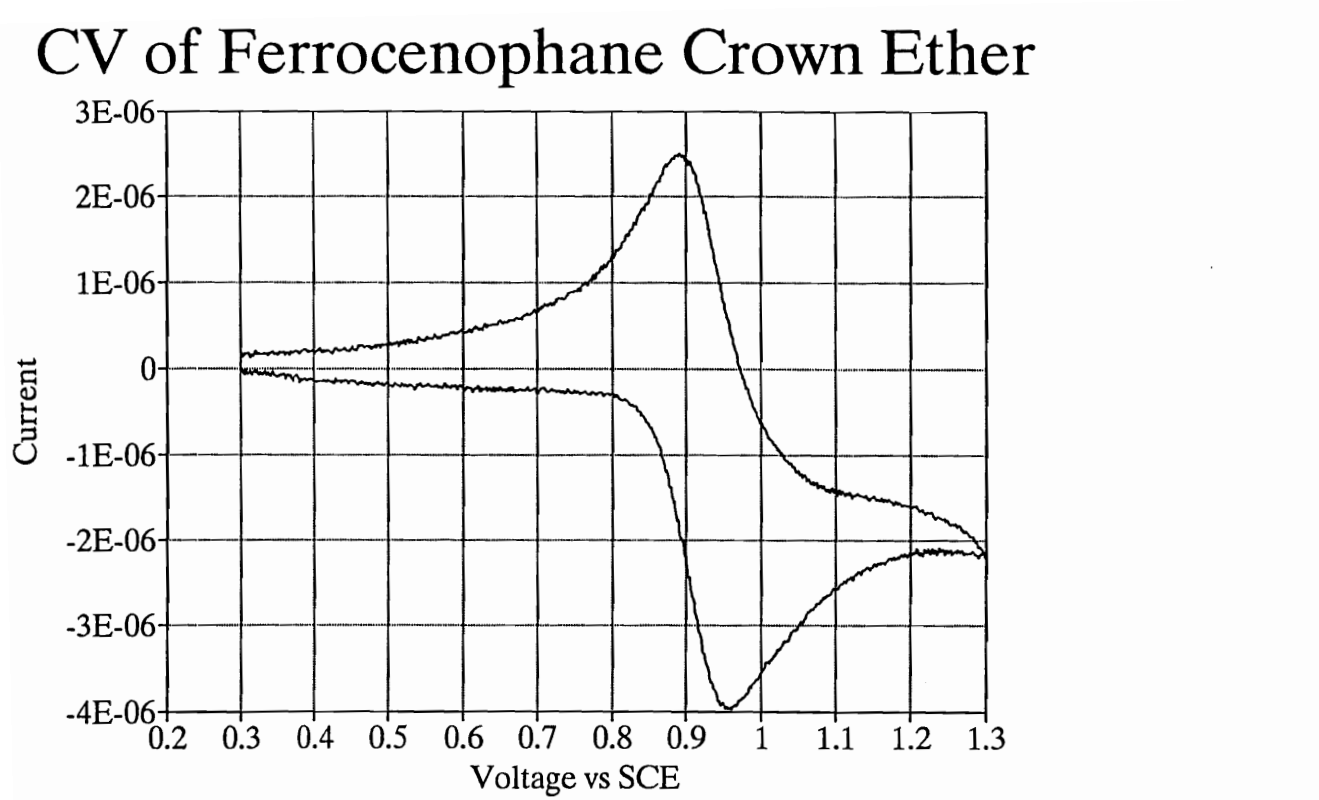

Figure 60. Cyclic Voltammagram for Ferroceneophane Crown Ether

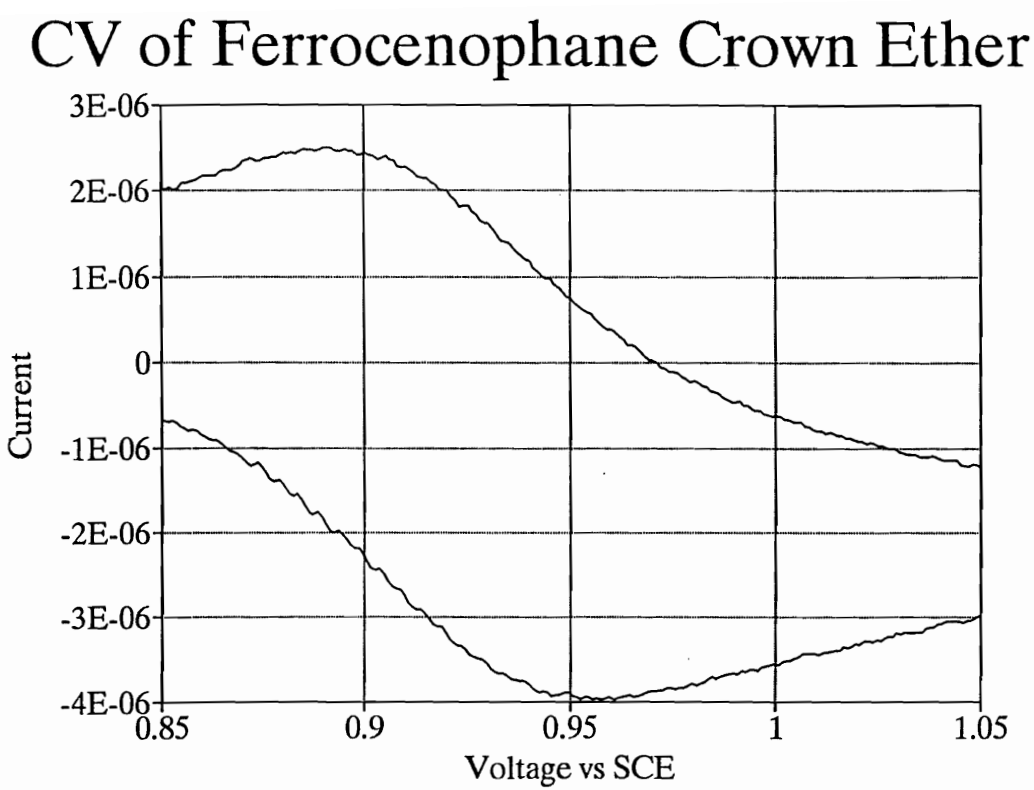

Figure 61. Expanded Cyclic Voltammagram for Ferroceneophane Crown Ether

Figure 62. They noted the half-wave potential increased with the number of attached carbonyl groups. As with the previously mentioned ultraviolet study, the effect of the carbonyl groups manifests itself on the overall oxidation potential of the ferrocene molecule through its π-π interactions with the p-orbitals of the cyclopentadienyl rings of the ferrocene moiety. A value of 921 mv (versus SCE) was reported for the dicarbonyl ferrocenophane. This is consistent with the half-wave potential of 0.9235 mv found for the newly synthesized ferrocenophane crown ether reported here. This correlation with literature values enhances the assignment of the structure for the unknown compound as that depicted in Figure 53.

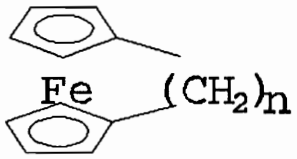

	E 1/2 (mv)
n=3	367
n=4	345
n=5	296

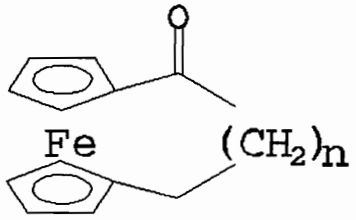

n=2	660
n=3	665
n=4	640

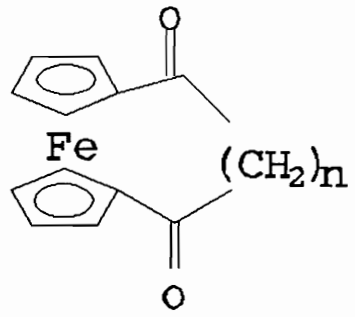

n=1	921
n=2	865
n=3	921

Figure 62. Potential Shifts Due to Addition of Ketone Groups to Ferrocenophanes

4) Conclusions

A previously unreported ferrocenophane crown ether has been synthesized, characterized and identified as the target compound depicted in Figure 53. Instrumental analysis (MS, NMR and UV) verifies the structure, and the cyclic voltammetry demonstrates electrochemical reversibility. Properties specified as essential for that of an ideal model carrier have been satisfied with the exception of selection of an appropriate cation for complexation studies. Suitability of the ferrocenophane crown ether for use as a model carrier compound to test the hypothesis of electrochemical facilitated transport will be addressed in the experimental section.

(B) Design of the Membrane Transport Experiments

As mentioned in the historical section, experimental studies utilizing crown ethers to transport metal ions across a bulk liquid membrane involve the use of a U-shaped experimental cell, and monitors the movement of a metal ion from an aqueous phase of high concentration across the membrane to an aqueous phase of lower concentration. This process will be referred to as Downhill transport (Figure 63). Later experiments, in an effort to mimic nature's ability to concentrate ions within cell membranes, focused on selecting systems where ions are preferentially driven against their concentration gradient to concentrate them on one side of the bulk liquid membrane (Figure 64). These experiments are typified by pH pumped systems where chemical energy in the form of acids or bases is used to concentrate the ion of choice. These experiments will be referred to as uphill transport. To demonstrate the feasibility of electrochemical facilitated transport it must be shown that an electrochemically modifiable carrier molecule can influence the movement of an ion both <u>with</u> (downhill) and <u>against</u> (uphill) it's concentration gradient.

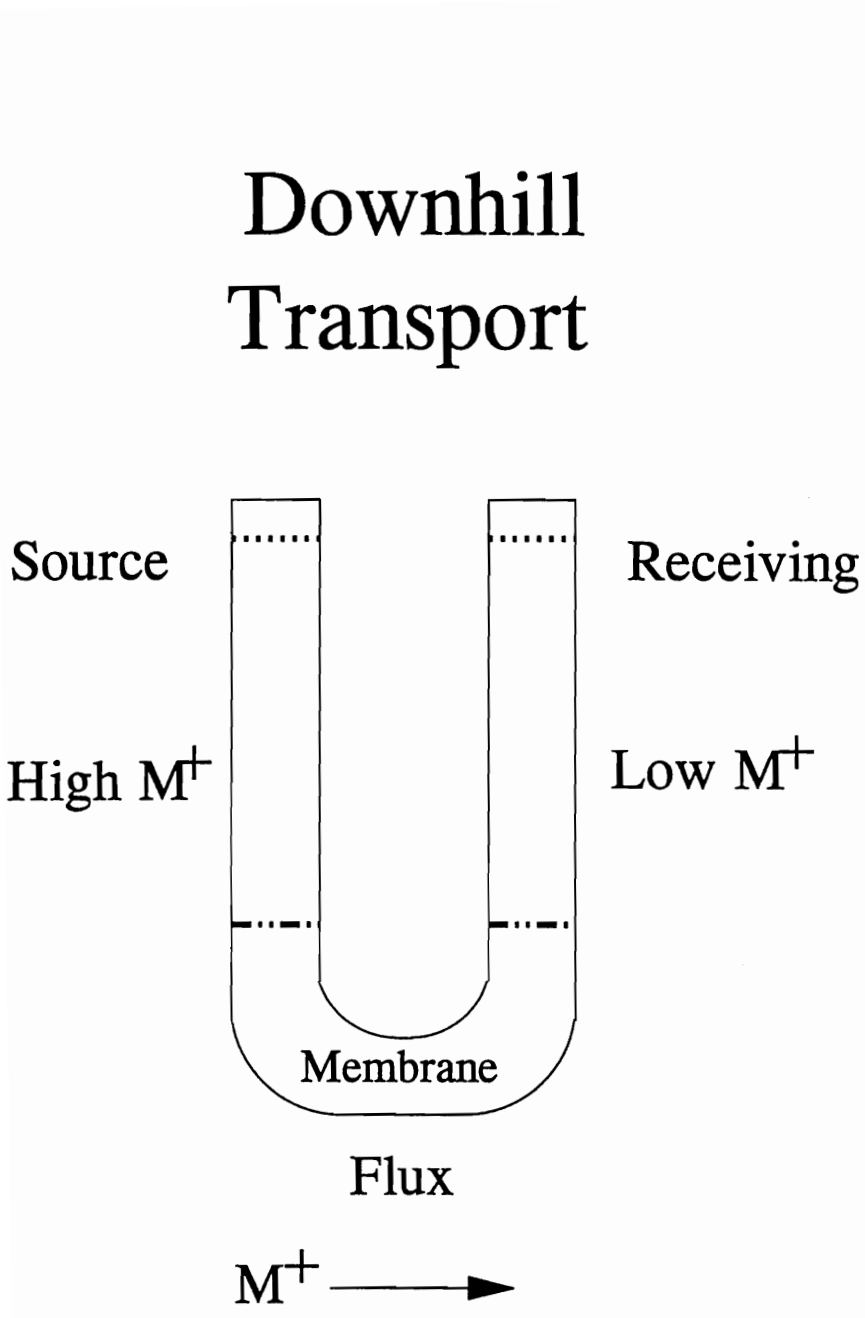

Figure 63. Downhill Transport U-Tube Diagram

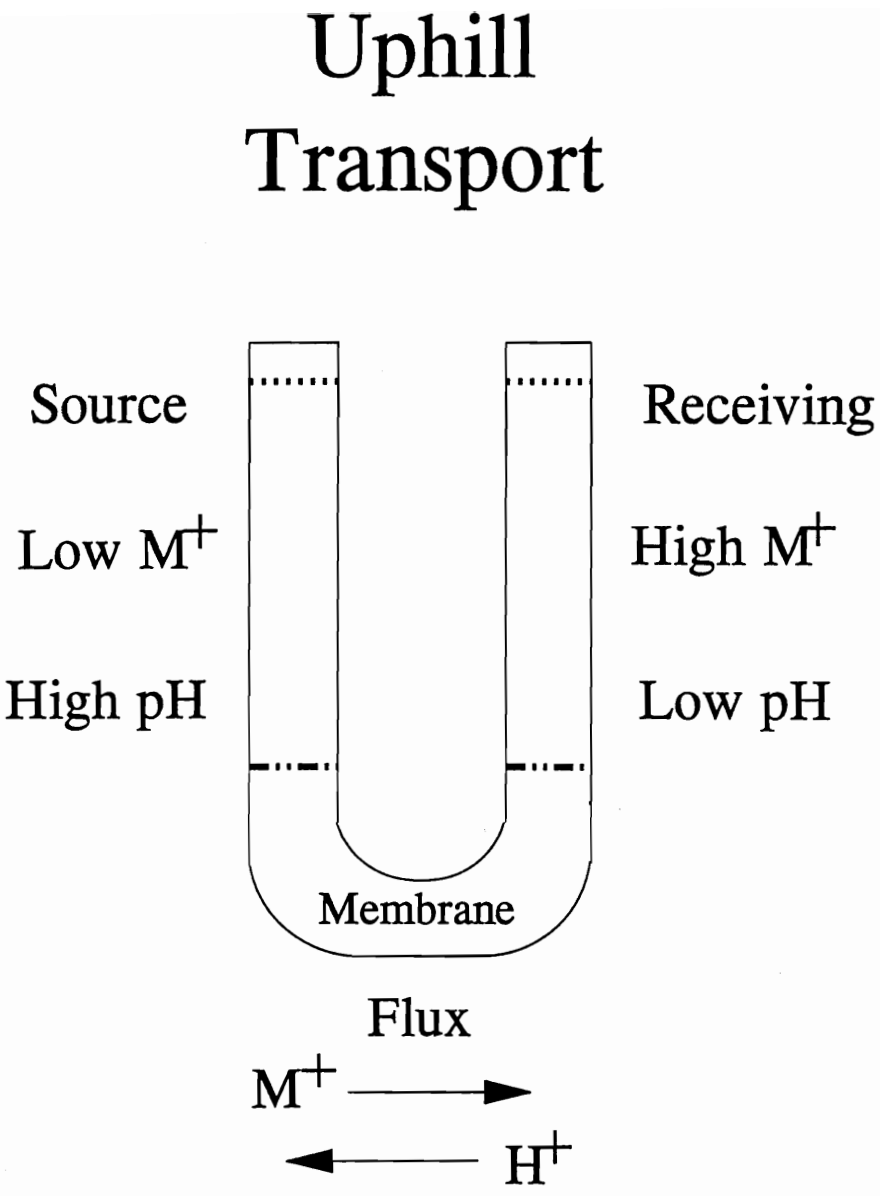

Figure 64. Uphill Transport U-Tube Diagram

1) Downhill

Experimental procedures for downhill membrane transport will closely mirror those studies reported in the literature with the addition of a supporting electrolyte to the membrane phase facilitating the electrochemical conversion of the carrier molecule. An amount of the ion to be studied will be placed in the source phase compartment of the experimental cell and distilled deionized water will comprise the receiving phase. The transport process will be monitored by sampling the receiving phase to determine the presence of the ion carried across the membrane.

Two variations of the downhill experiment will be performed, with the second differing only in the application of controlled potential voltammetry. Performing experiments in this manner illustrates whether electrochemistry can influence the ion complexation ability of the carrier molecule through observing the effect it has on the overall transport rate of the ion across the membrane. A difference in the transport rates between the two experiments will demonstrate that electrochemistry can influence the complexation ability of the ion/carrier system that comprise the transport process.

2) Uphill

The uphill experiment places an equal concentration of the ion to be studied in both aqueous phases. Controlled potential voltammetry is applied to the system and both phases are examined for changes in concentration. Starting with equal ion concentrations offers an analytical challenge not encountered with the downhill experiments. Quantifying the introduction of a small amount of an ion into a solution previously devoid of that ion is inherently easier than detecting the small increase or decrease in concentration of a phase already rich in that ion. To monitor the effects of electrochemical facilitated transport, the concentrations of both aqueous phases will be dilute in the hope that a small change in a relatively small concentration will be more readily measured. Samples from both phases were taken to monitor the movement of ions across the membrane. An increase in one phase accompanied with a decrease in the other demonstrates the viability of electrochemical facilitated transport.

Preliminary conclusions will be drawn during the course of the presentation of the experimental results. The inferences are a straight forward interpretation of the data. Doing so indicates the lessons learned from the current experiment and how those lessons lend themselves to the design of subsequent experiments. The experimental data will be dealt with in a more rigorous manner in the following chapter.

(C) Membrane Transport Experiments

1) Selection of Transport Ion

Several ions commonly used in membrane transport studies were chosen. They are as follows:

- Potassium [K(I)]
- Sodium [Na(I)]
- Lithium [Li(I)]
- Silver [Ag(I)]
- Thallium [Tl(I)]

Downhill and uphill transport experiments were performed utilizing the alkali earth metals with little evidence of electrochemical facilitated transport. While these experiment did little towards establishing the existence of electrochemical facilitated transport, they did afford the opportunity to enhance the skills needed to set up the membrane experiments, take samples, and analyze the metal ion samples by atomic emission spectroscopy. Experiments with silver and thallium ions demonstrated evidence for the transportability of the ions by the ferrocene crown ether. The following experiments will be presented.

(I) Silver Ion

(A) Uphill Membrane Transport

(B) Cyclic Voltammetry

(C) UV Spectroscopy

(II) Thallium Ion

(A) Uphill Membrane Transport

(B) Downhill Membrane Transport

(C) Cyclic Voltammetry

(D) UV Spectroscopy

For each transport experiment, atomic emission spectroscopy was used to determine the concentration of the ions. A three point working calibration curve for each ion was generated from standard solutions spanning the concentration range expected for each ion prior to analysis of the experimental aliquots. This is an accepted procedure. The calibration curve allow the emission readings from the samples to be converted into their corresponding concentration values. Graphs were generated from these values depicting concentration verses time profiles for each experiment.

2) Uphill Silver Ion Transport

The first experiment with the silver ion was chosen to be an uphill transport experiment. The experiment was designed with the following goals:

- Minimize the number of sample aliquots.
- Use dilute silver ion concentration (1.00×10^{-4}M) for the source and receiving phases.
- Achieve a mole ratio of total silver ion close to that of the ferrocene crown ether in the membrane phase.
- Pre-equilibrate membrane and aqueous phases

Prior to the filling of the experimental cell, the membrane and aqueous phases were equilibrated in a separatory funnel. Five ml of a 8.08×10^{-3}M ferrocene crown ether solution (0.1M TBAP/CH_2Cl_2) and 20 ml of a 0.1M TBAP/CH_2Cl_2 filling solution were pipetted into the separatory funnel to yield a total membrane phase volume of 25ml. Thirty five ml of a 1.00×10^{-4}M $AgClO_4$ aqueous solution was added to the separatory funnel and the contents were shaken to equilibrate the methylene chloride and aqueous phases. The phases were allowed to settle and a 1ml aliquot of the aqueous phase was removed from the system for later analysis by atomic emission spectroscopy. The methylene chloride membrane phase was placed

into the experimental cell with the aqueous phase evenly distributed between the two arms of the transport cell. A 0.10M TBAP/CH_2Cl_2 filling solution was introduced into the counter electrode compartments of the experimental cell. Electrodes were positioned in the cell and electrical connections were made to the two controlling potentiostats. Potentials were set to achieve an oxidation current at the receiving phase electrodes and a reduction current at the source phase electrodes. Samples were taken at 2, 6, and 14 hours.

Atomic emission spectroscopy for the determination of aqueous silver ion concentration was performed at the literature suggested wavelength[63] of 328 nm using an air and acetylene flame mixture. A set of secondary standard silver ion solutions were made by dissolving a known weight of silver perchlorate in 100 ml of water in a volumetric flask. Additional solutions were made by serial dilution techniques to form solutions of decreasing concentrations bracketing the range of concentration values expected from the membrane transport studies. Solutions ranging from 9.42×10^{-8} to 2.0×10^{-3} were prepared.

The Buck M200A Atomic Absorption Spectrophotometer was placed into emission mode and was allowed to warm up for at least 30 minutes prior to use to allow stabilization of the machine's electronics. The wavelength of the monochromator was adjusted for optimum response by aspirating silver ion solutions. The signal response was then optimized for 1.00×10^{-4} silver ion through an iterative process of adjustment of the air/acetylene flow rates and ratios, shifting the position

of the flame in reference to the monochromator path, and regulating the voltage of the photomultiplier tube. More dilute solutions were aspirated, and the above parameters were adjusted to allow for concentration determinations spanning at least 2 orders of magnitude. The built-in integration function of the Buck M200A Atomic Absorption Spectrophotometer was used to obtain reproducible, stable solution responses to the aspirated standard solutions. A working calibration curve was made using standard solutions. The concentration and emission readings are shown in Table 7. The calibration curve is shown in Figure 65.

In preparation for to AE analysis, the 1 ml sample volumes were diluted using an Ependorf pipette with an additional 3 ml of distilled deionized water to increase the total sample volume. Increasing the sample volume to 4 ml allowed approximately four integrated readings per sample. The aliquots from the uphill electrochemical transport experiment were subjected to atomic emission analysis. The raw atomic emission data for the silver ion transport study given in Table 8. The aliquot concentration values, from the raw emission data and the working curve, are shown in Table 9. A graph of concentration verses time for the experiment are shown in Figure 66.

Table 7. Uphill Silver Ion Transport
Working Calibration Curve

Concentration Silver Ion	Atomic Emission Readings 1	2	3	4	Average
1.00×10^{-6}	0.121	0.121	0.120	0.119	0.120
1.00×10^{-5}	0.205	0.212	0.215	0.212	0.211
1.00×10^{-4}	1.450	1.466	1.469	1.465	1.463

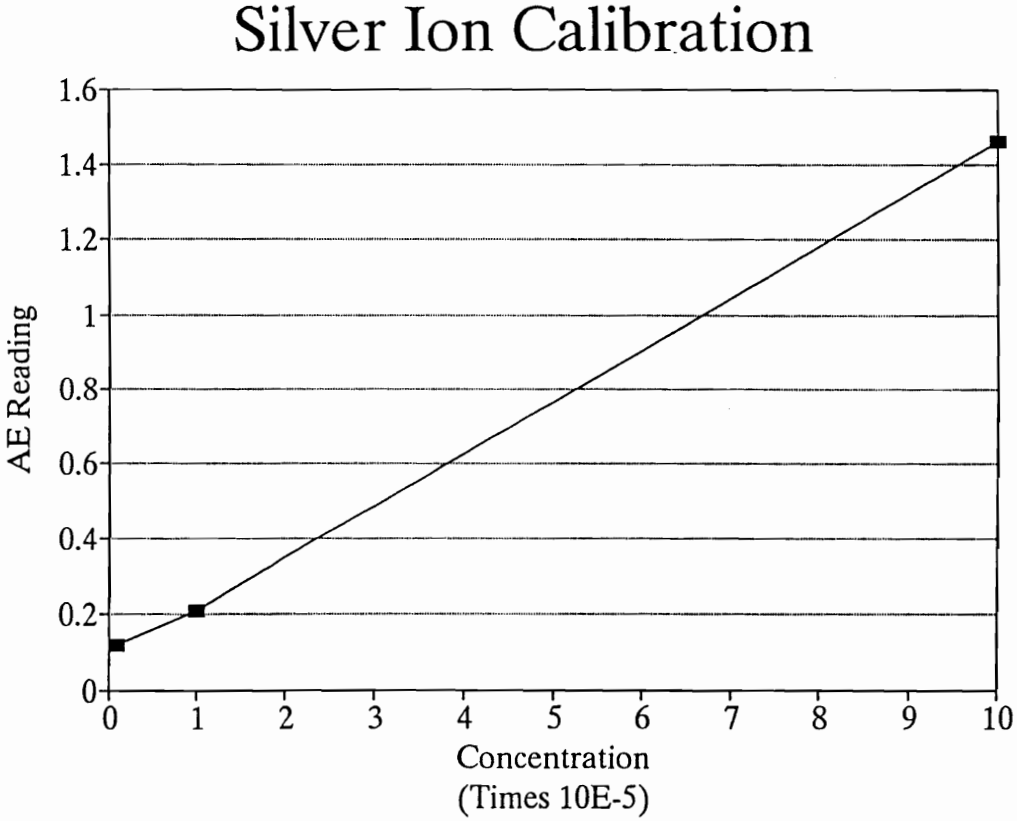

Figure 65. Calibration Curve for Silver (Uphill Pumping Experiment)

Table 8. Uphill Silver Ion Transport (AE Raw Data)

Time					
Source	1	2	3	4	Average
0	0.185	0.194	0.192	0.189	0.190
2	0.187	0.192	0.192	0.189	0.190
6	0.185	0.189	0.186	0.187	0.187
14	0.187	0.185	0.184	0.184	0.185
Receiving					
2	0.209	0.204	0.203	0.205	0.205
6	0.227	0.225	0.224	0.223	0.225
14	0.240	0.231	0.234	0.235	0.235

Table 9. Silver Uphill Transport (Experimental Results)

Time (Hours)	Source Concentration (M)	Receiving Concentration (M)
0	3.17×10^{-5}	3.17×10^{-5}
2	3.16×10^{-5}	3.84×10^{-5}
6	3.04×10^{-5}	4.40×10^{-5}
14	2.97×10^{-5}	4.69×10^{-5}

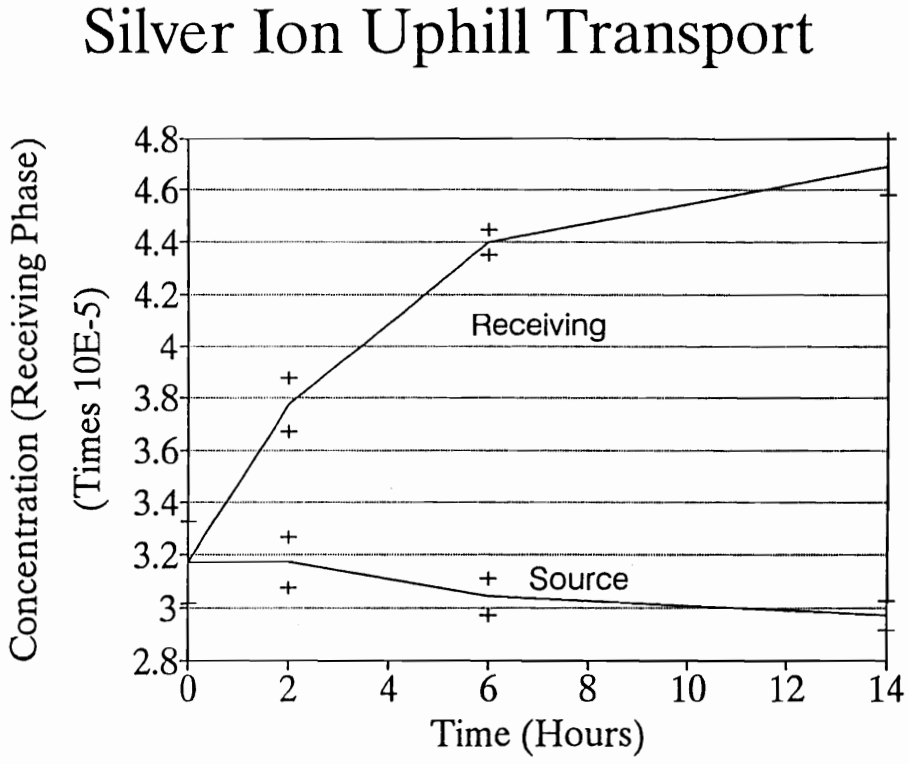

Figure 66. Experimental Data (Silver/Uphill Pumping Experiment)

a) Preliminary Experimental Conclusions

The following observations are made from the experimental data:

1) There is a decrease in the source phase concentration.

2) There is an increase in the receiving phase concentration.

3) Changes in concentration between the source and receiving phase is consistent with behavior expected from the applied electrochemical potentials and that of electrochemical facilitated transport.

4) Concentration in the source and receiving phase with respect to the initial filling solution indicate 70% of the initial aqueous silver ion migrated into the membrane phase. This is consistent with halving the amount of carrier in the membrane phase. A mass balance tracking of the silver ion follows this section.

5) There is formation of an insoluble material in the experimental cell. Cyclic voltammetry and ultraviolet experimental evidence of this side reaction follows the mass balance section.

b) Mass Balance for the Silver Ion

Examination of the sample aliquots of the source and receiving phases of the experimental transport cell show a significant decrease in the amount of aqueous silver ion present in both source and receiving phase sample aliquots compared with that of the initial filling solution. The silver ion transport study was constructed to equilibrate the membrane and aqueous phases prior to the start of the transport study and sample the aqueous phase before starting the controlled potential portion of the experiment. Measuring the concentration of the aqueous silver ion phase before and after equilibration makes it possible to measure a distribution coefficient for the system. By iterative calculations one can track the number of moles of silver ions as they move from one aqueous phase through the membrane and into the other aqueous phase.

The extraction coefficient for the system is defined as

$$K_{Ag} = \frac{[Ag]_{Aq}}{[Ag]_{Org}}$$

From the initial sample aliquot removed from the system directly after equilibration of phases in a separatory funnel, an aqueous silver ion concentration of 3.17×10^{-5} M was determined. Considering the concentration of the initial silver ion filling solution of 1×10^{-4}, the silver ion concentration in the membrane phase is 9.562×10^{-5}M and

the extraction coefficient for the system is 0.332. The membrane phase extracted roughly 75% of the available aqueous silver ion. The measured extraction coefficient is comparable with values reported in the literature for crown ethers of similar ring size and geometry.[64] A more thorough examination of extraction and complexation will be presented.

With the initial conditions established, the number of moles in each phase for each successive aqueous sample were calculated. The amount of material in each phase at the time of the sampling was used with the following mass balance equation to determine the amount of material in the membrane phase.

$$Total\,Ag = Ag(Src.) + Ag(Rec.) + Ag(Mem.) - Ag(AE\,Aliquots)$$

The total number of moles in the transport system is equal to the measured number of moles in each aqueous phases, less the number of moles removed from the aqueous layers as sample aliquots, plus the number of moles in the membrane phase. Using the mass balance, one calculates the number of moles in the membrane phase at the time of sampling by using the total number of moles in the system from the last set of measurements combined with the number of moles in each aqueous phases from the current measurements. The initial concentration of material in the membrane phase is determined using the concentration and amount of the aqueous filling solution combined with the t=0 aliquot for the aqueous phases. This process is repeated for

the remaining samples. This iterative process for tracking the number of moles in each phase of the experimental system was implemented using the Quattro Pro (Ver. 3.0) spread sheet.

Table 10 shows collated output of the spreadsheet calculations and presents the number of millimoles in each phase with respect to time. The overall decrease in the total number of moles in the system is due to the removal of silver ion by the sampling process. Several graphical representation of the data in Table 11 are given in the following Figures. Figure 67 shows the number of moles in both aqueous and membrane phases. Expanding the scale in Figure 68 to look at only the number of moles in the source and receiving phase, it can be seen that the number of moles in the receiving phase does indeed increase, while at the same time the number of moles in the source phase decreases.

Table 11 represents the data in Table 10 in terms of its mole percent with respect to the entire system. Using mole percentages as the criterion for plotting graphs yields similar results to the previous treatment. In Figure 69, it can be clearly seen that 70% of the total system moles of silver ion reside in the membrane phase and is consistent with the extraction coefficient calculated earlier. Enlarging the scale of the graph previous graph (Figure 70) shows the same trends of increasing concentration in the receiving phase and decreasing concentration of the source phase that is indicative of electrochemical facilitated transport. Examining the amount of

Table 10. Millimoles Mass Balance

Time Hours	Source x 10^{-4}	Receiving x 10^{-4}	Membrane x 10^{-4}	Total x 10^{-4}
0	5.38	5.38	23.92	35.68
2	5.05	6.136	22.80	34.68
6	4.56	6.59	22.79	33.94
14	4.16	6.57	22.45	33.17

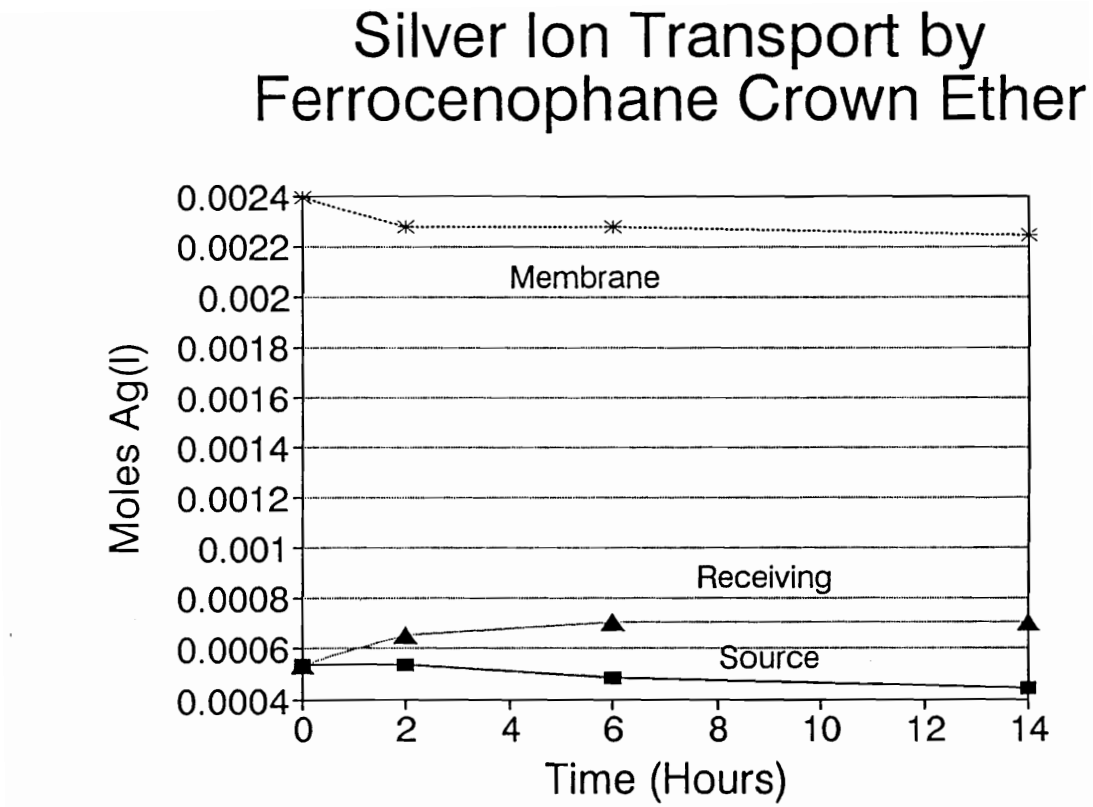

Figure 67. Millimoles Silver (All)

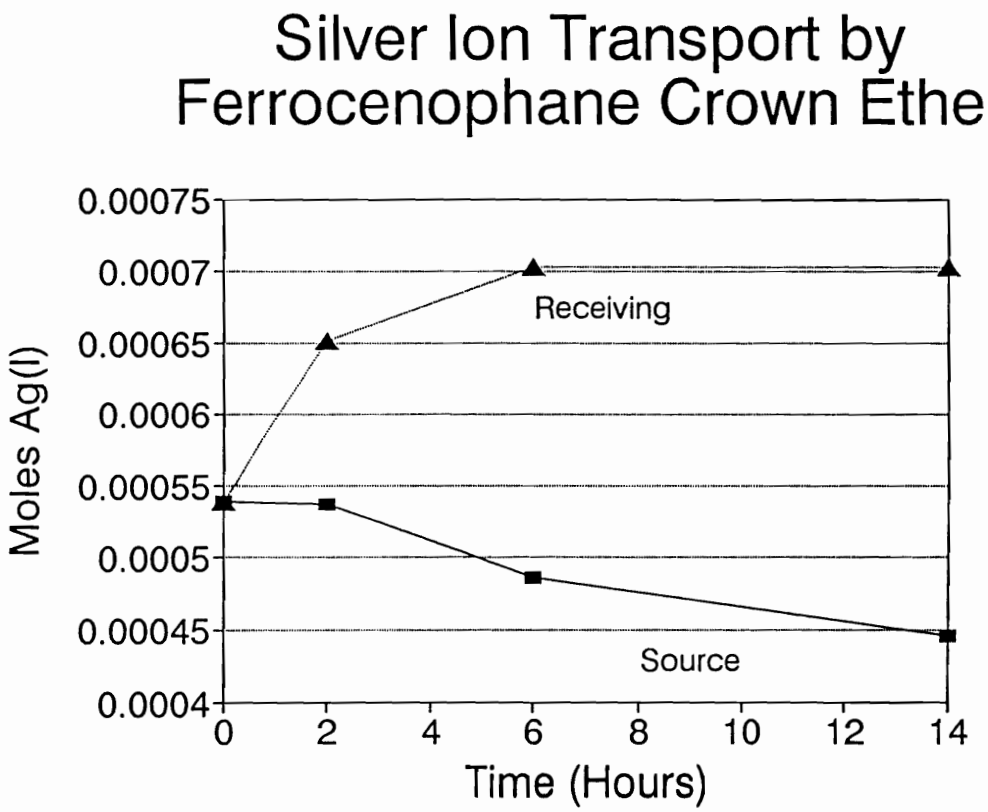

Figure 68. Millimiles Silver (Aqueous)

Table 11. %Moles Mass Balance

Time Hours	Source	Receiving	Membrane
0	15.52	15.52	68.95
2	15.47	18.80	65.73
6	14.01	20.28	65.71
14	13.12	20.73	66.15

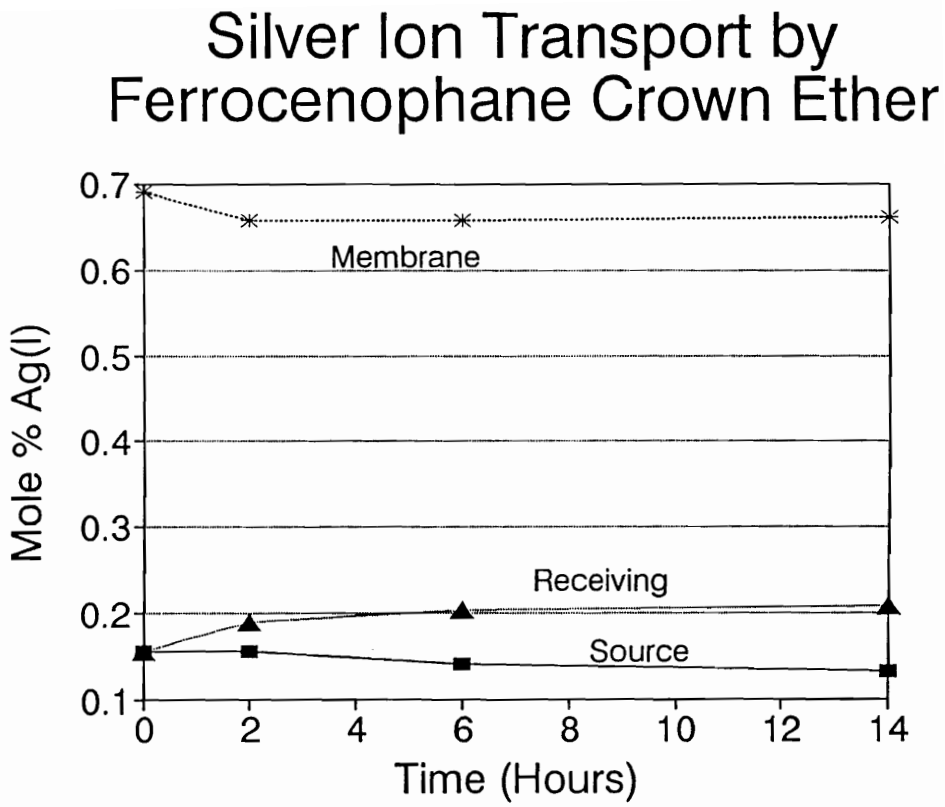

Figure 69. %Moles Silver (All)

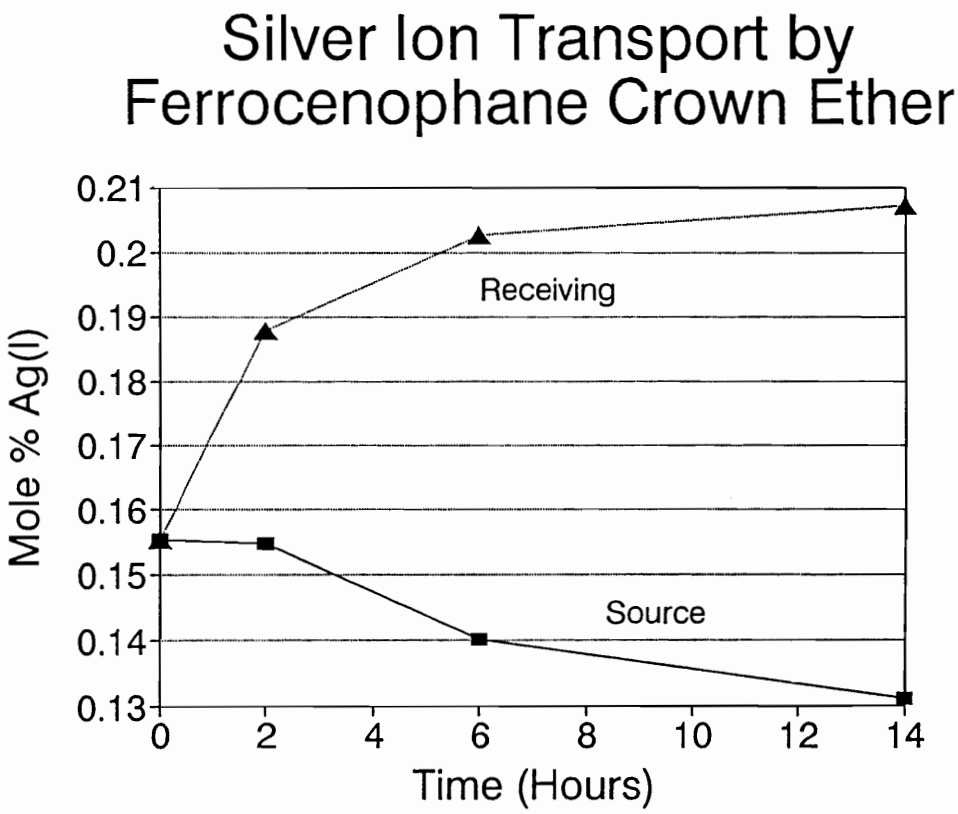

Figure 70. %Moles Silver (Aqueous)

material in the membrane phase in the graphs of Figures 67 and 69 shows that the number of moles contained in the membrane phase also decreases. The decrease in the number of moles in the membrane phase is consistent with the premise that oxidation of the carrier molecule decreases the crown ether's ability to complex with the silver ion. The silver ion system demonstrates the feasibility of electrochemical facilitated transport.

As mentioned earlier, an insoluble material was noted to form during the later stages of the transport experiment. This by-product is attributed to the chemical oxidation of the carrier molecule by the silver ion. The results of cyclic voltammetry and UV spectroscopic experiments will now be presented.

c) Cyclic Voltammetry of the Silver System

A series of cyclic voltammetry experiments were conducted over time. Cyclic voltammegrams for the ferrocene crown ether before and after addition of aqueous silver ion to the methylene chloride/TBAP/ferrocene crown ether system were measured. The intent of the experiments was to provide qualitative information as to the stability of the membrane phase containing the ferrocene crown ether in contact with the aqueous silver ion. To simulate conditions found in the membrane transport experiment the following experiment was performed. A small portion of ferrocene

crown ether was added to an electrochemical cell containing 10 ml of a 0.1M TBAP/CH_2Cl_2 filling solution. Platinum working and counter electrodes were used with an SCE serving as the reference electrode. Cyclic voltammetry experiments were performed. Previous CV characterization of the crown ether/electrolyte system showed the system to be stable over time.

A small portion of an aqueous silver perchlorate solution was added to the electrochemical cell and the system was stirred briefly. A CV was recorded with additional ones measured at 6 and 24 hours with respect to the addition of the silver ion. The resulting voltammegrams are shown in Figure 71-73 with Figure 74 showing all 3 spectra on one graph for ease of comparison. Examination of the voltammegrams showed a small distortion of the waveform at 6 hours with major distortions at the 24 hour mark. This distortion of the electrochemical waveform supports the hypothesis that the silver ion oxidizes the crown ether. The minimal degradation during the first hours of the experiment gives credence to the use of the silver ion data as validation of the concept of electrochemical facilitated transport.

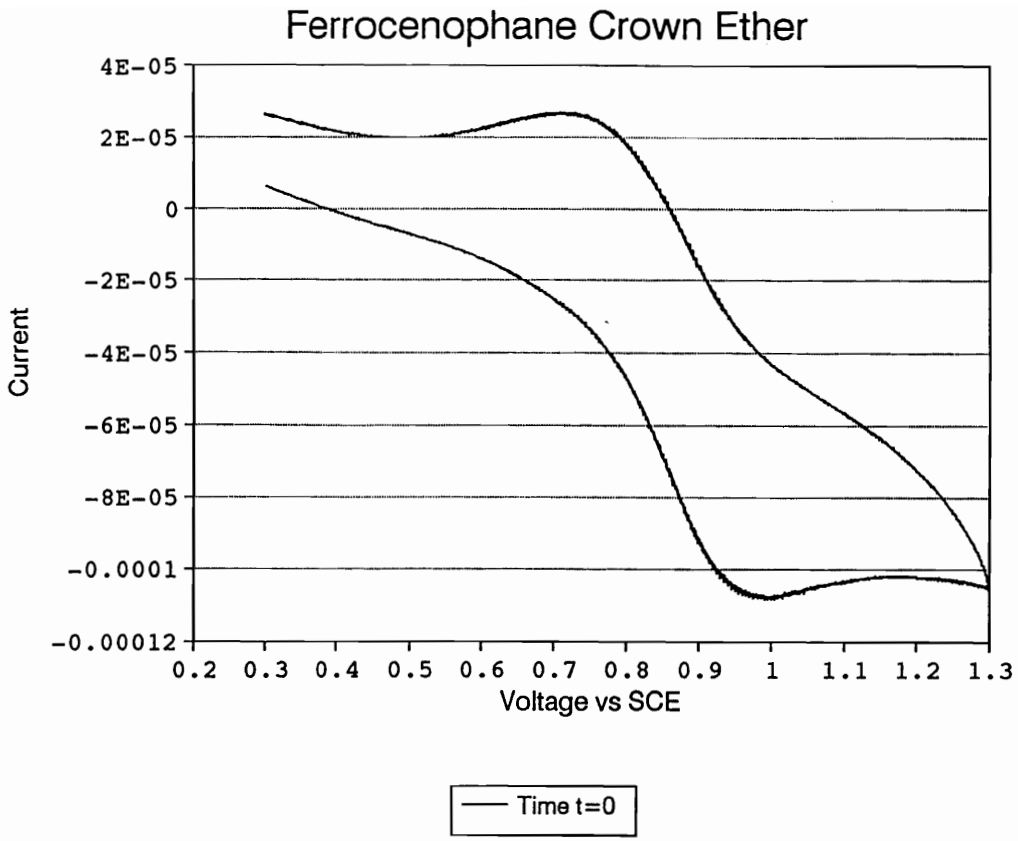

Figure 71. CV Ferrocenophane (Time = 0)

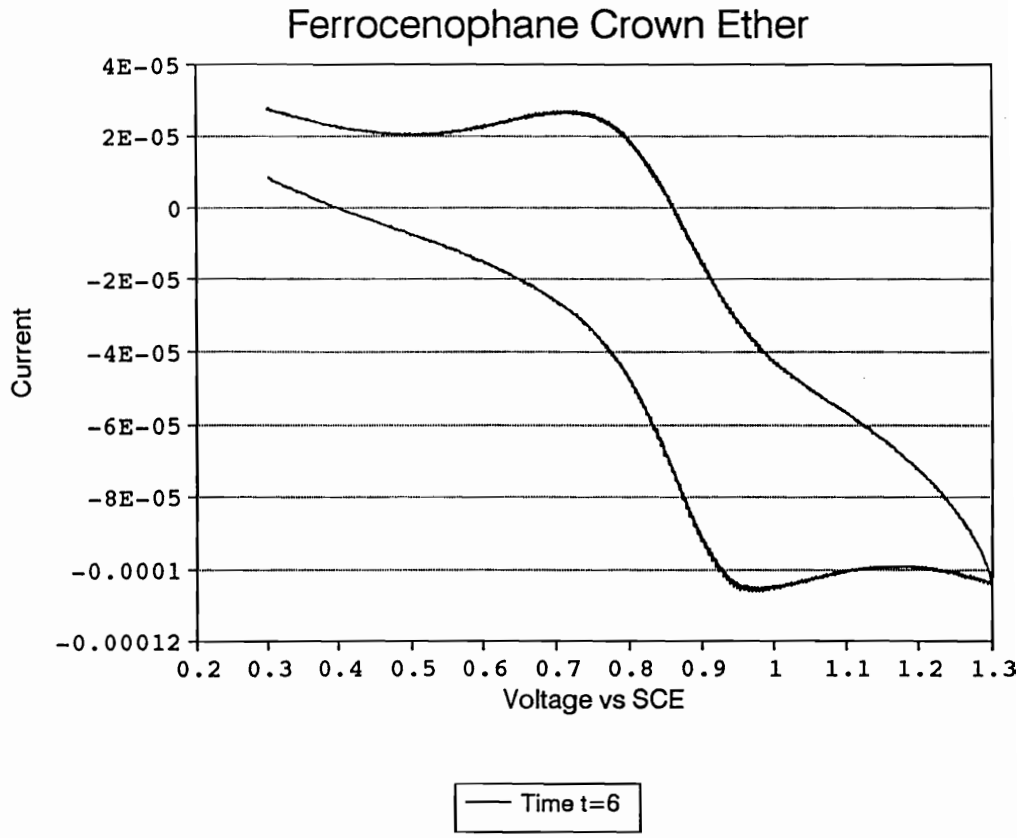

Figure 72. CV Silver Addition (Time = 6)

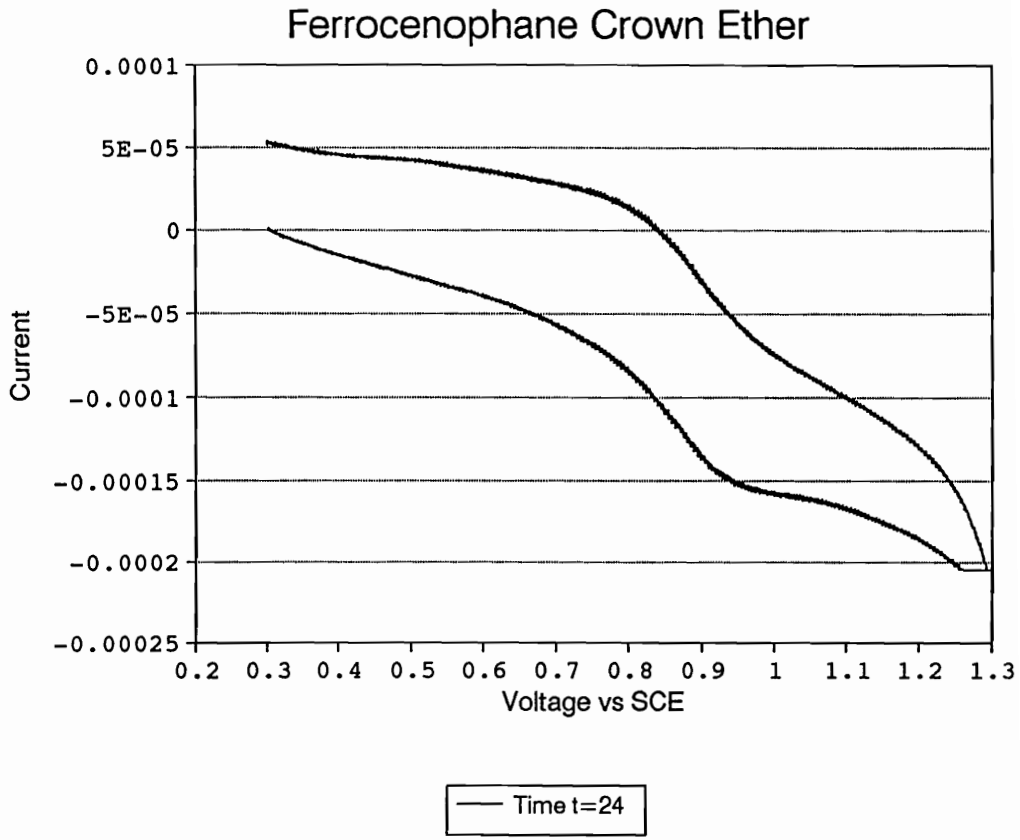

Figure 73. Silver Addition (Time = 24)

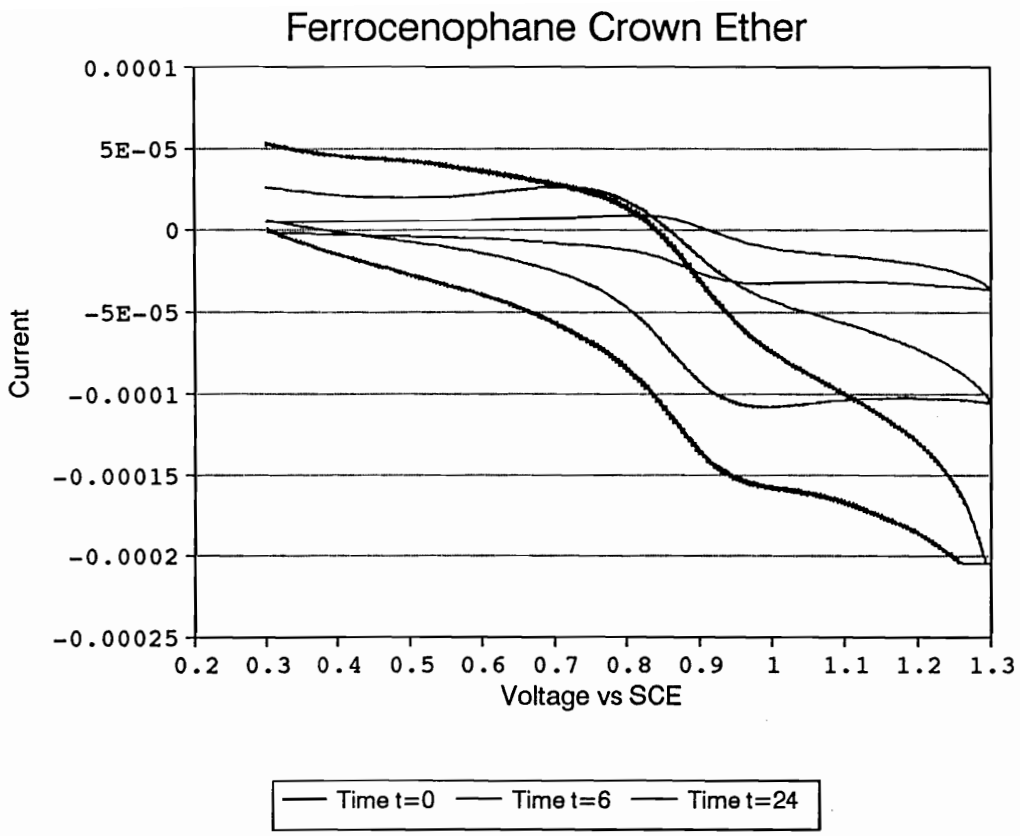

Figure 74. CV Silver Addition (Combined)

d) UV Evidence for the Silver Ion System

UV spectra for the ferrocene crown ether was performed on a Perkin Elmer Ultraviolet Spectrophotometer. A sample of the ferrocene crown ether in the methylene chloride/TBAP electrochemical filling solution was placed in the sample cuvette with the reference cuvette containing methylene chloride/TBAP solution. The cells were placed in the instrument and several spectra were collected to monitor the stability of the ferrocene crown ether solution upon exposure to UV radiation. The system was found to be stable with respect to time as shown by the repetitive wave forms shown in Figure 75.

To the sample cuvette, a small portion of aqueous silver perchlorate solution was carefully floated on top of the methylene chloride phase taking care not to wet the sides of cuvette in the area of the UV beam path. Spectra were taken with respect to time with the results shown in Figure 76. The signal for the ferrocene crown ether decreased with time after addition of the silver ion. An insoluble film similar to that noticed in the electrochemical membrane transport experiments formed at the interface of the two liquids as the experiment progressed. These results, complemented by those of the cyclic voltammetry experiments, demonstrate that silver ion attacks on the crown ether manifest themselves during the later experimental time frames.

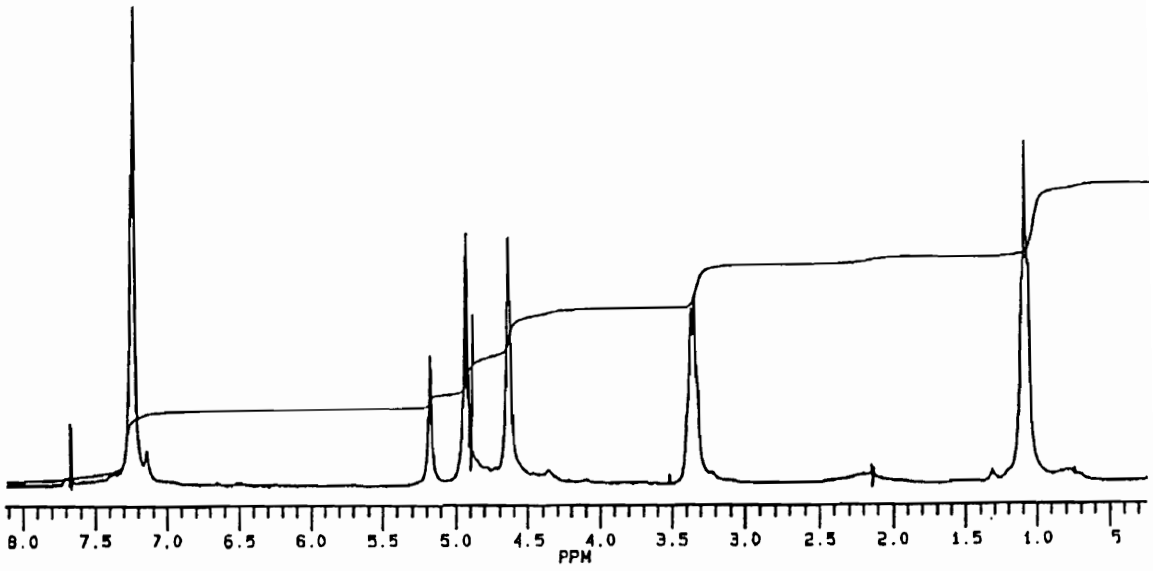

Figure 57. Proton NMR Spectrum for Ferrocenophane Crown Ether

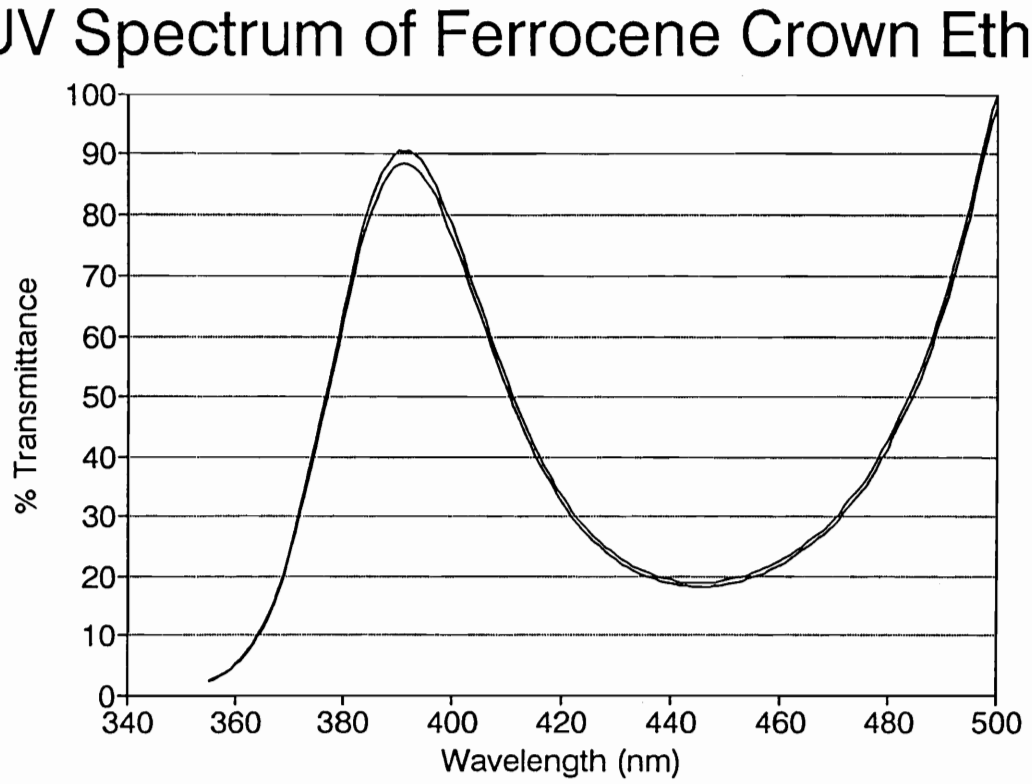

Figure 75. UV Spectrum of Ferrocenophane

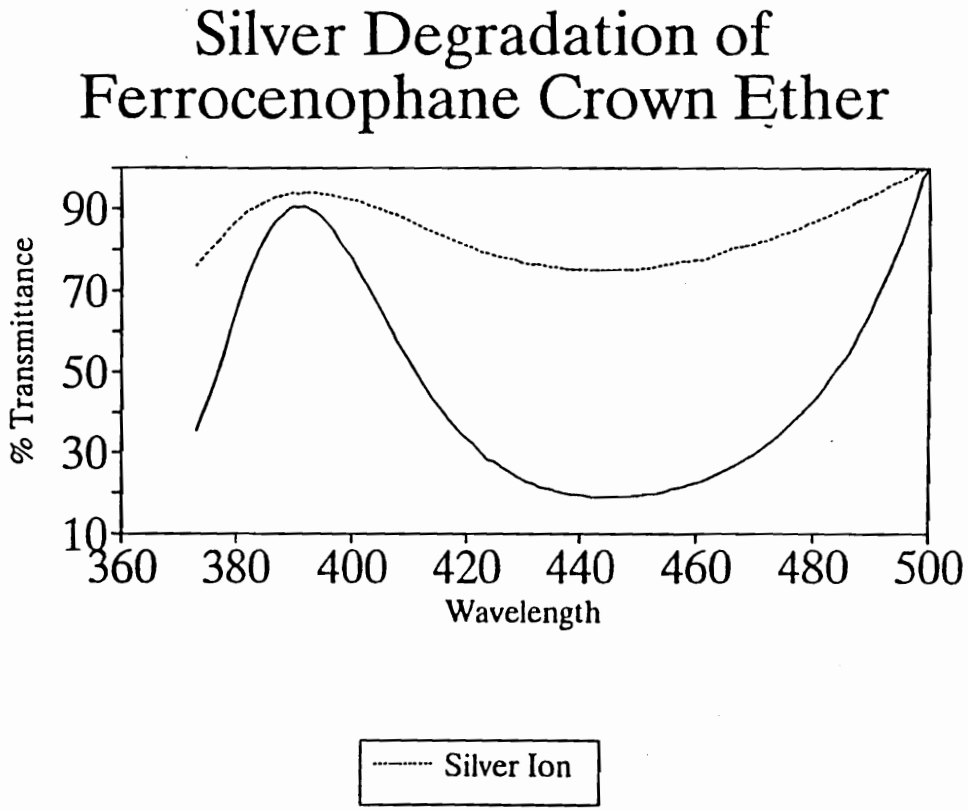

Figure 76. UV Spectrum of Ferrocenophane (Silver Degradation)

e) Evaluation of the Silver Ion System

The silver ion/ferrocene crown ether system demonstrates experimental results validating the concept of electrochemical facilitated transport. The uphill electrochemical pumped experiments shows the ability of the system to move ions against its concentration gradient by means of electrochemically altering the complexation ability of the carrier molecule. This is evidenced by noting the decrease in the source phase accompanied with increases in the receiving phase. One might argue the conclusions based on the experimental evidence is biased due to the formation of degradation product from the silver oxidation of the carrier molecule. This point was considered and can explain an increase in the concentration of the receiving phase due the release of complexed silver ions from the membrane phase as a chemically irreversible oxidation of the carrier molecule takes place releasing the silver ion into the nearest aqueous phase. But, it does not explain the decrease in concentration of the source phase. If chemical oxidation alone were responsible for the increase in the receiving phase concentration, the source phase would, by the same argument, also see an increase.

To further validate the concept, the thallium (I) ion was chosen for study since its physical properties are close to those of silver, but it does not possess silver's strong oxidation characteristics.

3) Uphill Thallium Ion Transport

The experimental cell was filled in accordance with the procedure outlined earlier. Ten ml of an 8.08 x 10^{-3}M ferrocene crown ether solution (0.1M TBAP/CH_2Cl_2) and 15 ml of a 0.1M TBAP/CH_2Cl_2 solution were pipetted into the experimental cell forming a membrane phase of 25ml. Fifteen ml of a 1.00 x 10^{-2}M TlCl aqueous solution was added each arm of the experimental cell. The phases were allowed to equilibrate for one hour, and a 1ml aliquot of each aqueous phase was taken for later analysis by Atomic Emission Spectroscopy. A 0.10M TBAP/CH_2Cl_2 filling solution was introduced to the counter electrode compartments of the experimental cell. Electrodes were positioned in the cell, and electrical connections were made to the two controlling potentiostats. Potentials were set to achieve an oxidation current at the receiving phase electrodes, and a reduction current at the source phase electrodes. Samples were taken with respect to time.

Determination of aqueous thallium ion concentration was performed at the literature suggested wavelength of 535nm using an nitrous oxide and acetylene flame mixture. Nitrous oxide/acetylene was chosen over air/acetylene to improve the limit of detection and linearity range of the thallium ion emission response. A set of secondary standard thallium ion solutions were made by dissolving a known weight of thallium chloride in 100 ml of water in a volumetric flask. Additional solutions were made by serial dilution techniques to form solutions of decreasing concentrations to

bracket the range of concentration values expected from the membrane transport studies. Solutions ranging from 1.0 x 10^{-7}M to 0.010M were made.

The atomic emission spectrometer was allowed to warm up for at least 30 minutes prior to use to allow the electronics to equilibrate. Wavelength response of the monochromator was adjusted for optimum response by aspirating standard thallium ion solutions. The signal response was then optimized for 0.01M thallium ion adjusting the nitrous oxide/acetylene flow rates and ratios to achieve a symmetrical flame. Flame position and the photomultiplier tube voltage were optimized for thallium. The integration function of the Buck Spectrophotometer was utilized to maintain reproducibility of solution response. A working calibration curve was made. The calibration data is shown in Table 12 and the calibration curve is shown in Figure 77.

The 1 ml sample aliquots taken from the uphill electrochemical experiment were diluted by Ependorf pipette to a total volume of 4 ml prior to AE analysis. The samples were subjected to atomic emission analysis after data values for the working calibration curve were obtained. The raw atomic emission data for the thallium ion transport study samples are given in Table 13. From the working curve for the experiment, the raw emission data values yield the concentration values listed in Table 14. A graph of concentration verses time for the experiment is shown in Figure 82.

Table 12. Uphill Thallium Ion Transport
Working Calibration Curve

Concentration Thallium Ion	Atomic Emission Readings 1	2	3	4	Average
0.000	-0.388	-0.395	-0.399	-0.401	-0.396
2.00×10^{-4}	-0.249	-0.250	-0.248	-0.250	-0.250
1.00×10^{-3}	0.332	0.340	0.339	0.347	0.340
2.00×10^{-3}	0.891	0.898	0.883	0.890	0.891

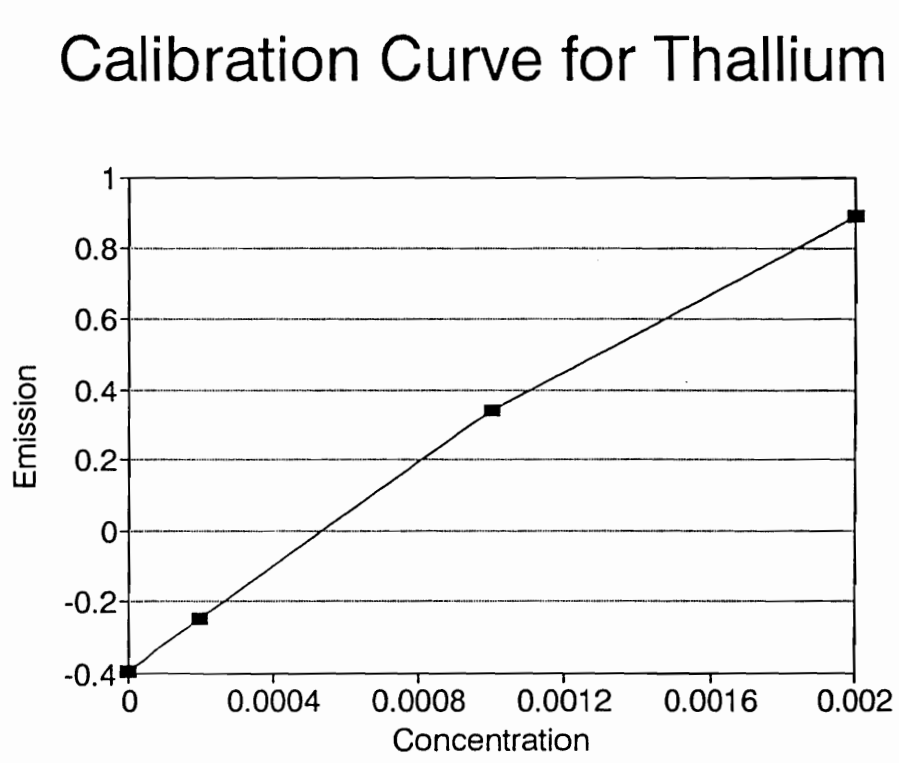

Figure 77. Calibration Curve for Thallium (Uphill Pumping Experiment)

Table 13. Uphill Thallium Ion Transport (AE Raw Data)

Source	Atomic Emission Reading				
Time	1	2	3	4	Average
0	0.364	0.374	0.373	0.371	0.371
6	0.367	0.367	0.367	0.367	0.367
12	0.339	0.341	0.341	0.340	0.340
Receiving					
0	0.370	0.370	0.366	0.367	0.368
6	0.396	0.399	0.397	0.397	0.397
12	0.501	0.507	0.508	0.505	0.505

Table 14. Thallium Ion Uphill Transport (Experimental Results)

Time (Hours)	Source Concentration (M)	Receiving Concentration (M)
0	4.22×10^{-3}	4.21×10^{-3}
2	4.20×10^{-3}	4.42×10^{-3}
6	4.00×10^{-3}	5.20×10^{-3}

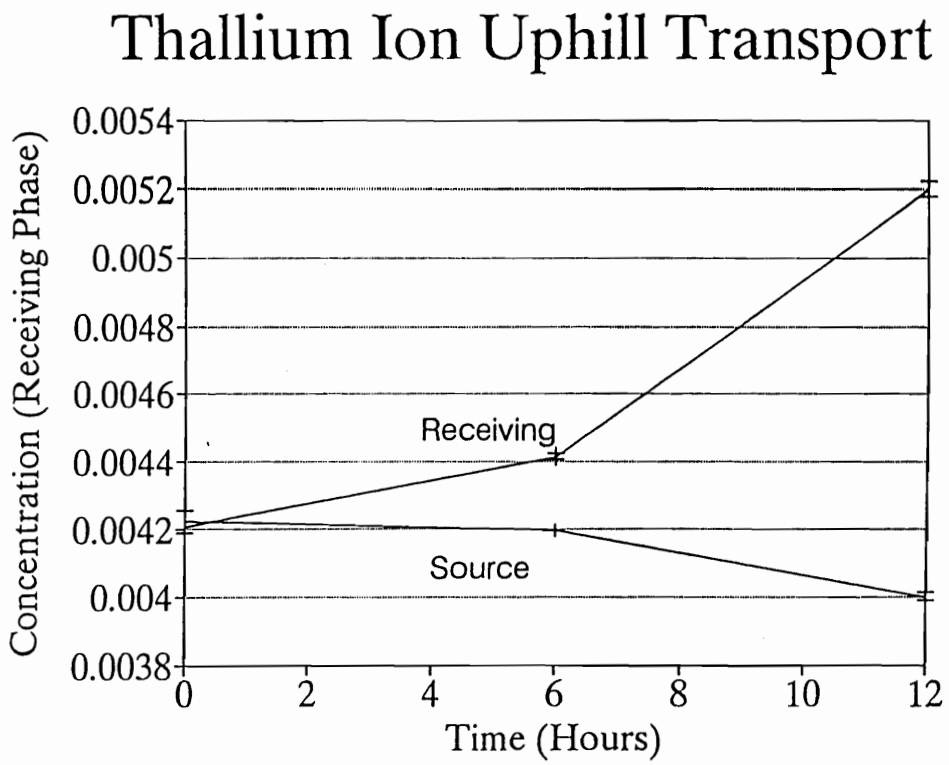

Figure 78. Experimental Data (Thallium Uphill Pumping Experiment)

a) Preliminary Experimental Conclusions

The following observations are made from the experimental data:

1) There is a decrease in the source phase concentration.

2) There is an increase in the receiving phase concentration.

3) Changes in concentration between the source and receiving phase is consistent with behavior expected from the applied electrochemical potentials and that of electrochemical facilitated transport.

4) Concentration in the source and receiving phase indicate over 55% of the initial aqueous thallium ion migrated into the membrane phase. Mass balance for the experiment follows.

5) Unlike the silver ion experiments, there is no observable formation of extraneous materials in the experimental cell. Ultraviolet experiments demonstrated the carrier molecule was not oxidized by the thallium ion.

b) Mass Balance for the Thallium Ion

As with the silver ion, examination of the aliquots from the source and receiving phases of the experimental transport cell shows a significant amount of aqueous thallium ion moved into the membrane phase. After the equilibration period and prior to initiation of the controlled voltammetry portion of the experiment, a 1 ml aliquot from both the source and receiving phases were sampled to measure the initial starting condition. Measuring these values, a distribution constant for the system was obtained. The extraction coefficient for the system is defined as:

$$K_{Tl} = \frac{[Tl]_{Aq}}{[Tl]_{Org}}$$

The initial sample aliquots yielded aqueous thallium ion concentration of 4.22×10^{-3}M and 4.21×10^{-3}M for the source and receiving phases respectively. Factoring in the initial concentration of the thallium filling solution of 0.01M yields the total millimoles of thallium ion in the membrane phase to be 0.174 millimoles. The calculated extraction coefficient for the experiment is 0.601.

Once the initial conditions are established, the number of moles in each phase be calculated. Similar to the silver ion, the total number of moles of thallium in the system represented by:

$$Total\ Tl = Tl(Src.) + Tl(Rec.) + Tl(Mem.) - Tl(AE\ Aliquots)$$

The total number of moles in the transport system is equal to the measured number of moles in each aqueous phases, less the number of moles removed from the aqueous layers as sample aliquots, plus the number of moles in the membrane phase. Using the mass balance, one calculates the number of moles in the membrane phase by using the total number of system moles from the last set of measurements and the number of moles in both aqueous phases from the current measurements. The number of moles in the membrane phase at the time of the sampling may be determined. This iterative process is repeated for the remaining sample values. The iterative process tracking the number of moles in each phase of the experimental system was implemented in a Quattro Pro (Ver. 3.0) spread sheet. Table 15 summarizes the output of the spreadsheet calculations in terms of the number of millimoles in each phase with respect to time. The decrease in the number of moles in the entire system is due to the removal of thallium ion by the sampling process. The millimoles in each phase are shown in Figure 79. Examining only the aqueous phases (Figure 80) one sees the now familiar trends of increasing receiving phase and decreasing source phase concentrations found in other concentration plots.

Examining the data in terms of mole percentages is shown in Table 16. The graph for the mole percent thallium for both aqueous and membrane phases with respect to time is shown in Figure 81. Examining the graph shows the bulk of the material resides in the membrane phase and is consistent with the extraction portion of

Table 15. Millimoles Mass Balance for Thallium

Time Hours	Source	Receiving	Membrane	Total
0	0.0633	0.06315	0.17355	0.3000
6	0.0588	0.06181	0.17096	0.29157
12	0.0520	0.0676	0.16336	0.28296

Uphill Transport of Thallium

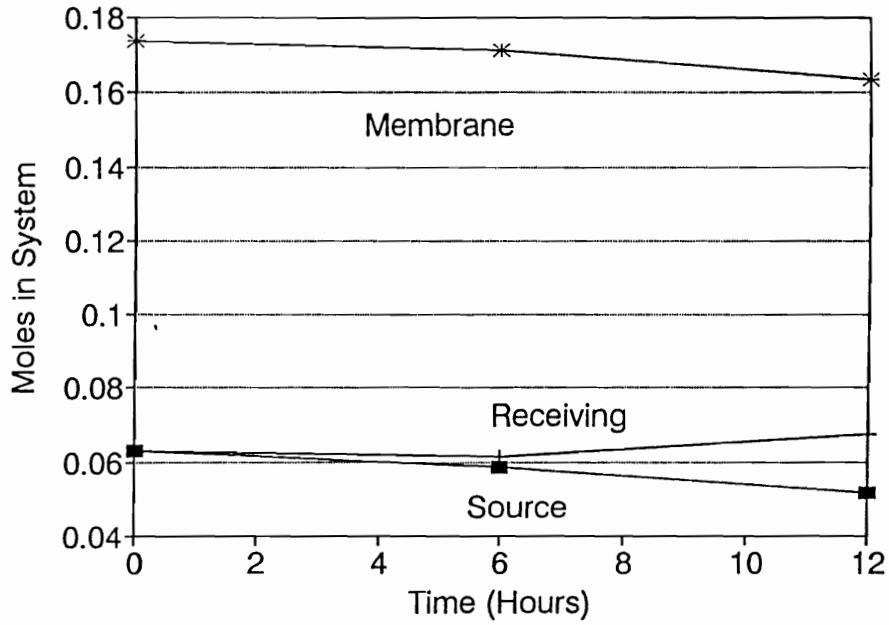

Figure 79. Millimiles Thallium (All)

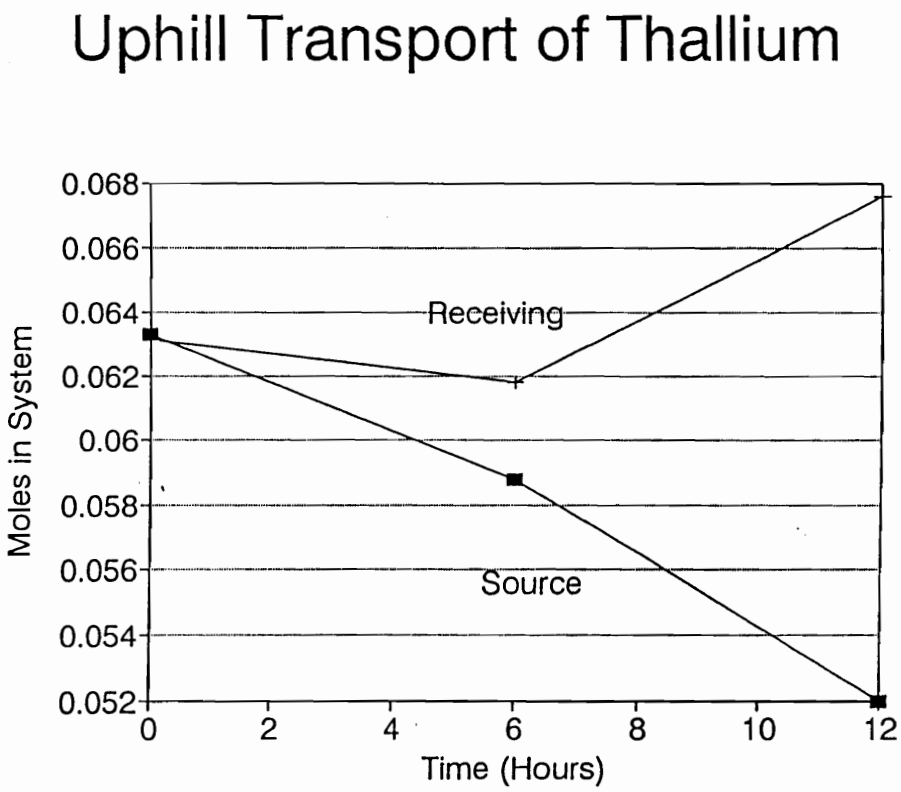

Figure 80. Millimoles Thallium (Aqueous)

Table 16. %Moles Mass Balance for Thallium

Time Hours	Source	Receiving	Membrane
0	21.10	21.05	58.85
6	20.17	21.20	58.63
12	18.38	23.89	57.73

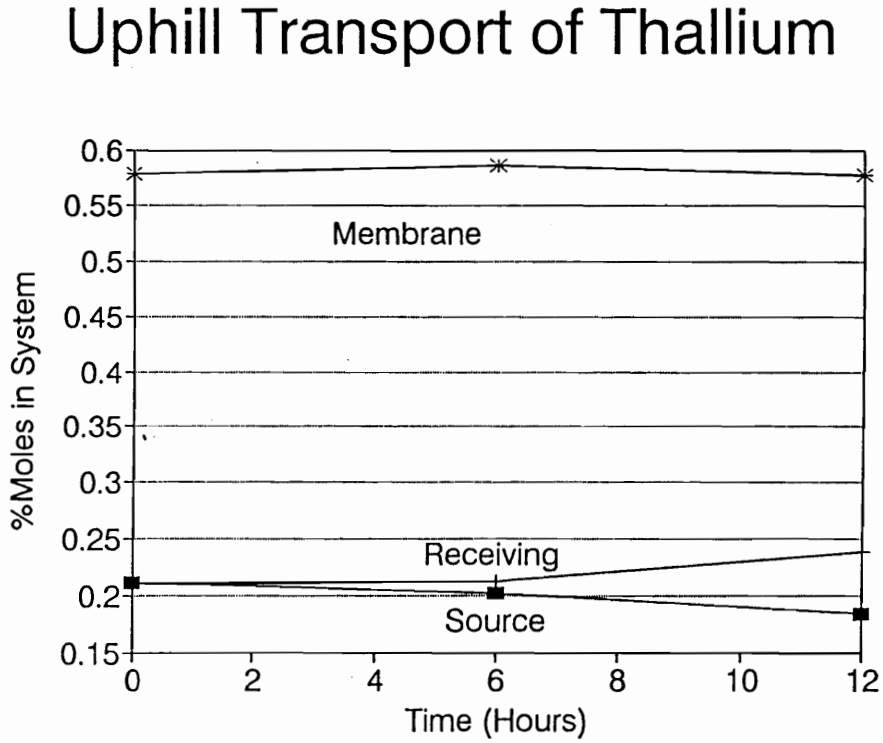

Figure 81. %Moles Thallium (All)

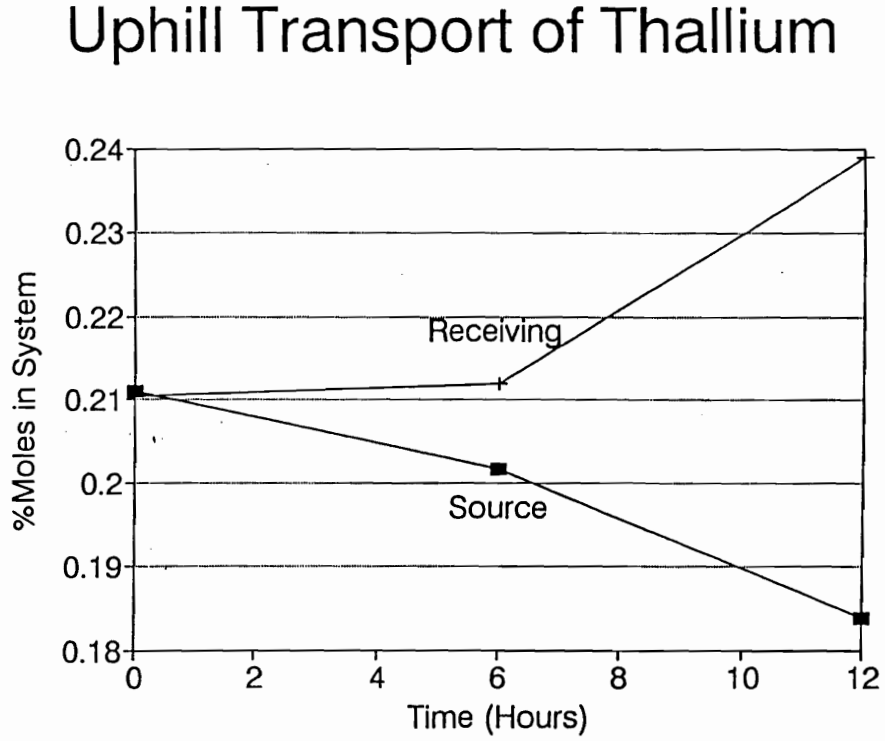

Figure 82. %Moles Thallium (Aqueous)

the experiment. Also, the total percentage of thallium that resides in the membrane decreases with respect to time. This indicates the crown ether looses its ability to complex and hold the thallium ion in the membrane phase upon electrochemical oxidation of the carrier. Expanding the scale of the plot (Figure 82) to examine the aqueous phases, the trends associated with electrochemical facilitated transport are apparent.

Comparison of the graphs for concentration (Figure 78), number of moles (Figure 80) and percentage of moles (Figure 82) verses time for each of the data treatments demonstrates an overall decrease in the number of moles found in the source phase, corresponding with a increase in the number of moles in the receiving phase. Throughout this process the number of thallium ion moles contained in the membrane phase also decreases. The decrease in the number of moles in the membrane phase is consistent with the premise that oxidation of the carrier molecule decreases the crown ether's ability to complex with the thallium ion.

4) Downhill Thallium Ion Transport

Having shown the viability of electrochemical facilitated transport through uphill transport studies using thallium, downhill membrane transport experiments were performed to provide complementary proof of concept. Two downhill experiments were run to verify that the conclusions from the simulation model were valid and to further validate the concept of electrochemical facilitated transport. Efforts were taken to ensure experimental conditions were duplicated differing only in application of controlled potential voltammetry. Upon completion of the matched set of downhill experiments, the concentration values for the two runs were plotted on a common axis to illustrate the effect of electrochemical pumping.

a) Experimental (Downhill with pumping)

The experimental cell was filled in accordance with the procedure outlined previously. Ten ml of a 8.08 x 10^{-3}M ferrocene crown ether solution (0.1M TBAP/CH_2Cl_2) and 15 ml of a 0.1M TBAP/CH_2Cl_2 solution were pipetted into the experimental cell forming a membrane phase of 25ml. Fifteen ml of a 1.00 x 10^{-2}M TlCl aqueous solution was added to the source phase of the experimental cell. The receiving phase was filled with 15ml of distilled deionized water. A solution of

0.10M TBAP/CH_2Cl_2 electrolyte filling solution was introduced to the counter electrode compartments of the experimental cell. Electrodes were positioned in the cell, and electrical connections were made to the two controlling potentiostats. No attempt was made to equilibrate the aqueous and membrane phases. Potentials were set to achieve an oxidation current at the receiving phase electrodes, and a reduction current at the source phase electrodes. Samples of the receiving phase were collected with respect to time at 0, 6, 12 and 20 hours.

Experimental (Downhill with no pumping)

The experimental cell was filled as in the previous experiment. Ten ml of a 8.08 x 10^{-3}M ferrocene crown ether solution (0.1M TBAP/CH_2Cl_2) and 15 ml of a 0.1M TBAP/CH_2Cl_2 solution were pipetted into the experimental cell forming a membrane phase of 25ml. Fifteen ml of a 1.00 x 10^{-2}M TlCl aqueous solution was added to the source phase of the experimental cell. The receiving phase was filled with 15ml of distilled deionized water. The phases were not allowed to equilibrate. A solution of 0.10M TBAP/CH_2Cl_2 electrolyte filling solution was introduced to the counter electrode compartments of the experimental cell. Electrodes were positioned in the cell, but no electrical connections were made to the two controlling potentiostats. Samples of the receiving phase were taken in accordance with the time

frames for the previous electrochemical downhill pumping experiment. The experiment was discontinued after the matching 20 hour sample was taken.

c) Experimental Results

A working curve for thallium was created. The raw data for the calibration curve is shown in Table 17. The working curve is shown in Figure 87. The one ml sample aliquots taken from the both the uphill and downhill electrochemical experiment were diluted by Ependorf pipette to a total volume of 4ml. They were subjected to AE analysis subsequent to tuning of the instrument and obtaining values needed to construct the working calibration curve. The raw atomic emission data for the thallium ion downhill transport studies is given in Table 18. The resulting concentrations from the working curve are shown in Table 19.

A graph of concentration verses time for the experiments are shown in Figure 88. It is apparent that the application of electrochemistry to the system increases the transport rate of thallium ions across the bulk liquid membrane. This increase in the delivery rate is predicted by the mathematical equations used to derive the simulation data presented earlier and further validates the concept of electrochemical facilitated transport.

Table 17. Downhill Thallium Ion Transport
(Working Calibration Curve)

Concentration Thallium Ion	Atomic Emission Readings 1	2	3	Average
1.00×10^{-6}	0.244	0.238	0.233	0.238
1.00×10^{-5}	0.311	0.313	0.319	0.314
1.00×10^{-4}	1.341	1.353	-	1.347

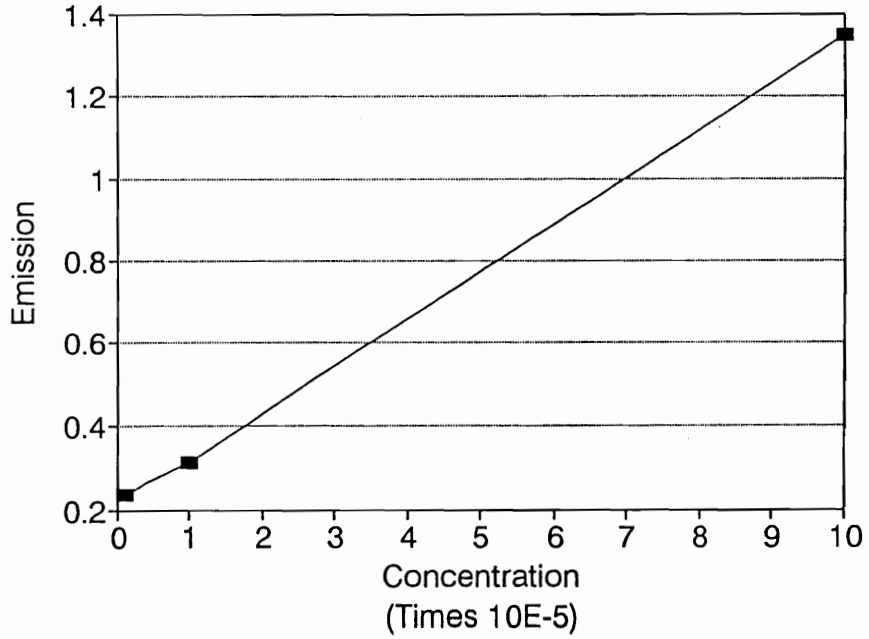

Figure 83. Calibration Curve for Thallium (Downhill Transport Experiment)

Table 18. Downhill Thallium Ion Transport (AE Raw Data)

Pumping	Atomic Emission Reading				
Time	1	2	3	4	Average
6	1.005	1.002	1.002	1.003	1.003
12	1.142	1.143	1.143	1.141	1.142
30	1.202	1.199	1.204	1.200	1.201
No Pumping					
0	0.251	0.250	0.252	0.251	0.251
12	0.253	0.256	0.257	0.255	0.255
30	0.255	0.257	0.257	0.237	0.257

Table 19. Downhill Thallium Ion Transport (Experimental Data)

Time (hours)	Pumped	Unpumped
0	0.0	0.0
6	2.80×10^{-4}	1.0×10^{-5}
12	3.29×10^{-4}	1.2×10^{-5}
20	3.49×10^{-4}	1.3×10^{-5}

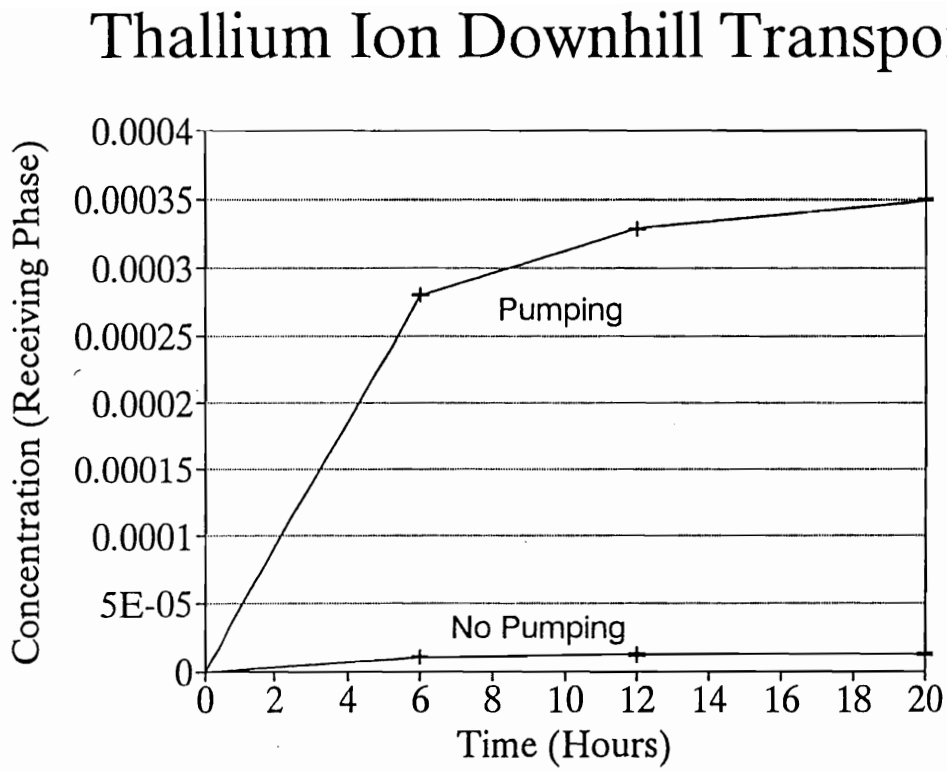

Figure 84. Experimental Data (Thallium Downhill Pumping Experiment)

5) Exhaustive Electrolysis and Extraction

To further elucidate the change in complexation ability between the oxidized and neutral form of the ferrocene crown ether, two matched aqueous/membrane extraction experiments were run involving shaking equal volumes of aqueous thallium ion solution with a methylene chloride solution containing the ferrocene crown ether and the TBAP supporting electrolyte. The concentration of the aqueous phase after equilibration was measured to determine the amount of thallium ion moving into the membrane phase. The second extraction experiment differed from the first in that the equilibration of the two phases was preceded by an exhaustive electrolysis experiment to oxidize the bulk of the ferrocene crown ether in the membrane phase. The concentration of the aqueous phase was measured for loss of thallium ion.

A weight 0.0119 grams of TlCl was measured using a Mettler balance, and dissolved in a final volume of 25 ml of deionized distilled water in a volumetric flask yielding a thallium molarity of 1.98×10^{-3} M. Two milliliters of an 8.08×10^{-3} M crown ether solution was pipetted into two separate vials, and an additional 8 ml of methylene chloride and TBAP solution was added to each vial bringing the total non-aqueous phase volume to 10 ml. To the first vial, 10 ml of the aqueous thallium ion solution was added to the crown ether phase and equilibrated by vigorous shaking the two phases. The two immiscible phases were allowed to separate, and left to stand until subjecting the aqueous layer to ICP analysis.

A three electrode assembly consisting of platinum counter and working electrodes and a SCE reference electrode were positioned in the second vial for the exhaustive electrolysis portion of the experiment. Connections were made to the PAR Model 173 potentiostat, and an oxidizing potential was selected. The electrolysis was allowed to continue until the oxidation current was perceived to have decayed to a constant small value. The electrolysis continued for 30 minutes. After removal of the electrodes from the vial, 10 ml of the aqueous thallium solution was added to the oxidized crown ether membrane phase. The phases were equilibrated as with the first vial, and left to settle before analysis by the ICP.

Analysis of the thallium ion was performed by a departmental inductively coupled plasma unit. A calibration curve for the ICP experiment was performed using primary standard solution for the thallium ion. The data for the calibration curve is:

Primary Standard Concentration (ppm)	ICP Reading
0	206.5
50	264.2
100	325.5
1000	1662.8

The working curve is presented in Figure 89. The aqueous phases from the extraction experiments were entered directly into the ICP stream without any further preparation. The data for the extraction experiments is shown in Table 20. The ppm concentrations were converted into their molarity equivalent for later equilibrium analysis.

From the two matched experiments, one can see a difference in the ability of the oxidized crown ether molecule to extract thallium ion from the aqueous phase. This experiment supports the simulation model presented earlier. Further information about the complexation of the crown ether thallium complex may be obtained by determining the complexation coefficients for the experiment. The complexation coefficient is defined as:

$$K_{eq} = \frac{[Crn^{+} \cdot Tl^{+}]_{org}}{[Tl^{+}]_{aq} \cdot [Crn^{+}]_{org}}$$

Knowing the original amount of starting materials for both the thallium and the crown ether, as well as the ending concentrations for the aqueous phase after the extraction experiment, it is possible to calculate the concentrations of each species in both phases using a mass balance as described earlier. Performing this procedure, the equilibrium constants for the neutral and oxidized species are listed below.

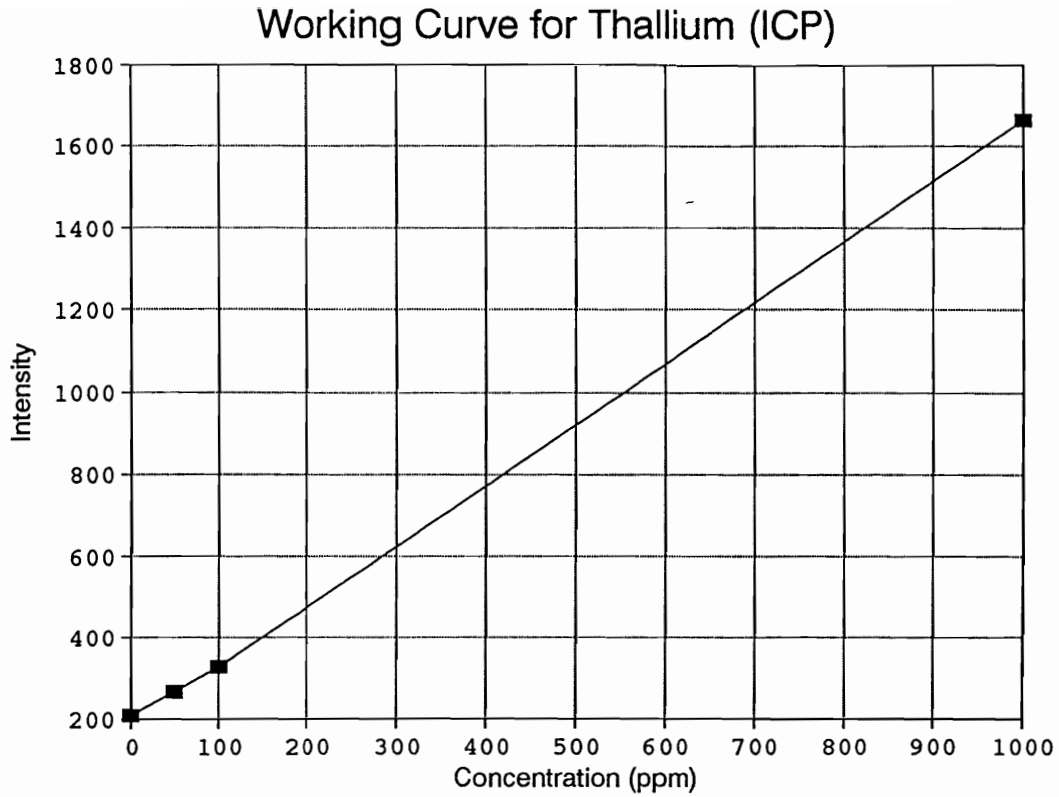

Figure 85. ICP Working Curve for Thallium

Table 20. Extraction Experiments

Vial	ICP Value	ppm	Molarity
No Electrolysis	497.4	215.7	0.899×10^{-3}
Electrolysis	537.0	242.3	1.011×10^{-3}

Initial moles of crown ether:	1.62×10^{-5}
Initial moles aqueous thallium ion:	1.98×10^{-5}
Moles aqueous thallium ion after equilibration:	0.899×10^{-5}
Moles organic crown/thallium ion complex after equilibration:	1.081×10^{-5}

The distribution coefficient as defined earlier in the uphill membrane transport experiments measures ration of the amount of cation in the aqueous phase divided by the amount of cation in the membrane phase. The distribution coefficient is 0.83. The calculated equilibrium coefficient is 2231. For the extraction experiment preceded by exhaustive electrolysis the data values are:

Initial moles of crown ether:	1.62×10^{-5}
Initial moles aqueous thallium ion:	1.98×10^{-5}
Moles aqueous thallium ion after equilibration:	1.011×10^{-5}
Moles organic crown/thallium ion complex after equilibration:	0.969×10^{-5}

The distribution coefficient is 1.043, and the equilibrium coefficient of the oxidized carrier is 1472. Examining the ratio of the two equilibrium constants, it becomes clear that the oxidation of the carrier molecule diminished the complexation ability of the ferrocene crown ether, but did not eliminate the possibility of complexation. This coincides with the experimental evidence from the silver and thallium ion transport studies where it was evident that the membrane phase was able to absorb a high percentage of the cation during the equilibration stage, and the observation that the overall amount of the percentage of cation within the membrane decrease with the increasing presence of oxidized carrier within the membrane phase.

D) Summary of Experimental Results

The experimental results from the silver and thallium membrane transport studies combined with the extraction and electrochemical studies demonstrate that the oxidation state of the carrier molecule effects the change of its complexation ability for cations. For the ferrocenophane crown ether being studied, the oxidized molecule is less able to complex with the cation as compared with its neutral state. Electrochemically cycling the molecule between its complexing and less complexing forms at the source and receiving interfaces of the membrane respectively, allow the membrane to electrochemically facilitate the movement of ion across the membrane.

Uphill transport for both silver and thallium demonstrates electrochemical facilitated transport can effect the transfer of aqueous metal ions from an initial equimolar source phase to an ever increasing receiving phase. The downhill thallium transport shows electrochemical facillitated transport increases the transport rate of thallium ions across the membrane phase approximately 25 times greater than the corresponding "unpumped" downhill transport experiment. A mechanism to explain the effect of electrochemical process on the complexation of the crown and cation will presented in the next chapter.

EXPERIMENTAL ANALYSIS

The historical and simulation chapters laid the groundwork outlining the theory and criteria required to validate the concept of electrochemical facilitated transport. The synthetic and experimental sections demonstrated it was possible to create a class of molecules with complexation constants capable of being electrochemically altered, and that it is possible to harness this ability, and to externally control the movement of ions across a bulk liquid membrane both with and against the ion's concentration gradient. The interaction of the ferrocenophane in the complexation process will now be examined as to its role in electrochemical facilitated transport.

A) Structure of Ferrocenophane Crown Ether

As presented in the historical section, the complexation of ions by crown ethers is influenced by the freedom of motion and the number of atoms in the ring linkages as well as the nature of the groups contained in and around the binding sites. To examine how the ferrocenophane molecule synthesized for this study complexes with the silver or thallium cation, it is necessary to determine the preferred geometry of the molecule and examine its role in the complexation process.

Currently, the preferred geometry of a complex in solution is approximated by obtaining a crystal of the compound and submitting it to X-ray crystallography analysis. The ferrocenophane compound for this study was obtained as an red oil. Frustrating attempts to crystallize the oil to obtain a crystal for structure analysis were terminated after considering many literature references reported several ferrocene compounds, as well as crown ether analogs, exist only as oils.

The use of CPK space filling molecules and computer molecular modeling packages capable of determining energy minimized structures of molecules were used to examine the possible 3-D configurations for the ferrocenophane molecule. The structure for the ferrocenophane is shown in Figure 86, with the CPK structure shown in Figure 87.

The CPK model shows the size and shape of the ring cavity is subject to change due to its large ring size, the freedom of motion associated with the ether linkages comprising the ring, and the rotation of the ferrocene cyclopentadienyl rings about the central iron atom. Manually rotating the bonds of the CPK model demonstrates a wide variation of cavity sizes are possible with differing numbers of oxygen atoms being spatially available for complexation with the metal cation. CPK views in Figures 88 and 89 depict two ring orientations (with complexed ion) that seem reasonable based on reported crown ether crystal structures for 24C8 and 27C9 crown ethers[4].

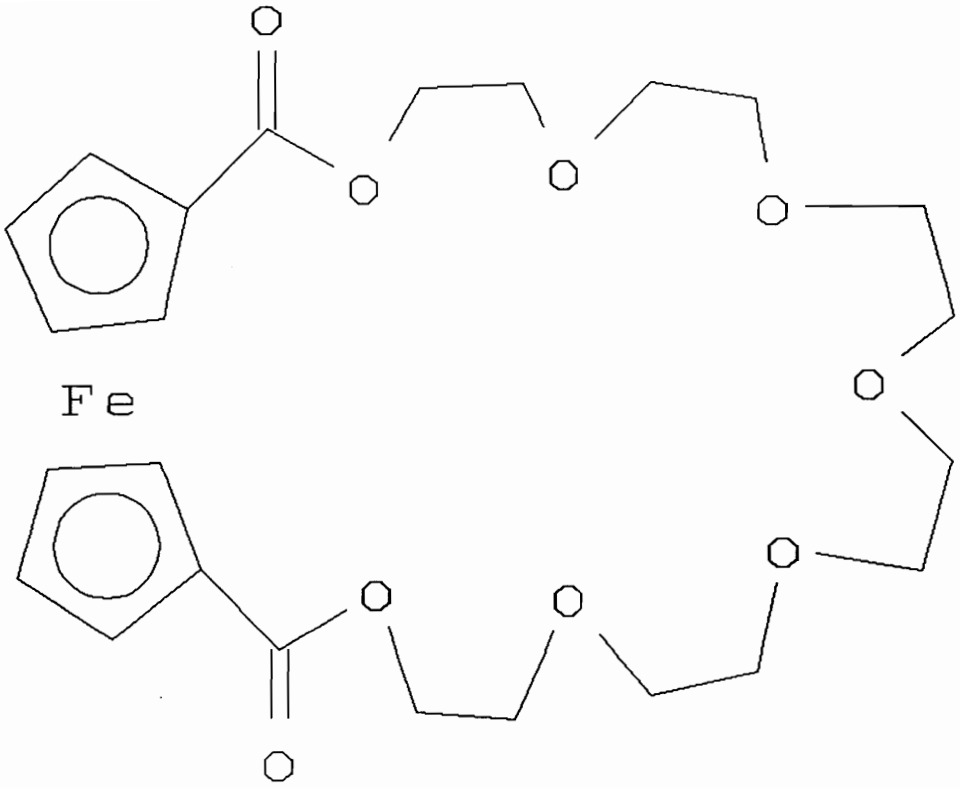

Figure 86. 2,5,8,11,14,17,20-heptaoxa[21]
(1,1')ferrocenophane-1,21-dione

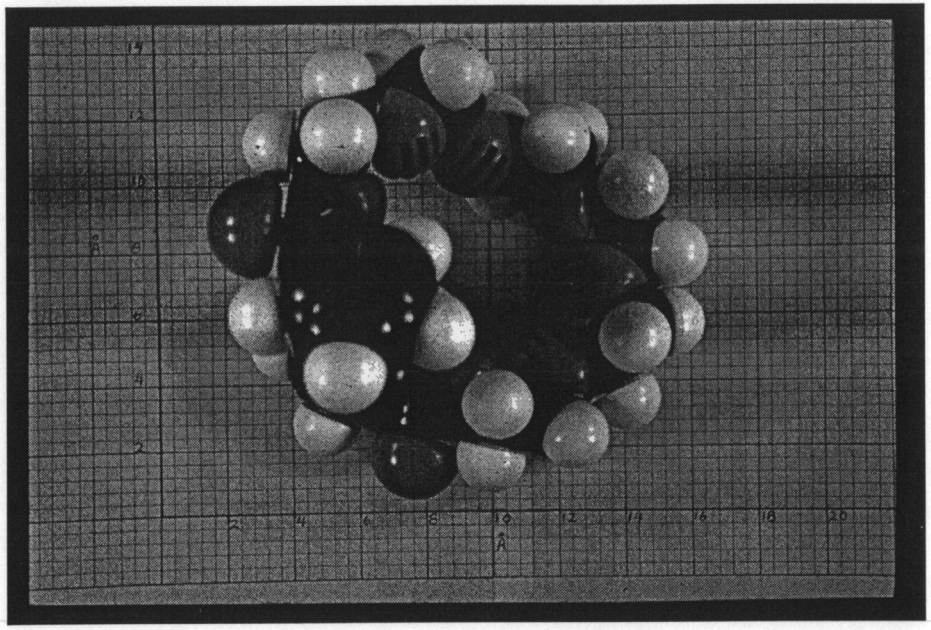

Figure 87. CPK Model of Ferrocenophane Crown Ether

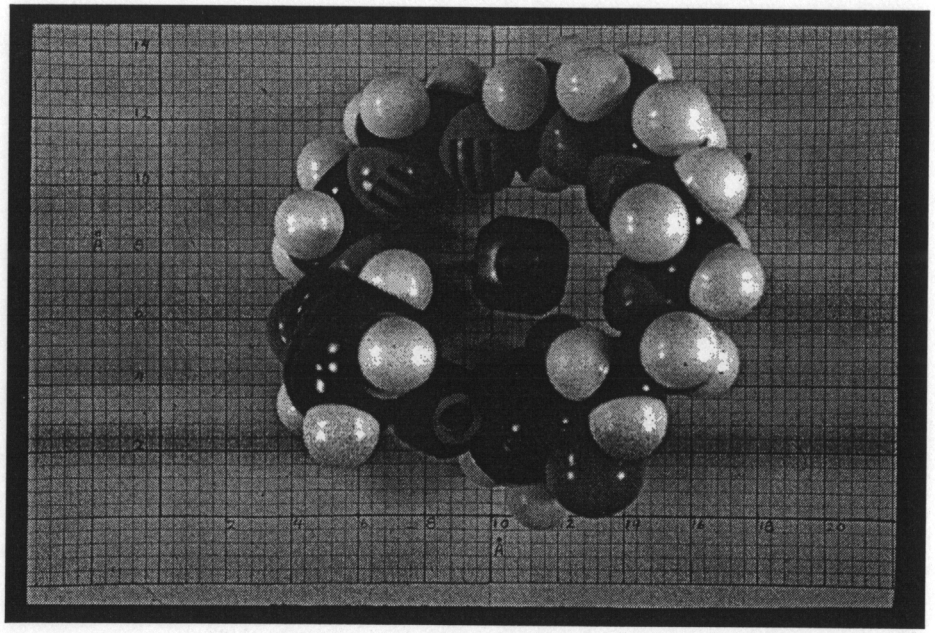

Figure 88. CPK Model of Ferrocenophane Crown Ether Complexed with Ion

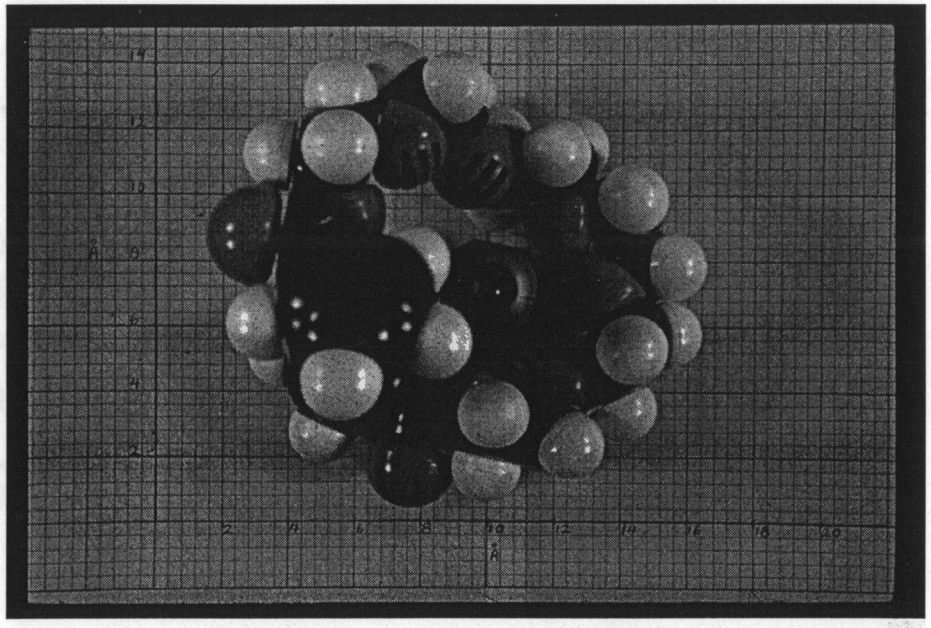

Figure 89. CPK Model of Ferrocenophane Crown Ether Complexed With Ion

B) Computer Generated Molecular Model Structures

Several computer-based molecular modeling packages available in the Virginia Tech Chemistry Department (both IBM compatible and Macintosh computer platforms), were utilized to obtain the preferred geometry of the ferrocenophane and that of its thallium complex. Unfortunately, current modeling packages have not yet advanced to a point where they can handle inorganic interactions. Attempts to achieve an energy minimized structure on existing Mac and IBM platforms failed. A newly released modeling system named Insight (BIOSYM Technologies Inc.), running on a Sun Workstation, comes closest to being able to model transition metal based molecules and their interactions. Their technical staff provided images of energy minimized structures for the ferrocenophane and its complex with thallium (Figures 90-92). Many approximations and "fixes" were made to permit the program to reach a solution. BIOSYM is continuing their research and development efforts to permit effective representation of the interactions of inorganic compounds. Despite these existing deficiencies, the program did produce structures that compared well with those obtained by CPK models.

The role of the iron (in its +2 and +3 oxidation state) of the ferrocenophane on the complexed transition metal ion being transported will now be addressed.

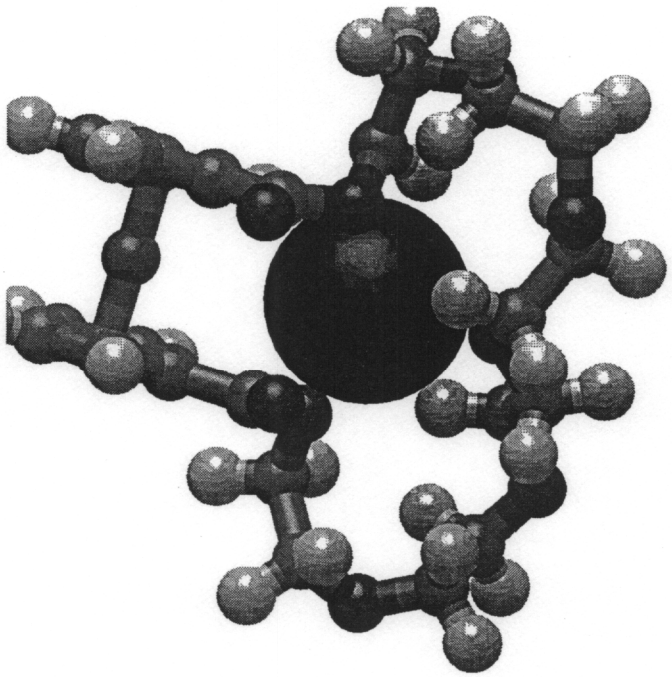

Figure 90. Computer Model of Ferrocenophane
Crown Ether Complexed With Ion (View 1)

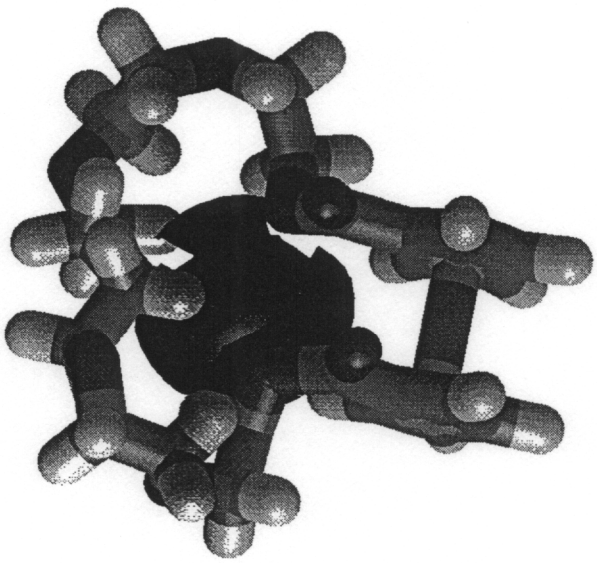

Figure 91. Computer Model of Ferrocenophane
Crown Ether Complexed With Ion (View 2)

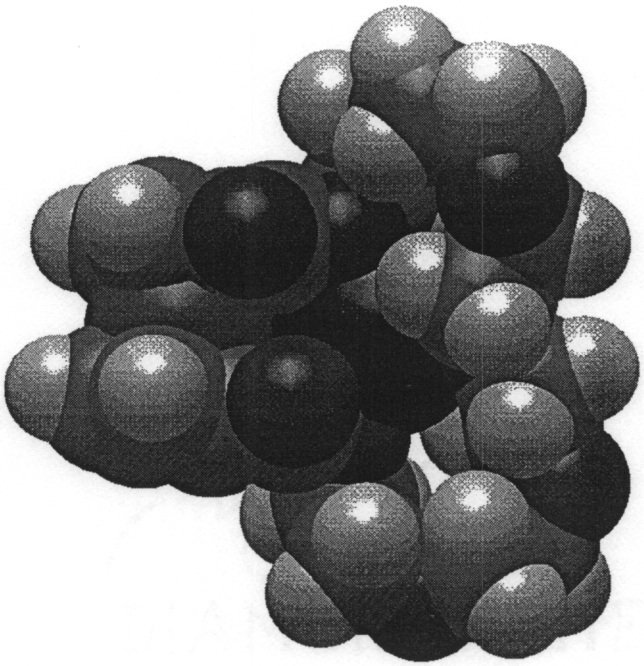

Figure 92. Computer Model of Ferrocenophane
Crown Ether Complexed With Ion (View 3)

C) Electronic Structure of Ferrocenophane

To gain insight as to how the reversible electrochemical oxidation of ferrocene influences the equilibrium complexation constant for the ferrocenophane/transition metal (Ag(I),Tl(I)) complex, it is necessary to evaluate the effects of the ferrocene entity on the binding cavity of the crown ether. The CPK model reveals a complexation cavity size large enough to accommodate the thallium or silver cations. The nature of the ring ether linkages and the freedom of rotation of the cyclopentadienyl rings of the ferrocene unit about the iron allow the ring oxygens to move into positions favorable for complexation. The observed change in the complexation constants due to oxidation of the ferrocene must result from a through-space interaction between the charge on the ferrocene moiety with that of the bound cation. Two approaches will be taken to examine this effect. The first considers electrostatic repulsion of two like charges in a vacuum. The second examines the electronic structure of ferrocene, and the changes that occur in the structure during electrochemical oxidation.

To obtain a qualitative understanding of the through-space electrostatic forces involved in the ferrocenophane/ion complex, an electrostatic repulsion model of two like charges in a vacuum was examined. Simplifications were made by reducing the entire ferrocenophane to a point charge of +2 or +3 located at the iron. The attractive forces of the ring oxygen's lone pair electrons for cation were treated as a

constant that did not change during the oxidation of ferrocene, and will not be considered in the model. The complexed ion was also treated as a point charge of +1. This reduces the system to a two-body attraction/repulsion model (Figure 93). The through-space electrostatic force equation for two point charges in a vacuum is given by:

$$F = \frac{Q_1 Q_2}{r^2}$$

where Q_1 and Q_2 represent the electronic charges of the two ions and r is the distance between the two point charges. Consider an initial two body system where the two entities of charges +2 and +1 co-exist at a distance r from one another. As the charge on the +2 species is increased to +3, the equation predicts the electrostatic repulsive force will increase by 50 percent if the point charges were to remain at the same distance. This increase in the repulsive force would certainly make the charges separate to a greater distance. For the case of a cation held within the cavity of a ferrocenophane crown ether, this increase in distance forces the cation to move to a region in the complexing cavity where there is a lower availability of oxygen lone pair electrons for complexation. This decrease in attractive force lowers the formation constant for the carrier/ion complex.

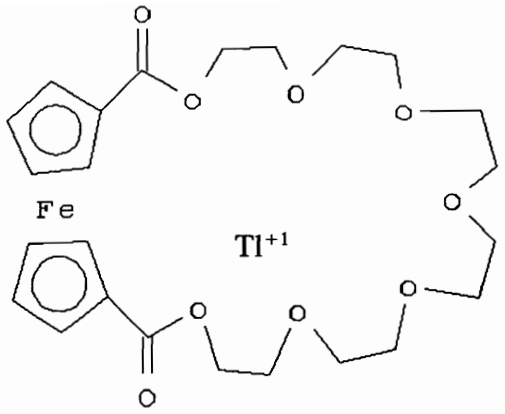

Reduced to:

Fe^{+2} --- r --- Tl^{+1}

Where r is defined by:

$$F = \frac{Q_1 Q_2}{r^2}$$

Consider change in distance (r') due to oxidation of Iron keeping the forces of repulsion (F and F') constant

Fe^{+3} ----- r' ----- Tl^{+1}

Figure 93. Electrostatic Repulsion Model

To examine the distances involved in the complexation process, refer to the CPK models in Figures 88 and 89. The distance between the centers of the iron and the cation point charges can vary from 4.3 Å to 6.21 Å. A value of 6 Å is used as a nominal value to calculate the repulsive force of the iron(II) center on the thallium(I) ion using the above electrostatic equation. For the repulsive force between the iron and thallium to remain the same, as the charge of the iron atom increases to +3, the thallium ion must move to a distance of 7.35 Å. To achieve this distance, the thallium moves outward from the complexing cavity of the crown ether. This movement leads to a lowered stability for the complex. While this simplistic model provides a qualitative explanation for the lowered complexation constants upon electrochemical oxidation of the ferrocene, it ignores quantitative views of the changes in equilibrium constants as indicated by the thallium extraction experiments, and ignores possible changes due to alteration of the ferrocene structure.

The electronic structure of ferrocene, the effective charge on the iron of ferrocene, and its effect on the through-space interactions must be considered. The electronic structure for ferrocene and ferrocenium have been published.[65,66] References agree the charge on the iron is dispersed evenly over the cyclopentadienyl rings of ferrocene. Further, the charge orbitals of the iron is shielded by the orbitals of the cyclopentadienyl rings. A Mossbauer spectroscopic study published in 1976 (ref. 61) measured the ionicity of ferrocene's iron in both neutral and oxidized states. They reported values of +1.39 for ferrocene and +1.47 for the ferrocenium ion.

Placing these numbers into the above electrostatic model, the resulting change in distance is much less (6.17 Å), and more closely explains the change in transport rates observed in the experimental section.

The electronic structure for ferrocene[60] involves hybridization of the molecular orbitals between the iron and the cyclopentadienyl rings. The wave functions are shown in Table 21. The resulting orbitals a_{1g}, a_{1u} and e_{1u} are associated with the rings, while the d_{z^2}, $d_{x^2-y^2}$ and d_{xy} orbitals are located on the metal ion. The four electrons in the strongly bonding e_{1g} orbital are distributed evenly about the rings to form two covalent single bonds.

Oxidation of ferrocene to the ferrocenium ion removes an electron from an e_{2g} anti-bonding molecular orbital. This causes an alteration of the orbitals between the iron and the rings. Four molecular orbitals, ψ_6-ψ_9, change significantly, while the rest remain virtually unchanged. The wave functions for ferrocenium are given in Table 22. The over-all effect of the oxidation is an increase in the d-character of the e_{1g} molecular orbitals comprising the covalent bonds between the iron and the rings. The distance between the iron and the plane of the rings increases from 1.66 to 1.71 Å. The ionicity of the iron is increased only slightly (+1.39 to +1.47) as a result of the oxidation, with the bulk of the charge being evenly distributed over both of the cyclopentadienyl rings. The electron distribution around the iron also changes to a more spherical nature that does not extend as far from the iron center as the oblate orbitals of the neutral molecule.

Table 21. Ferrocene Molecular Orbitals

Molecular Orbitals	No. of Electrons
$\psi_1(a_{1g}) = 0.49\psi_{4s}+0.84\varphi(a_{1g})$	2
$\psi_2(a_{2g}) = 1\psi_{3dz^2}$	2
$\psi_3(a_{1u}) = 0.1\psi_{4pz}+0.99\varphi(a_{1u})$	2
$\psi_4(e_{1u}) = 0.59\psi_{4px}+0.81\varphi(e_{1u})$	4
$\psi_5(e_{1u}) = 0.59\psi_{4py}+0.81\varphi(e_{1u})$	
$\psi_6(e_{1g}) = 0.37\psi_{3dxz}+0.93\varphi(e_{1g})$	4
$\psi_7(e_{1g}) = 0.37\psi_{3dyz}+0.93\varphi(e_{1g})$	
$\psi_8(e_{2g}) = 0.85\psi_{3dxy}+0.52\varphi(e_{2g})$	4
$\psi_9(e_{2g}) = 0.85\psi_{3dx^2-y^2}+0.52\varphi(e_{2g})$	

ψ = Iron or Hybrid Orbitals

φ = Cyclopentadienyl Orbitals

Table 22. Ferrocenium Ion Molecular Orbitals

Molecular Orbitals	No. of Electrons
$\psi_1(a_{1g}) = 0.49\psi_{4s}+0.84\varphi(a_{1g})$	2
$\psi_2(a_{2g}) = 1\psi_{3dz^2}$	2
$\psi_3(a_{1u}) = 0.1\psi_{4pz}+0.99\varphi(a_{1u})$	2
$\psi_4(e_{1u}) = 0.59\psi_{4px}+0.81\varphi(e_{1u})$	4
$\psi_5(e_{1u}) = 0.59\psi_{4py}+0.81\varphi(e_{1u})$	
$\psi_6(e_{1g}) = 0.45\psi_{3dxz}+0.89\varphi(e_{1g})$	4
$\psi_7(e_{1g}) = 0.45\psi_{3dyz}+0.89\varphi(e_{1g})$	
$\psi_8(e_{2g}) = 0.94\psi_{3dxy}+0.35\varphi(e_{2g})$	3
$\psi_9(e_{2g}) = 0.94\psi_{3dx^2-y^2}+0.35\varphi(e_{2g})$	

ψ = Iron or Hybrid Orbitals

φ = Cyclopentadienyl Orbitals

Thus, one might conclude that the effective electrostatic repulsive influence exerted by the ferrocenium ion of the ferrocenophane involved in this study with the complexed ion results from the increase in charge density that is spread over the ferrocene entity countered by orbital rearrangement and bond lengthening (1.66 to 1.71 Å) that may change the geometry of the ferrocenophane. It is this author's opinion that the increase in charge density for the ferrocenophane ion is the major cause of the decrease in complexation/transport rate seen in the experimental section.

This interpretation of the interaction of the ferrocenophane/transition metal complexes is strengthened by examining studies performed on a class of compounds known as biferrocenes. Biferrocenes are a class of compounds containing two ferrocene units linked by their cyclopentadienyl rings. This causes the irons to come within close proximity to one another (analogous to that of a complexed cation). Studies for biferrocenylene (Figure 94) show the iron atoms reside 3.98 Å from one another. This iron-to-iron distance is 6 pm longer than is expected based on perfectly aligned ferrocene molecules and the linkages connecting their cyclopentadienyl rings.[67] The literature ascribes this lengthening as due to a repulsive through-space interaction between the two irons. The published explanation, including Mossbauer Spectroscopy, concludes that the electron density around ferrocene's iron is located mainly in the hybrid orbitals formed from the interaction of the iron's orbitals and those of the two cyclopentadienyl rings.[65,68] This results in an asymmetric, oblate

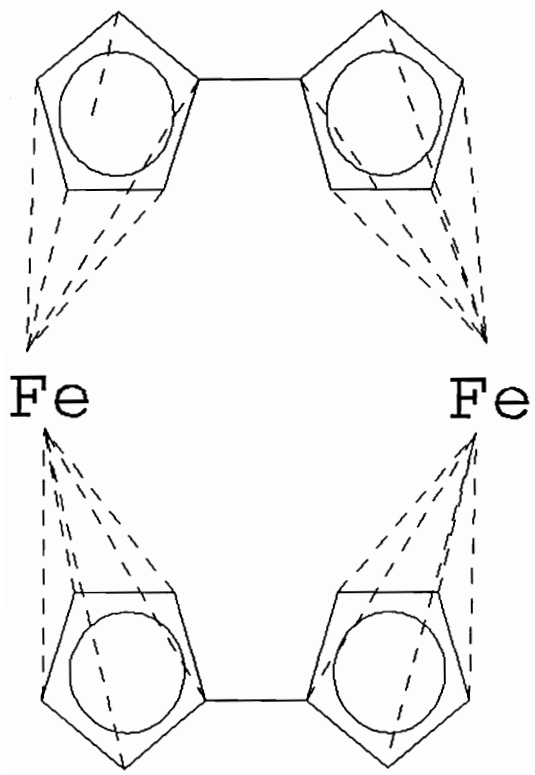

Figure 94. Biferrocenylene

electron distribution oriented along the axis of the ferrocene molecule that disperses the charge of the iron over the rings.

The concept of electrochemical facilitated transport implies that the changing electrochemical state of the carrier molecule alters its ability to complex with a cation. The experimental uphill and downhill membrane transport and extraction experiments support the above arguments, and show that the neutral form of the ferrocenophane is a better complexing (transporting) agent than the oxidized form. The combination of theory and experimentation show the above concept is valid and that it merits further work.

CONCLUSIONS: Future Work and Lessons Learned

In this work, several areas have been brought to bear on the concept of electrochemical facilitated transport. It is with no small amount of satisfaction that this author can now report the above concept is valid and worthy of future study. It is the hope of this author that the concepts presented in this work, along with the diffusion modeling tools and experimental procedures and apparatus, will provide the basis for additional work in this area.

The synthesis of electrochemically alterable crown ethers is likely to increase as new base compounds and applications are found. Physical chemists and biochemists will have new series of externally alterable compounds by which to examine the effects of complexation/transport phenomena. Creation of additional ferrocene-based crown ethers will allow organometallic chemists a modifiable tool that they may use to probe the interactions of ferrocene with other ferrocene units and metal ions.

Another possible area of application deals with electrochemically altering the growth profiles of polymers. Wanigatunga and Wagener[69] report that a broad range of poly(siloxane)-graft-poly(picalolactone) copolymers can be generated via crown ether mediated chemistry. Copolymers of dichloro-dimethylsilane and (dichloromethyl)(3-cyanopropyl)silane can be prepared by hydrolyzing the cyano

group to an acid. The potassium salt of this acid acts as an initiator to graft pivalolactone onto the poly(siloxane) backbone. They note that grafting does not occur in the absence of the crown compound. In this senario, growth of various grafts could be influenced or moderated by an electroactive carrier molecule bound to a mesh electrode system. Applying alternating redox potentials to the crown ether would allow creation of graft copolymers that would otherwise be unobtainable by traditional methods.

Perhaps of most importance is the personal realization that research will continue to cross the classical boundaries of science, and the successful researcher will be one that can apply the knowledge gained in many areas to the project at hand.

Appendix I

Cyclic Voltammetry Routines

201 LIST

```
 0 ( SYSTEMS DEFINITIONS)
 1 9 , : <CREATE>  BLK @ , (CREATE) ; ' <CREATE>  'CREATE !
 2 : KEY  0 0  'S 1 EXPECT  SWAP DROP  255 AND ;
 3 : EMIT  'S 1 TYPE DROP ;
 4 10 CONSTANT B/H  ( # BYTES/HEAD)  ( DICTIONARY)  10 LOAD
 5 ( 32-BIT ARITHEMETIC)  203 LOAD
 6 ( ADDT'L TERMINALS)  24 LOAD  26 LOAD
 7 ( EXTENSIONS)  37 LOAD  38 LOAD
 8 ( ERRORS)  21 LOAD
 9
10
11
12 : UNIQUE  ['] ?CREATE  'CREATE ! ;
13 : -UNIQUE  ['] <CREATE>  'CREATE ! ;
14
15 202 LOAD
```

202 LIST

```
 0 ( SATELLITE  LOAD BLOCK)                : SATELLITE ;
 1 : ASK  PAD 12 EXPECT  PAD 1- NUMBER ;
 2 : REV# CR CR ." AL REV 7 DEC 87 " CR CR ; REV#
 3 CONTEXT GOLDEN 20 MOVE  HERE H 2+ !
 4 EMPTY-BUFFERS
 5
 6 204 LOAD
 7 205 LOAD
 8 206 LOAD
 9 207 LOAD
10 208 LOAD
11 209 LOAD
12 210 LOAD
13 211 LOAD
14
15
```

Appendix I (Cont.)

203 LIST

```
 0 ( NEEDED 32 BIT ROUTINES )
 1 CODE D+  0 S )+ MOV  2 S) S )+ ADD  0 ADC  S ) 0 ADD  NEXT
 2 CODE DMINUS  2 S) NEG  S ) ADC  S ) NEG  NEXT
 3 : D-  DMINUS D+ ;  : D0=  0= SWAP 0= AND ;  : D=  D- D0= ;
 4 : DABS  DUP 0<  IF DMINUS  THEN ;  : 0. 0 0 ;
 5
 6 CODE */MOD  1 S )+ MOV  0 2 S) MOV  0 S S) MOV  2 S) 1 MOV  S )+ 0 MUL
 7   S ) 0 DIV  S ) 1 MOV  S -) 0 MOV  NEXT
 8 : */  */MOD  SWAP DROP ;  : MOD  /MOD DROP ;
 9 CODE /  2 S )+ MOV  1 S )+ MOV  0 SXT ( CLR ***)
10   2 0 DIV  S -) 0 MOV  NEXT
11
12
13
14
15
```

204 LIST

```
 0 ( POTENTIOSTAT VARIABLE BLOCK ) OCTAL
 1 VARIABLE  V/C-BUF  40000 ALLOT  ( DATA ARRAY )
 2 VARIABLE  BUF-PTR              ( DATA BUFFER POINTER )
 3 : RESET-PTR V/C-BUF BUF-PTR ! ;  RESET-PTR
 4 : CLR-BUF V/C-BUF  40000 ERASE ;  ( CLEAR DATA BUFFER )
 5 VARIABLE DAT.BLK                ( NXT DSK STORAGE LOCATION )
 6 VARIABLE BLK/SCAN               ( # DSK BLKS WRITTEN/SCAN )
 7 VARIABLE PTS/SCAN               ( # DATA VALUES PER SCAN )
 8 VARIABLE CLOCK  0 CLOCK !       ( CLOCK ROUTINE )
 9 VARIABLE CNTR   0 CNTR !        ( CLOCK ROUTINE )
10 VARIABLE MV/SEC                 ( SWEEP RATE )
11 VARAIBLE TICS                   ( CLOCK TICK PER VOLTAGE STEP )
12 176760 CONSTANT 0DAC
13 ASSEMBLER  BEGIN  CNTR DEC  CLOCK I) WAKE # MOV
14                        200 200 INTERRUPT
15 FORTH  DECIMAL
```

Appendix I (Cont.)

205 LIST

```
 0 ( POTENTIOSTAT VARIABLE BLOCK )
 1 OCTAL
 2 VARIABLE IPOT  0 IPOT !    ( INITIAL POTENTIAL DAC VALUE )
 3 VARIABLE UPOT  0 UPOT !    ( UPPER POTENTIAL DAC VALUE )
 4 VARIABLE LPOT  0 LPOT !    ( LOWER POTENTIAL DAC VALUE )
 5 VARIABLE SPOT  0 SPOT !    ( BEGINNING SCAN POTENTIAL )
 6 VARIABLE EPOT  0 EPOT !    ( ENDING    SCAN POTENTIAL )
 7 VARIABLE DIR   1 DIR  !    ( SCAN DIRECTION )
 8 VARIABLE DTIM  1000 DTIM ! ( DELAY TIME IN 0.01 SECONDS )
 9
10
11
12
13
14
15 DECIMAL
```

206 LIST

```
 0 ( D/A AND A/D CONVERSION ROUTINES FOR ADAC BOARDS )
 1 DECIMAL
 2 : V>DAC ( DEC# -- DAC# ) SWAP ABS 4096 100 */  SWAP
 3       MINUS IF MINUS 5 - ELSE 5 + THEN 10 / ;
 4 : DAC>V ( DAC# -- DEC# )  1000 4096 */ DUP 0< IF
 5       5 - ELSE 5 + THEN 10 / ;
 6 : MV>TICS 24414 MV/SEC @ / 50 + 100 /
 7         DUP 0= IF DROP 1 THEN 1 - TICS ! ;
 8 : TICS>MV  24414 TICS @ 1 + / 50 + 100 / MV/SEC ! ;
 9
10
11
12 : .VOLTS DUP ABS 0 <# # #  46 HOLD #S SIGN #>
13                 TYPE SPACE ." VOLTS" ;
14
15
```

Appendix I (Cont.)

207 LIST

```
 0 ( POTENTIOSTAT SETTINGS LISTING )
 1
 2 : .IPOT  ." INIT POT " IPOT @ DAC>V .VOLTS CR  ;
 3 : .UPOT  ." UPPR POT " UPOT @ DAC>V .VOLTS CR  ;
 4 : .LPOT  ." LOWR POT " LPOT @ DAC>V .VOLTS CR  ;
 5 : .SWP   ." SWEEP RATE " MV/SEC @ . ." MV/SEC" CR ;
 6
 7 : .DTIM  DTIM @ 0 <# # # # 46 HOLD #S #> TYPE ." SEC DELAY" CR ;
 8 : .DAT.BLK ." NEXT BLOCK FOR STORAGE IS : DAT.BLK @ . CR ;
 9 : .SETTINGS .IPOT .UPOT .LPOT .DTIM .SWP .DAT.BLK ;
10
11
12
13
14
15
```

208 LIST

```
 0 ( POTENTIOSTAT SETUP )
 1 : ?IPOT  ." INIT. POTENTIAL X.XX V " ASK V>DAC IPOT ! CR ;
 2 : ?UPOT  ." UPPER POTENTIAL X.XX V " ASK V>DAC UPOT ! CR ;
 3 : ?LPOT  ." LOWER POTENTIAL X.XX V " ASK V>DAC LPOT ! CR ;
 4 : ?DTIM  ." DELAY TIME IN 0.01 SEC " ASK DTIM ! CR ;
 5 : ?MV    ." SWEEP RATE XXX MV/SEC "  ASK MV/SEC !
 6          MV>TICS TICS>MV CR ;
 7 : ?DAT   ." STORAGE BLOCK " ASK DAT.BLK ! CR ;
 8
 9 : ?TICS  ." TICS PER POINT " ASK TICS ! TICS>MV CR ;
10
11 : SETUP  ?IPOT ?UPOT ?LPOT ?DTIM ?MV ?DAT .SETTINGS ;
12
13
14
15
```

Appendix I (Cont.)

209 LIST

```
 0 ( POTENTIOSTAT DATA STORAGE ROUTINES )
 1 ( RAW A/D VALUES STORED TO ALLOW GREATER SWEEP SPEED )
 2 DECIMAL
 3 : DM1 ." BLOCK " DAT.BLK @ . ;
 4 : DM2 ." THRU " DAT.BLK A 1- . ." WRITTEN" ;
 5 : STORE 29999 BUF-PTR @ . ;            ( EOF MARKER )
 6       BUF-PTR @ 2 + V/C-BUF            ( DATA LIMITS )
 7       DO I                        ( SOURCE )
 8         DAT.BLK @ BLOCK              ( DESTINATION )
 9         1024 MOVE UPDATE FLUSH        ( NUMBER OF BYTES PER BLOCK )
10         1 DAT.BLK +! 1024 +LOOP ;     ( ALL DATA TRANSFERRED? )
11
12
13 : MSTORE DM1 STORE DM2 ;
14
15
```

210 LIST

```
 0 ( SCAN ROUTINE  STORES D/A AND CURRENT  9/3/88   )
 1 OCTAL ASSEMBLER
 2 : FOOLISH ;
 3 CODE SCAN    0 BUF-PTR MOV  1 SPOT MOV
 4     BEGIN
 5       BEGIN CNTR TST 0< END  176770 1 # MOV  CNTR TICS MOV
 6       0 )+ 1 MOV  1 DIR ADD
 7       BEGIN 176770 TST B 0< END   0 )+ 176772 MOV
 8       176760 1 MOV  1 EPOT CMP 0= END
 9     BUF-PTR 0 MOV  170000 0 # MOV   NEXT   FORTH
10
11
12
13
14 DECIMAL
15
```

Appendix I (Cont.)

```
211 LIST

 0 ( SCAN ROUTINES ) OCTAL
 1 : USC  EPOT !  SPOT !  1 DIR !
 2       CLOCK GET  104 170000 !  SCAN  CLOCK RELEASE ;
 3 : DSC  EPOT !  SPOT !  -1 DIR !
 4       CLOCK GET  104 170000 !  SCAN  CLOCK RELEASE ;
 5 CODE  TDEL  BEGIN CNTR TST  0< END 170000 # MOV NEXT
 6 : TDELAY  DTIM @ CNTR !  CLOCK GET  104 170000 !
 7          TDEL          CLOCK RELEASE ;
 8
 9 : FSC  RESET-PTR      IPOT @ 176760 !    TDELAY
10       IPOT @ UPOT @ USC UPOT @ LPOT @ DSC LPOT @ IPOT @ USC ;
11 : BSC  RESET-PTR      IPOT @ 176760 !    TDELAY
12           IPOT @ LPOT @ DSC LPOT @ UPOT @ USC UPOT @ IPOT @ DSC ;
13
14
15 DECIMAL
```

Appendix II
Diffusion Simulation Routines
Written in Microsoft Fortran V.5.0

```
C MAIN.FOR  March 16, 1991
$LARGE
      REAL*8 SALTS(200),SALTR(200),CN(100),CC(100),
     1CNSALT(100),CCSALT(100)
      INTEGER*4 NXTIT(200)
      CHARACTER*64 FNAME
      D=0.45
      WRITE(*,'(A\)')' IS THIS A NEW SIMULATION? (Y/N) '
      READ(*,'(A)')FNAME
      IF(FNAME.EQ.'Y') GOTO 50
      GOTO 100
   50 CALL SETUP(FRCTCNVS,FRCTCNVR,EQK,CEQK,SALTSI,SALTRI,
     1CI,CSALTI,CN,CC,CCSALT,CNSALT,SALTS,SALTR)
      ITOT=0
      GOTO 200
  100 CALL READFILE(ITOT,FRCTCNVS,FRCTCNVR,EQK,CEQK,CN,CC,
     1SALTR,SALTS,CCSALT,CNSALT)
  200 FRCTLFTS=1.0-FRCTCNVS
      FRCTLFTR=1.0-FRCTCNVR
C NXTIT ARRAY CONTAINS VALUES TELLING PROGRAM WHEN TO STORE
C DATA VALUES.  1 NUMBER IN INPUT FILE DESIGNATES NUMBER OF
C DATA SETS TO STORE.  SUBSEQUENT VALUES ARE ITERATION VALUES
C THAT ARE TO BE STORED
      WRITE(*,'(A\)')' ENTER FILE NAME OF ITERATIVE SAVE PARAMETERS '
      READ(*,'(A)')FNAME
      OPEN(7,FILE=FNAME,ACCESS='SEQUENTIAL',STATUS='OLD')
      I=1
  300 READ(7,996)NXTIT(I)
      IF(NXTIT(I).EQ.-9)GOTO 350
      I=I+1
      GOTO 300
  350 LASTSET=I-1
      CLOSE(7)
C MAIN DIFFUSION LOOP
      DO 1000 M=1,LASTSET
      DO 500  N=ITOT+1,NXTIT(M)
C CONSIDER ELECTROCHEMISTRY AT INTERFACES
C SALT1  :  NON-AQUEOUS ( C CP CSALT CPSALT )  :  SALT2
C RECEIVING INTERFACE: FRCTCNVR AMOUNT OF CN GOES TO CC
      CC(100)=FRCTCNVR*CN(100)+CC(100)
      CN(100)=FRCTLFTR*CN(100)
      CCSALT(100)=FRCTCNVR*CNSALT(100)+CCSALT(100)
      CNSALT(100)=FRCTLFTR*CNSALT(100)
      CALL EQUIL(SALTR(1),CN(100),CC(100),CCSALT(100),CNSALT(100),
```

Appendix II (Cont.)

```
     1EQK,CEQK)
C SOURCE INTERFACE: FRCTCNVS AMOUNT OF CC GOES TO CN
      CN(1)=FRCTCNVS*CC(1)+CN(1)
      CC(1)=FRCTLFTS*CC(1)
      CNSALT(1)=FRCTCNVS*CCSALT(1)+CNSALT(1)
      CCSALT(1)=FRCTLFTS*CCSALT(1)
      CALL EQUIL(SALTS(1),CN(1),CC(1),CCSALT(1),CNSALT(1),EQK,CEQK)
C SIMULATE DIFFUSION
      CALL DIFUSE(D,100,CN)
      CALL DIFUSE(D,100,CC)
      CALL DIFUSE(D,100,CNSALT)
      CALL DIFUSE(D,100,CCSALT)
      CALL DIFUSE(D,200,SALTR)
      CALL DIFUSE(D,200,SALTS)
  500 CONTINUE
      ITOT=NXTIT(M)
      CALL WRITFILE(ITOT,FRCTCNVS,FRCTCNVR,EQK,CEQK,CN,CC,
     1SALTR,SALTS,CCSALT,CNSALT)
 1000 CONTINUE
      STOP
  996  FORMAT(I8)
 2001 FORMAT(1H0,'  MAIN  ',\,3(F20.16,2X),\,2(F20.16,2X))
      END
```

Appendix II (Cont.)

```
C SETUP.FOR March 16, 1991
      SUBROUTINE SETUP(FRCTCNVS,FRCTCNVR,EQK,CEQK,SALTSI,SALTRI,
     1CI,CSALTI,CN,CC,CCSALT,CNSALT,SALTS,SALTR)
      REAL*8 SALTS(200),SALTR(200),CN(100),CC(100),
     1CNSALT(100),CCSALT(100),CI,CSALTI,SALTSI,SALTRI
      REAL*4 EQK,CEQK
      CHARACTER*64 FNAME
   50 WRITE(*,'(A\)')' ENTER SOURCE PHASE SALT CONCENTRATION '
      READ(*,'(F12.9)')SALTSI
      CSALTI=0.0
      WRITE(*,'(A\)')' ENTER RECEIVING PHASE SALT CONCENTRATION '
      READ(*,'(F12.9)')SALTRI
      WRITE(*,'(A\)')' ENTER INITIAL CARRIER CONCENTRATION '
      READ(*,'(F12.9)')CI
      WRITE(*,'(A\)')' ENTER CARRIER EQUILIBRIUM CONSTANT '
      READ(*,'(F12.9)')EQK
      WRITE(*,'(A\)')' ENTER CHARGED CARRIER EQUILIBRIUM CONSTANT '
      READ(*,'(F12.9)')CEQK
      WRITE(*,'(A\)')' ENTER ELECTROCHEMICAL CONVERSION FACTOR AT SOURCE
     1 INTERFACE '
      READ(*,'(F12.9)')FRCTCNVS
      WRITE(*,'(A\)')' ENTER ELECTROCHEMICAL CONVERSION FACTOR AT RECEIV
     1ING INTERFACE '
      READ(*,'(F12.9)')FRCTCNVR
      WRITE(*,'(A\)')' DO YOU WISH TO PRE-EQUILIBRATE MEMBRANE PHASE?'
      READ(*,'(A\)')FNAME
      IF(FNAME.EQ.'N') GOTO 75
      WRITE(*,'(A\)')' ENTER EQUIL. SOURCE PHASE SALT CONCENTRATION '
      READ(*,'(F12.9)')SALTSI
      WRITE(*,'(A\)')' ENTER EQUIL. RECEIVING PHASE SALT CONCENTRATION '
      READ(*,'(F12.9)')SALTRI
      WRITE(*,'(A\)')' ENTER EQUIL. CARRIER CONCENTRATION '
      READ(*,'(F12.9)')CI
      WRITE(*,'(A\)')' ENTER EQUIL. CARRIER/COMPLEX CONCENTRATION '
      READ(*,'(F12.9)')CSALTI
   75 WRITE(*,994)EQK,CEQK,CI,CSALTI,SALTSI,SALTRI,FRCTCNVS,FRCTCNVR
      WRITE(*,'(A\)')' ARE VALUES CORRECT?'
      READ(*,'(A\)')FNAME
      IF(FNAME.EQ.'N') GOTO 50
      DO 100 I=1,200
      SALTS(I)=SALTSI
      SALTR(I)=SALTRI
  100 CONTINUE
      DO 200 I=1,100
```

Appendix II (Cont.)

```
      CN(I)=CI
      CC(I)=0.0
      CCSALT(I)=0.0
      CNSALT(I)=CSALTI
  200 CONTINUE
  994 FORMAT(1X,'EQK CEQK ',2(F12.9,2X),1H0,' CARRIER CMP ',2(F12.9,2X)
     1,1H0,'SALT S/E ',2(F12.9,2X),1H0,' CONV. FACT. S/R ',2(F12.9,2X))
      RETURN
      END
```

Appendix II (Cont.)

```
C READFILE.FOR  March 16, 1991
      SUBROUTINE READFILE(ITOT,FRCTCNVS,FRCTCNVR,EQK,EQKP,CN,CC,
     1SALTR,SALTS,CCSALT,CNSALT)
      REAL*8 SALTR(200),SALTS(200),CN(100),CC(100)
     1,CCSALT(100),CNSALT(100)
      CHARACTER*64 FNAME
      WRITE(*,'(A\)')' DOUBLE PREC. DATA ARRAY NAME '
      READ(*,'(A)')FNAME
      OPEN(7,FILE=FNAME,ACCESS='SEQUENTIAL',STATUS='OLD',
     1FORM='UNFORMATTED')
      READ(7)(CN(I),I=1,100)
      READ(7)(CC(I),I=1,100)
      READ(7)(CNSALT(I),I=1,100)
      READ(7)(CCSALT(I),I=1,100)
      READ(7)(SALTR(I),I=1,200)
      READ(7)(SALTS(I),I=1,200)
      READ(7)ITOT,FRCTCNVR,FRCTCNVS,EQK,EQKP
      CLOSE(7)
      RETURN
      END


C WRITFILE.FOR  March 16,1991
      SUBROUTINE WRITFILE(ITOT,FRCTCNVS,FRCTCNVR,EQK,CEQK,CN,CC,
     1SALTR,SALTS,CCSALT,CNSALT)
      REAL*8 SALTR(200),SALTS(200),CN(100),CC(100),
     1CCSALT(100),CNSALT(100)
      CHARACTER*64 FNAME
      FNAME = '        .DAT'
      WRITE(FNAME(1:8),'(I8.8)')ITOT
      OPEN(7,FILE=FNAME,ACCESS='SEQUENTIAL',STATUS='NEW',
     1FORM='UNFORMATTED')
      WRITE(7)(CN(I),I=1,100)
      WRITE(7)(CC(I),I=1,100)
      WRITE(7)(CNSALT(I),I=1,100)
      WRITE(7)(CCSALT(I),I=1,100)
      WRITE(7)(SALTR(I),I=1,200)
      WRITE(7)(SALTS(I),I=1,200)
      WRITE(7)ITOT,FRCTCNVR,FRCTCNVS,EQK,CEQK
      CLOSE(7)
      WRITE(*,'(A\)')'  ',FNAME,' HAS BEEN WRITTEN'
      RETURN
      END
```

Appendix II (Cont.)

```
C EQ.FOR March 16, 1991
      SUBROUTINE EQUIL(SALT,CN,CC,CCS,CNS,EQK,CEQK)
      REAL*8 SALT,CN,CC,CCS,CNS,RATIO
      IF(CN.LT.0) WRITE(*,'(A\)')' NEUTRAL CARRIER CONC. NEGATIVE '
      IF(CC.LT.0) WRITE(*,'(A\)')' CHARGED CARRIER CONC. NEGATIVE '
      IF(SALT.LT.0) WRITE(*,'(A\)')' SALT CONC. NEGATIVE '
      IF((SALT.EQ.0).AND.(CNS.EQ.0).AND.(CCS.EQ.0)) GOTO 200
      IF((CC.GT.0).AND.(CN.GT.0)) GOTO 100
C CALCULATE FOR NEUTRAL CARRIER ONLY
     CN=CN+CNS
     SALT=SALT+CNS
     CNS=SALT*CN*EQK
     CN=CN-CNS
     SALT=SALT-CNS
      GOTO 200
C CALCULATE FOR COMPETING CARRIERS
 100   CST=SALT+CCS+CNS
      CCT=CC+CCS
      CNT=CN+CNS
      RATIO=(EQK*CN)/(CEQK*CC)
      SALT=CST/(1+CC*(RATIO+1))
      CCS=(CST-SALT)/(RATIO+1)
      CNS=CST-SALT-CCS
      CN=CNT-CNS
      CC=CCT-CCS
 200   RETURN
      END
```

Appendix II (Cont.)

```
C DIFUSE.FOR  March 16, 1991
      SUBROUTINE DIFUSE(D,N,ARRAY)
      REAL*8 ARRAY(200),C1,C2,C3
C ROUTINE TAKES N VALUES FROM THE CALLING ROUTINE PLACING THEM IN
C ARRAY.  IT THEN SIMULATES DIFUSSION USING DIMENSIONLESS DIFFUSION
C COEFFICIENT D.
      C1=ARRAY(1)
      C2=ARRAY(2)
      ARRAY(1)=C1+D*(C2-C1)
      DO 100 I=2,N-1
      C3=ARRAY(I+1)
      ARRAY(I)=C2 + D*(C1-C2-C2+C3)
      C1=C2
      C2=C3
  100 CONTINUE
      ARRAY(N)=C2+D*(C1-C2)
      RETURN
      END
```

Bibliography

1. C. J. Pedersen, J. of the American Chemical Society 89(26), 7017 (1967)

2. K. H. Pannell, B. J. Rodriguez, S. Chiocca, L. P. Jones and J. Molinar, Journal of Membrane Science (1982)

3. S. R. Cooper, "Crown Compounds: Towards Future Applications," VCH Publichers (1992)

4. G. Gokel, "Crown Ethers & Cryptands," The Royal Society of Chemistry (1991)

5. S. Patai, "Chemistry of the Ether Linkage"

6. J. H. Fendler, "Membrane Mimetic Chemistry", Wiley (1982)

7. R. M. Izatt and J. J. Christensen, "Progress in Macrocyclic Chemistry", Wiley, (1979)

8. S. Patai, "Chemistry of Ethers, Crown Ethers, Hydroxyl Groups, and Their Sulfur Analogues," Wiley (1980)

9. M. Hiraoka, "Crown Compounds: Their Characteristics and Applications," Elsevier (1982)

10. E. Weber, "Crown Ethers and Analogs," Wiley (1982)

11. C. J. Pedersen and H. K. Frensdorff, Angew Chem., 11(1), 16 (1972)

12. J. D. Lamb, R. M. Izatt, C. S. Swain and J. J. Christensen, J. of the American Chemical Society, 102(2), 475 (1980)

13. J. D. Lamb, R. M. Izatt, D. G. Garrick, J. S. Bradshaw and J. J. Christensen, J. of Membrane Science, 146 (1981)

14. E. Kleinpeter, M. Stoss and W. Schroth, Magnetic Resonance in Chemistry, 27, 676 (1989)

15. K. Hashimoto, H. Togo, K. Morihashi, Y. Yokoyama and O. Kikuchi, Bulletin of the Chemical Society of Japan, 64, 3245 (1991)

16. G. W. Leisegang, M. M. Farrow, F. A. Vazquez, N. Purdie and E. M. Eyring, Journal of the American Chemical Society, 99(10), 3240 (1977)

17. S. Stoss, W. Schroth and E. Kleinpeter, Journal of Magnetic Resonance, 28, 425 (1992)

18. R. G. Pearson, Journal of the American Chemical Society, 85(22), 3533 (1963)

19. J. March, "Advanced Organic Chemistry: Reactions, Mechanisms, and Structure," McGraw Hill, 253 (1977)

20. M. C. Mackey, "Ion Transport Through Biological Membranes: An Integrated Theoretical Approach"

21. N. Lakshminarayanaiah, "Equations of Membrane Biophysics," Academic Press (1984)

22. H. Nishida, M. Tazaki, M. Takagi and K. Ueno, Mikrochimica Acta, 281 (1981)

23. K. Hiratani, I. Nozawa, T. Nakagawa and S. Yamada, Journal of Membrane Science, 12(1982), 207 (1982)

24. S. Shinkai, K. Inuzuka, O. Miyazaki and O. Manabe, J. of the American Chemical Society, 107(13), 3950 (1985)

25. S. Shinkai, M. Ishihara, K. Ueda and O. Manabe, Journal of the Chemical Society: Perkins Transactions II, 511 (1985)

26. "Perkin Elmer Atomic Absorption User Manual", Perkin Elmer, Inc. (1976)

27. K. M. Klein, C. Park and A. F. Tasch, IEEE Trans. on Electron Dev., 40(7), 1446 (1992)

28. R. Kircher, "Three-Dimensional Simulation of Semiconductor Devices" (1991)

29. C. Catlow, S. Parker and M. Allen, "Computer Modeling of Fluids, Polymers, and Solids," (1989)

30. R. J. Roe, "Computer Simulation of Polymers" (1991)

31. A. Warshel, "Computer Modeling of Chemical Reactions in Enzymes and Solutions" (1991)

32. R. E. Keen, "Computer Simulation in Biology" (1992)

33. R. M. Izatt, R. Bruening, M. Bruening, G. Lindh and J. J. Christensen, Anal. Chem., 61, 1140 (1989)

34. M. Meyer and M. Hayoun, J. Chem. Phys., 89(2), 1067 (1988)

35. A. J. Bard and L. R. Faulkner, "Electrochemical Methods: Fundamentals and Applications," Wiley (1980)

36. Kissinger and Heineman, "Laboratory Techniques in Electroanalytical Chemistry" (1984)

37. C. Reusch and E. Cussler, AIChE J., 19, 736 (1973)

38. J. Lamb, J. Christensen, S. Izatt, K. Bedke, M. Austin and R. Izatt, J. Am. Chem. Soc., 102 3399 (1980)

39. R. W. Ramette, "Chemical Equilibrium and Analysis," 450-460 (1981)

40. M. Baizer, "Organic Electrochemistry: An Introduction and a Guide," M. Dekker (1973)

41. A. J. Fry, "Synthetic Organic Electrochemistry," Plenum Press (1986)

42. C. K. Mann, "Electrochemical Reactions in Nonaqueous Solvents" (1973)

43. D. Root, R. Pendarvis and W. Smith, J. Org. Chem., 43(4), 778 (1978)

44. M. Maruyama and K. Murakami, J. Electroanal. Chem., 102, 221 (1979)

45. D. G. I. Felton, "Phenazines" (1957)

46. F. Ullman and F. Mauthner, Ber., 35, 4302 (1902)

47. F. King, P. Clark and P. Davis, J. Chem Soc., 3012 (1949)

48. K. Ley and F. Seng, Synthesis, July, 415 (1975)

49. A. Romer, H. Scholl and H. Budzikiewicz, Z. Naturforsch, 36b, 1037 (1981)

50. A. Romer and M. Sammet, Z. Naturforsch, 38b, 866 (1983)

51. N. Takashi and T. Hishida, Bull. Chem. Soc. Jpn., 48(12), 3709 (1975)

52. W. Horspool, P. Smith and J. Tedder, J. Chem. Soc. C, 138 (1971)

53. M. Abu El-Haj, B. Dominy, J. Johnston, M. Haddadin and C. Issidorides, J. Org. Chem., 37(4), 589 (1972)

54. C. Chandler and L. Deady, J. Heterocyclic Chem, 18, 599 (1981)

55. F. W. Knobloch and W. H. Rauscher, J. of Polymer Chem, 657 (1967)

56. R. Silverstein, G. C. Bassler and T. Morrill, "Spectrometric Identification of Organic Compounds" (1981)

57. K. Yamakawa and M. Hisatome, J. Organomat. Chem., 52, 407 (1973)

58. T. Barr and W. Watts, Tetrahedron, 24, 3219 (1968)

59. Ibid, 24, 6111 (1968)

60. Ibid, 25, 5245 (1969)

61. T. Barr and W. Watts, J. Organomet. Chem., 15, 177 (1968)

62. S. Toma and E. Solcaniova, J. Organomet. Chem., 288, 331 (1985)

63. ref. 26

64. E. Shchori, et. al., J. Chem. Soc., Dalton, 2381 (1975)

65. V. I. Goldanski and R. H. Herber, "Chemical Applications of Moessbauer Spectroscopy", Academic Press, 268-311 (1968)

66. P. S. Bagus, U. I. Walgren and J. Almlof, Journal of Chemical Physics, 64(6), 2324 (19)

67. M. Hillman and A. Kvick, Organometallics, 2(12), 1780 (1983)

68. N. J. Singletary, M. Hillman and H. Dauplaise, Organometallics, 3, 1427 (1984)

69. S. Wanigatunga and K. B. Wagener, Macromolecules, 22, 4156 (1989)